REPORT DOCUMENTATION PAGE

Form Approved
OMB No. 0704-0188

1. REPORT DATE *(DD-MM-YYYY)*	2. REPORT TYPE	3. DATES COVERED *(From - To)*
06-05-2010		

4. TITLE AND SUBTITLE

A Feedforward Compensation Technique for use in Mitigating Platform Induced Jitter

5a. CONTRACT NUMBER

5b. GRANT NUMBER

5c. PROGRAM ELEMENT NUMBER

6. AUTHOR(S)

Roberts, Matthew Lynn

5d. PROJECT NUMBER

5e. TASK NUMBER

5f. WORK UNIT NUMBER

7. PERFORMING ORGANIZATION NAME(S) AND ADDRESS(ES)

8. PERFORMING ORGANIZATION REPORT NUMBER

9. SPONSORING/MONITORING AGENCY NAME(S) AND ADDRESS(ES)

U.S. Naval Academy
Annapolis, MD 21402

10. SPONSOR/MONITOR'S ACRONYM(S)

11. SPONSOR/MONITOR'S REPORT NUMBER(S)

Trident Scholar Report no. 392 (2010)

12. DISTRIBUTION/AVAILABILITY STATEMENT

This document has been approved for public release; its distribution is UNLIMITED

13. SUPPLEMENTARY NOTES

14. ABSTRACT

To mitigate jitter in a directed-energy laser system, caused by mechanical vibrations without feedback from the target, a feedforward compensation technique is proposed. The technique requires that the position of the beam at the target be calculated in real time, which is accomplished by determining the exact position and orientation of the platform that fires the laser beam. Once the position of the beam at the target is calculated, it is used in a feedforward control algorithm to mitigate the platform induced jitter. This research demonstrates that it is possible to calculate a beam's position at a target approximately 5 m away with micro-meter accuracy for a complex motion in real time based solely on platform and mirror positions. This calculated beam position is then used in a feedforward compensation technique to mitigate platform induced jitter by over 90%. These results have the potential to improve the aimpoint maintenance on a target and significantly reduce the power required for a directed energy weapon system.

15. SUBJECT TERMS

Directed Energy Laser System, Jitter Reduction, Feedforward Control System

16. SECURITY CLASSIFICATION OF:			17. LIMITATION OF ABSTRACT	18. NUMBER OF PAGES	19a. NAME OF RESPONSIBLE PERSON
a. REPORT	b. ABSTRACT	c. THIS PAGE		96	19b. TELEPHONE NUMBER *(Include area code)*

U.S.N.A. --- Trident Scholar project report; no. 392 (2010)

A FEEDFORWARD COMPENSATION TECHNIQUE FOR USE IN MITIGATING PLATFORM INDUCED JITTER

by

Midshipman 1/c Matthew L. Roberts
United States Naval Academy
Annapolis, Maryland

_____
(signature)

Certification of Advisers Approval

CDR R.J. Watkins, USN
Mechanical Engineering Department

_____
(signature)

_____
(date)

Professor Oscar Barton, Jr.
Mechanical Engineering Department

_____
(signature)

_____
(date)

RADM Craig E. Steidle, USN (ret.)
Aerospace Engineering Department

_____
(signature)

_____
(date)

Acceptance for the Trident Scholar Committee

Professor Carl E. Wick
Associate Director of Midshipman Research

_____
(signature)

_____
(date)

Abstract

Directed energy weapons are a potential "game changer" of modern naval warfare that will dramatically increase capability while decreasing the risk of collateral damage, and as a result, the Office of Naval Research has developed a Directed Energy Program. Beam control is one of the five main fields of study in this program and is essential for the development and operation of a directed energy weapon system. The United States Naval Academy has constructed a unique Laser Jitter Control Testbed which is used in this research to study jitter, the deviation of an optical beam from its intended path due to platform induced vibrations and atmospheric effects. To mitigate jitter caused by mechanical vibrations without feedback from the target, a feedforward compensation technique is proposed. This technique requires that the position of the beam at the target be calculated in real time which is accomplished by determining the exact position and orientation of the platform which fires the beam. Once the position of the beam at the target is calculated, it is used in a feedforward control algorithm to mitigate the platform induced jitter. This research demonstrates that it is possible to calculate a beam's position at a target approximately 5 m away with micro-meter accuracy for a complex motion in real time based solely on platform and mirror positions. This calculated beam position is then used in a feedforward compensation technique to mitigate platform induced jitter by over 90%. These results have the potential to improve the aimpoint maintenance on a target and significantly reduce the power required for a directed energy weapon system.

Acknowledgements

A project of this magnitude is never an individual effort but the result of multiple contributors. While difficult to describe in such few words, I would like to thank the following people for their help in assisting my Trident Scholar research project:

I would first like to thank my primary adviser, Commander Joe Watkins. Simply put, this project would not have been possible if it were not for his tireless efforts and constant encouragement. I attribute a major portion of not only my academic success, but also my professional development to the time I have spent with CDR Watkins and I will forever be grateful for his help and support. Secondly, I would like to thank Professor Oscar Barton of the Mechanical Engineering Department here at USNA. Professor Barton was instrumental in my engineering education and invited me to join him and CDR Watkins in this research project. I would also like to thank Rear Admiral Craig Steidle (Ret.) who has been essential to my education in the Aerospace Engineering Department and professional development. RADM Steidle has helped me understand what it means to be both an officer and an engineer in the U.S. Navy and I am very grateful for the time I have spent with him.

Besides my advisers, there are many additional individuals I would like to thank. My research would not have been possible if it were not for Jesse Baldwin and Curtis Mayes of the Technical Support Division here at USNA. Their efforts have provided me with an exceptional laboratory to work in and we are truly fortunate to have such incredible people working here at USNA. I would also like to thank the Office of Naval Research for funding my project. I would especially like to thank Michael Deitchman, Deputy Chief of Naval Research, and Quentin Saulter, Directed Energy Program Manager. I would like to thank Distinguished Professor Brij Agrawal and Captain Al Scott (Ret.) of the Naval Postgraduate School who provided me with an incredible internship at NPS over the summer of 2009. They provided me with an introduction to directed energy and beam control research and helped lay a foundation for my Trident Scholar research project. I am also very grateful to the Trident Scholar Committee here at USNA who have made this project possible. I would especially like to thank Professor Carl Wick, Professor

Daryl Boden, and Professor Kiriakos Kiriakidis. Also worth mentioning is Cindi Gallagher of MSC who helped me prepare my final poster.

Lastly, and most importantly, I would like to thank my family and friends for their constant help and support. My parents, Mike and Jane Roberts, are largely responsible for what I have accomplished in my life and for who I am today. My grandfather, Larry Speaker, who is a role model for me not only as an engineer, but as a father and husband. My younger brother, Kevin Roberts, who has provided me with a reason to continue to excel and work hard so that I may be a good role model for him. And finally, my fiancée, Laura Schmalhorst, who is my best friend and the love of my life.

Table of Contents

Abstract 1
Acknowledgements 2
Table of Contents 4
List of Figures 5
List of Tables 6
List of Symbols 6
1 Introduction 7
1.1 Motivation 7
1.2 History 8
2 Experimental Setup and Procedure 11
2.1 Description of Major Components 11
2.2 Experimental Method 13
2.3 Tunnel Isolation Effects on Jitter 16
3 Theory 18
3.1 Calculated Beam Position 18
3.2 Proportional-Integral Control 21
3.3 Least Mean Squares Control 24
3.4 SIMULINK Model 27
4 Experimental Results 32
4.1 Platform Motion 32
4.2 Spectral Analysis of System with No Control and Residual Jitter 33
4.3 Beam Calculation Results 36
4.4 Experiment Description 40
4.5 PI and LMS Control Experimental Results 41
4.6 Comparison 46
5 Conclusion 48
5.1 Results 48
5.2 Future Work 48
APPENDIX A: Newport Fast Steering Mirror 50
APPENDIX B: Newport Breadboard 55
APPENDIX C: CSA Engineering Inertial Actuator 58
APPENDIX D: On-Trak PSM 59
APPENDIX E: Newport Compact Air-Mount 61
APPENDIX F: Newport Optical Table 64
APPENDIX G: Newport Pneumatic Isolators 69
APPENDIX H: Laser Diode 72
APPENDIX I: Kistler Accelerometer Model 8690C5 73
APPENDIX J: MATLAB Scripts 76
APPENDIX K: Additional Simulink Blocks 90

List of Figures

Figure 1. USNA Directed Energy Control Laboratory 11
Figure 2. Newport FSM 12
Figure 3. Newport Breadboard 12
Figure 4. Experimental Configuration 14
Figure 5. Experimental Configuration 15
Figure 6. Tunnel 16
Figure 7. Tunnel Effects 17
Figure 8. PI Controller Block Diagram 22
Figure 9. Mirror Position before Critical Gains 23
Figure 10. Mirror Position at Critical Gains 24
Figure 11. Filter for LMS Algorithm 25
Figure 12. LMS block diagram 26
Figure 13. SIMULINK Model Block Diagram 28
Figure 14. Beam Calculation Sub-Blocks 29
Figure 15. PI Controller 30
Figure 16. LMS Controller 31
Figure 17. Platform Motion for 17 Hz Disturbance 32
Figure 18. Platform Motion for Multiple Frequency Disturbances 33
Figure 19. Spectral Analysis, No Disturbance, No Control 34
Figure 20. Filtered System Residual Jitter 35
Figure 21. Spectral Analysis, 17 Hz Disturbance, No Control 36
Figure 22. Spectral Analysis, Multiple Frequency Disturbances, No Control 36
Figure 23. Actual vs. Calculated Beam Position at Target for 17 Hz Disturbance 37
Figure 24. Actual vs. Calculated Beam Position at Target for Multiple Frequency Disturbances 38
Figure 25. 50 msec Moving Average of Error between Actual and Calculated Jitter Angle at Target for 17 Hz Disturbance 39
Figure 26. 50 msec Moving Average of Error between Actual and Calculated Jitter Angle at Target for Multiple Frequency Disturbances 40
Figure 27. PI Jitter Control for 17 Hz Disturbance 42
Figure 28. PI Spectral Analysis for 17 Hz Disturbance 42
Figure 29. LMS Jitter Control for 17 Hz Disturbance 43
Figure 30. LMS Spectral Analysis for 17 Hz Disturbance 43
Figure 31. PI Jitter Control for Multiple Frequency Disturbances 45
Figure 32. PI Spectral Analysis for Multiple Frequency Disturbances 45
Figure 33. LMS Jitter Control for Multiple Frequency Disturbances 46
Figure 34. LMS Spectral Analysis for Multiple Frequency Disturbances 46

List of Tables

Table 1. PI Controller Gains 23
Table 2. Improvement in Jitter Angle for 17 Hz Disturbance 47
Table 3. Improvement in Jitter Angle for Multiple Frequency Disturbances 47

List of Symbols

n_i	i^{th} component of the direction of the normal to a plane
$\vec{r}$	Direction vector
$\bar{x}$	Intercept point of a vector
m_{ij}	i^{th} component of the j^{th} coordinate on the intercept plane
$\lfloor T_{ref} \rfloor$	Reflection matrix
$[T_{rot}]$	Rotation matrix
Δ	Rotation angle
d	Distance along a beam direction to the intercept plane
K_i	Integral gain
K_p	Proportional gain
K_u	Ultimate gain
P_u	Oscillation period
$x(n)$	Reference signal at step n
$\bar{w}(n)$	Vector of weights at step n
$u(n)$	Control input at step n
$s(n)$	Desired output at step n
$d(n)$	Actual output at step n
μ	LMS filter adaptation rate
$e(n)$	Error at step n

1 Introduction

1.1 Motivation

The Directed Energy Program at the Office of Naval Research (ONR) is a potential "game changer" of modern naval warfare that will dramatically increase U.S. capability while decreasing the risk of collateral damage. Five fields make up this program: (1) free electron laser weapon system, (2) free electron laser for weapons of mass destruction detection, (3) high power microwave weapon, (4) electric fiber weapon system, and (5) beam control. Beam control is essential for the development and operation of all four directed energy systems, especially when operating in the air or on the sea in a combat maritime environment. Specific technological challenges include tracking maritime targets in high clutter ocean seas, aimpoint maintenance on a rapidly maneuvering target, aiming and firing from a highly dynamic platform, and compensation for atmospheric effects in a maritime environment.[1] ONR has tasked researchers at the Naval Postgraduate School (NPS) and the United States Naval Academy (USNA) to investigate these unique challenges. It is the purpose of this research project to address the aimpoint maintenance challenge to aid the development of a directed energy weapon system suitable for use by the Navy in a combat maritime environment.

Directed energy beams are highly susceptible to jitter which is the deviation of a light beam from its intended path due to mechanically induced vibrations and atmospheric effects. For example, a 1 cm diameter directed energy beam with only 1 micro-radian (μrad) of jitter will result in roughly a 9 fold decrease in the intensity of the beam at 10 km. Due to the high amount of energy needed to destroy a target (roughly 100 kW or more),[2] this decrease in intensity is

---

[1] Deitchman, Michael B., "Naval S&T Strategic Plan-Defining the Strategic Direction for Tomorrow," Presentation to the U.S. Naval Academy, Annapolis MD, 24 October 2008

[2] Shachtman, Noah, "Weapons-Grade Lasers by the End of '08?" 02 September 2008, <http://blog.wired.com/defense/2008/09/weapons-grade-l.html>

unacceptable and must be minimized. In addition, many control problems are more easily solved if feedback is available from the intended target. However, this weapon system will be employed in a highly dynamic environment and the beam's precise location on the target must be maintained to ensure burn through with the minimum amount of energy. Because of this, the use of target feedback by means of visual detection methods may not be feasible. Instead, feedforward control is desirable which will involve calculating the error in the system and then correcting that error in real time as the weapon system is fired. USNA has developed a Directed Energy Beam Control Laboratory which will be used in this research project to determine an error signal that may be used to correct platform induced jitter using feedforward control techniques.

1.2 History

While the control of disturbances from unwanted vibrations has been under investigation since the early 1900s, only relatively recently have researchers explored the control of these disturbances in optical beams. The first efforts in this area were in overcoming the problem of image stabilization. Smith[3] wrote one of the first papers, published in 1928, on the algebraic theory behind systems of plane reflecting surfaces. Beggs[4] developed an algorithm in 1960 for quantifying mirror-image kinematics. Both of these methods used matrix algebra to solve the image location on a focal plane for a series of reflections. In 1990, Royalty[5] applied these matrix techniques to a gimbaled mirror in anticipation of using these systems on vehicles that could impart motion to the mirror itself. DeBruin and Johnson[6] applied vector analysis to establish a line of sight reference frame, again for a mirror disturbed by motion of the base. In depth research into the control of optical beams first began in the 1980's and 1990's for use in satellite

---

[3] Smith, T., "On systems of Plane Reflecting Surfaces", *Trans. Opt. Soc.* 30 68-78

[4] Beggs, Joseph S., "Mirror Image Kinematics", *Journal of the Optical Society of America*, Vol 50, Number 4, April, 1960

[5] Royalty, J., "Development of Kinematics for Gimbaled Mirror Systems", *Proc. SPIE, Vol. 1304, 262-274, Acquisition, Tracking, and Pointing IV,* 1990

[6] DeBruin, James, C. and Johnson, David B., "Line of Sight Reference Frames: A Unified Approach to Plane-Mirror Optical Kinematics", *Proc. SPIE Vol. 1697, p. 111-129, Acquisition, Tracking, and Pointing VI,* 1992

communications[7], and adaptive control has been proposed for use in control systems to accomplish accurate beam pointing.[8] The use of directed energy beams as weapons was explored during this time, but laser systems and power requirements were too large, thus making them impractical for naval applications. The recent advent of smaller lasers with high power output has prompted the Navy to explore the use of directed energy systems on tactical naval platforms. For the Navy to move forward with a directed energy system, beam control technology must be advanced to minimize the power dissipating effects of jitter.

In the 1990's, the Air Force began work on a high altitude directed energy system that had the potential to shoot down theater ballistic missiles.[9] A downfall of this technology is the extremely large and complex energy source which is not suitable for use in a tactical naval platform. In addition, a directed energy system on a tactical naval platform will be exposed to a much richer disturbance frequency spectrum than a high altitude one, thus making the Air Force program not well suited for naval applications. There are currently several ground-based directed energy programs in development as well. These systems have demonstrated the ability to detect, track, and destroy targets, but they do not experience the dynamics of a tactical naval platform and are therefore not subject to the higher amplitude mechanical vibrations expected to be encountered in a combat maritime environment. More importantly, the dynamic nature of the maritime and/or low altitude combat environment may make obtaining accurate feedback of the beam's location on the target problematic. Therefore, a jitter mitigation technique that uses feedforward, as opposed to feedback, control is desirable.

The following technique develops an algorithm to compute the beam's motion based on the platform's motion and mirror kinematics. While previously unavailable, today's faster CPUs and I/O cards present an opportunity to exploit extraordinarily sensitive sensors to determine the

---

[7] Skormin, V.A.; Tascillo, M.A.; Nicholson, D.J., "A jitter rejection technique in a satellite-based laser communication system," *Aerospace and Electronics Conference, 1993. NAECON 1993., Proceedings of the IEEE 1993 National* , vol., no., pp.1107-1115 vol.2, 24-28 May 1993.

[8] Skormin, V.A.; Busch, T.E.; Givens, M.A., "Model reference control of a fast steering mirror of a pointing, acquisition and tracking system for laser communications," *Aerospace and Electronics Conference, 1995. NAECON 1995., Proceedings of the IEEE 1995 National* , vol.2, no., pp.907-913 vol.2, 22-26 May 1995

[9] Forden, G.E., "The airborne laser," *Spectrum, IEEE* , vol.34, no.9, pp.40-49, Sep 1997

platform's motion. Combined, this research has the potential to improve the aimpoint maintenance on a target, thus significantly reducing the power required for a directed energy system. This paper is organized as follows: first is a discussion of the experimental setup. Following that, the theory used to develop the feedforward signal is explained. Finally, experimental results and conclusions are presented.

2 Experimental Setup and Procedure

2.1 Description of Major Components

Research for this project was conducted in the USNA Directed Energy Control Laboratory as seen in Figure 1. The laboratory is located in Rickover Hall.

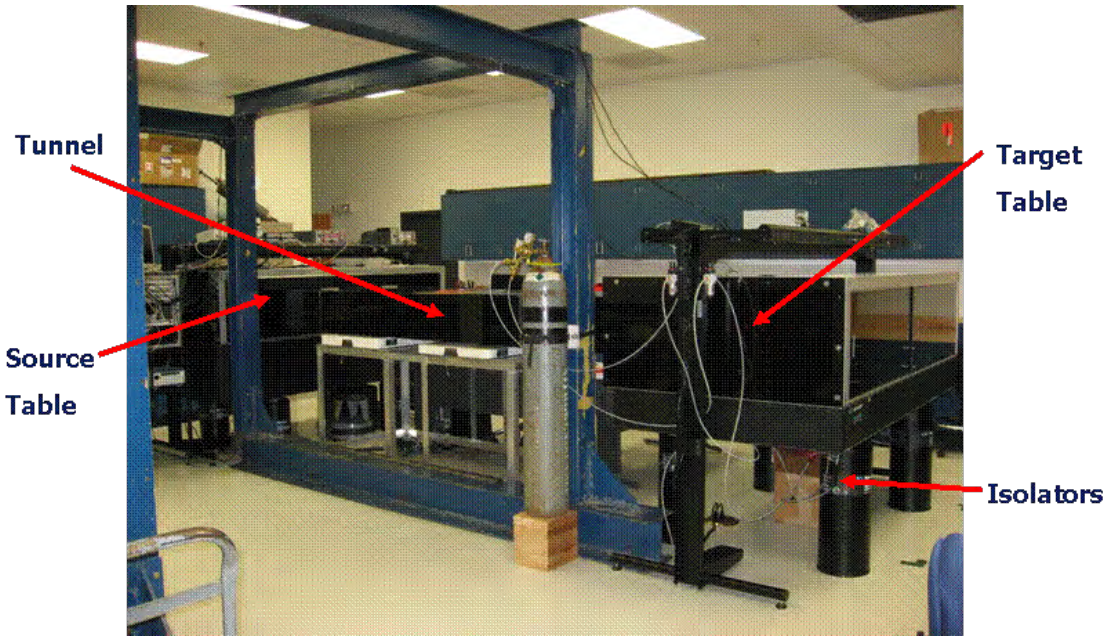

Figure 1. USNA Directed Energy Control Laboratory

The Newport Corporation's Fast Steering Mirrors (FSMs) are the heart of beam control system as they are used to rapidly and accurately direct the beam through the system. The FSM provides two-axis, high-bandwidth rotation with sub-microradian resolution by using four voice coil actuators. Used in push-pull pairs, the actuators provide smooth, even torque to the mirror. The FSM used for this experiment has a control bandwidth of 800 Hz. using a 2.54 cm (1 inch) mirror and is shown in Figure 2.

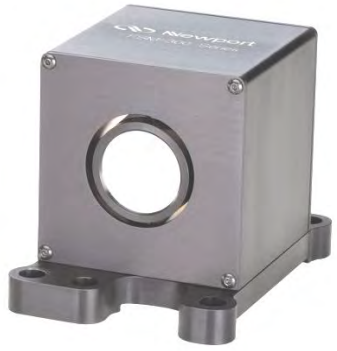

Figure 2. Newport FSM

A Newport research grade breadboard with constrained layer damping simulates the directed energy beam's source platform. This breadboard is a 91.44 by 91.44 by 5.08 cm (36 by 36 by 2 in) honeycombed breadboard constructed to eliminate torsional and bending modes below about 200 Hz. The mass is 71.3 kg.

Figure 3. Newport Breadboard

The breadboard is mounted on a Newport research grade optical table using four compression springs and four isolators. The stainless steel springs are approximately 3.8 cm long with an outer diameter of 2.8 cm and have a stiffness of 20 kN/m. Simulation of the vibrations that would be encountered on an aircraft will be accomplished by inertial actuators. The actuators are manufactured by CSA Engineering (SA-10) and have a rated force output of 10 lbf for frequencies up to 1,000 Hz. The actuators are configured such that one actuator is mounted vertically and imparts roll motion to the platform while the second actuator is mounted at a 45 degree angle to the vertical and imparts both pitch and yaw motion to the platform (see

Figure 4). The isolators are Newport SLM-1A air mounts and are pressurized to 275 kPa, resulting in a natural frequency of 3.5 Hz for the mount. The Newport optical table is a RS 4000 series that measures 1.2 m by 1.8 m by 45.7 cm (4 ft by 6 ft by 18 in) thick and is mounted on Newport I-2000 Pneumatic Isolators with Automatic Leveling.

To determine the position and orientation of the platform as well as the beam's position on target, On-Trak's Position Sensing Detectors (PSD) and mountings (designated a Position Sensing Module (PSM)), are driven by an On-Trak OT301 Position sensing amplifier. The combination is used to measure the movement of the main beam and positioning beams. The PSMs have a detection area of 10x10 mm and provide the position of the center of the laser beam in two dimensions. The minimum resolution of the PSM is approximately 0.5 micrometers when combined with the OT301 amplifier. The lasers used on the platform and for the main beam are 5 mW, 635 nm diode lasers, with an elliptical beam measuring 3.8 mm x 0.9 mm. The main beam is circularized by an anamorphic prism pair. Technical specifications and additional details for each laboratory component can be found in the Appendix.

The computer control system is based on MATLAB R2006b with SIMULINK from Mathworks, and the xPC Targetbox from SpeedGoat. The main computer for control implementation and experiment supervision is a Dell Precision 690 work station with a CPU speed of 3.8 GHz. The xPC Targetbox is an Intel Core 2 Duo running at 2.13GHz.

2.2 Experimental Method

This research project uses the configuration in Figure 4 and Figure 5 to calculate an error signal by determining the position and orientation in real time for the full beam control system. The configuration contains the platform, two inertial actuators mounted on the platform's surface, four PSMs, and the laser. Three position PSMs are on the platform, with a diode laser mounted next to them off the platform, to develop the position of three points on the surface. The PSMs will move with the platform and their associated diode laser will remain fixed on the optical table. The motion of the PSMs translates into an x-y laser position on each PSM's detection area. Assuming the positions of the PSMs do not change, the known distance between the position PSMs can be used to find the equation of the plane. The fourth PSM will be the target, approximately 5 meters away. It is recognized that this type of measurement system can

not be used on a mobile platform. However, if an error signal can be developed that is suitable for correcting the beam, the calculated beam error as a function of accuracy in the position and orientation may be known. The specifications for an on-board inertial measurement unit (IMU) may then be determined to accomplish the desired accuracy for the error signal.

In the experiment, the platform is disturbed by two inertial actuators using multiple frequencies along with random noise. The position of three points on the platform, in two dimensions, is measured using the position PSMs in a time step of 500 µsec as the platform is disturbed by the inertial actuator. These measurements are used to generate an algorithm to determine the position and orientation of the platform as a function of time. Knowing this motion and each reflective surface's orientation, the beam intercept point is then calculated and compared to the laser motion at the target.

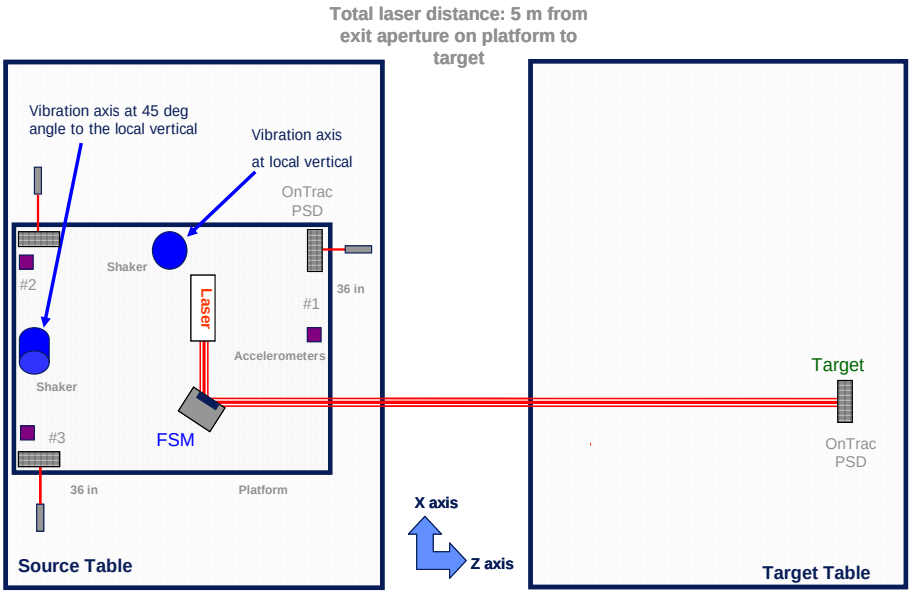

Figure 4. Experimental Configuration

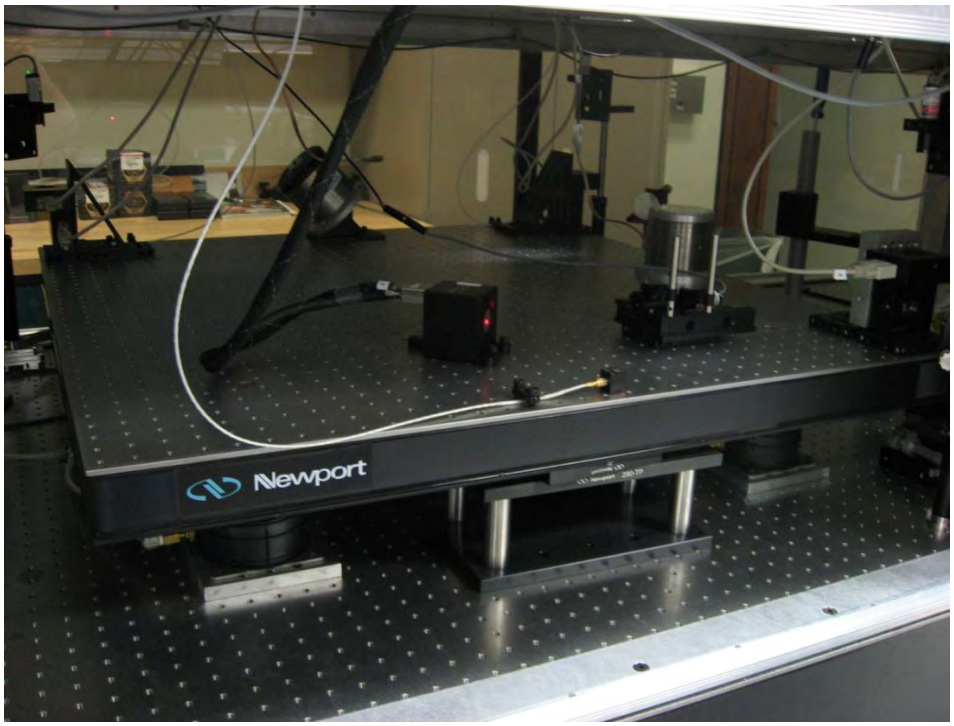

Figure 5. Experimental Configuration

2.3 Tunnel Isolation Effects on Jitter

The entire laboratory setup is enclosed by acrylic windows in an effort to mitigate possible atmospheric or acoustic disturbances. After the beam is reflected off of the FSM, it travels through a tunnel (

Figure 6) approximately 5 meters before it intercepts the target PSM. Figure 7 shows the effects of the tunnel on the beam's vertical position at the target. For this experiment, the platform was not disturbed and the FSM was held at a fixed position. This figure shows that the jitter is noticeably reduced, and the transverse motion of the platform due to acoustic and seismic disturbances within the laboratory is clearly seen. This setup will allow experimental verification that the platform induced jitter has been mitigated.

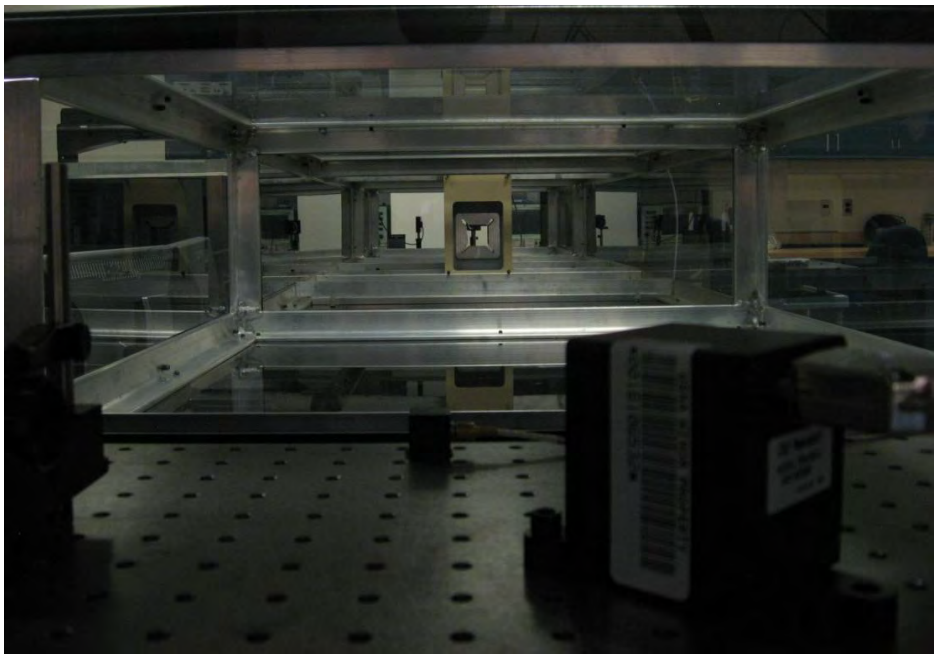

Figure 6. Tunnel

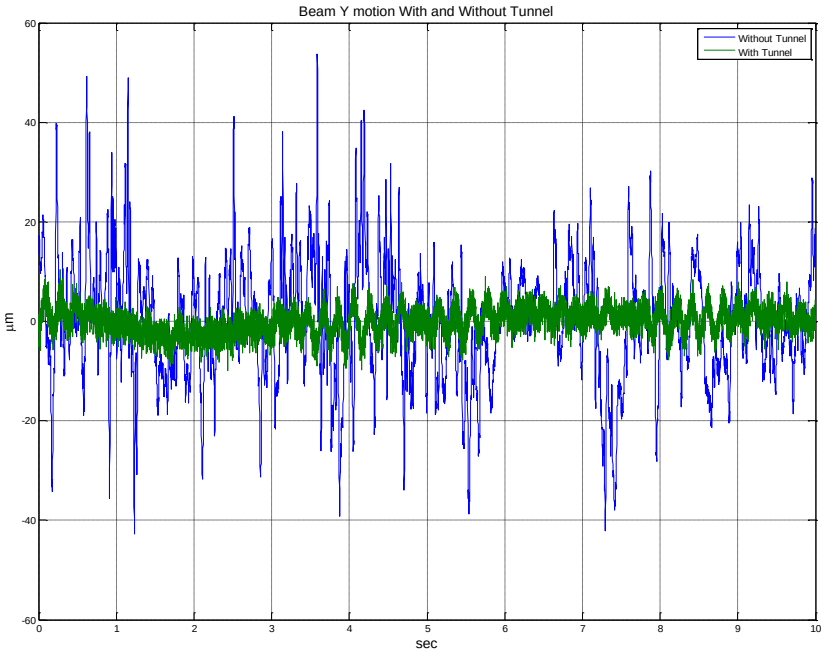

Figure 7. Tunnel Effects

3 Theory

3.1 Calculated Beam Position

To correct platform induced jitter, the error between the beam's actual impact and its intended impact point must be determined. This is normally accomplished by using feedback from the target. Obtaining feedback may be problematic in the expected environment. Therefore a feedforward control system is proposed to mitigate the jitter imposed by the platform. A feedforward system will require the beam's path to be predicted in real time. Applying rigid body kinematics for the platform and the laws of geometric optics to the optical control system provides the means of determining the position of the impact of the beam at the target based only on platform motion. Atmospheric effects may be corrected by other means such as deformable mirrors and probe beams. Assuming the platform on which the beam source and control mirrors are mounted is rigid, the position and orientation of the platform, and any point on it, can be determined, given accurate sensory input. The platform used in the experimental apparatus rests atop four springs which allows limited displacement and rotation in six degrees of freedom. From sensors, the position of the platform at three points can be measured and using these three points, the equation for the platform's surface can be determined. This equation is used to find the displacement and orientation of the composite bodies on the platform, specifically the starting location of the beam and the orientation of the reflective surfaces that controls the beam. From this information, the plane for each reflective surface is determined. Geometric optics are introduced to calculate where the beam will travel given the orientation of its source and the reflective surface that controls it. In addition to the orientation of the reflective surface on the platform, the mirrors can rotate about two axes to control the beam's direction. The rotation of the mirror is reported by the mirror's sensing system which provides the necessary information required to compute the normal vector to each reflective surface. The normal is then used to generate a reflection matrix, $\lfloor T_{ref} \rfloor$

$$\left[T_{refl}\right]=\begin{bmatrix}1-2n_1^2 & -2n_1n_2 & -2n_1n_3\\ -2n_1n_2 & 1-2n_2^2 & -2n_2n_3\\ -2n_1n_3 & -2n_2n_3 & 1-2n_3^2\end{bmatrix} \quad (1)$$

where n_i is the i^{th} component of the vector normal to the plane calculated from the mirror and platform position and orientation. The original direction of the beam, $\vec{r}$, is multiplied by this reflection matrix to determine the new direction of the beam, $\vec{r}'$

$$\vec{r}' = \left[T_{refl}\right]\vec{r} \quad (2)$$

This new direction, along with the starting point, $\bar{x}$, and distance to the next point, d, is used to determine the intercept point of the beam, $\bar{x}'$, on the next intercept plane:

$$\bar{x}' = \bar{x} + \vec{r}'d \quad (3)$$

d is calculated as

$$d = \frac{\det\begin{bmatrix}1 & 1 & 1 & 1\\ m_{1,1} & m_{2,1} & m_{3,1} & x_1\\ m_{1,2} & m_{2,2} & m_{3,2} & x_2\\ m_{1,3} & m_{2,3} & m_{3,3} & x_3\end{bmatrix}}{\det\begin{bmatrix}1 & 1 & 1 & 0\\ m_{1,1} & m_{2,1} & m_{3,1} & r_1\\ m_{1,2} & m_{2,2} & m_{3,2} & r_2\\ m_{1,3} & m_{2,3} & m_{3,3} & r_3\end{bmatrix}} \quad (4)$$

where the $m_{i,j}$ are the i^{th} component of the j^{th} coordinate on the intercept plane. Three arbitrary points on the intercept plane (the $m_{i,j}$) are required to find the intercept point. The intercept point and the beam direction from the last reflective surface on the platform are determined in the

platform coordinate system. To find the point in the target's coordinate system, the last reflective surface's intercept point and beam direction are multiplied by a rotation matrix, $[T_{rot}]$

$$[T_{rot}] = \begin{bmatrix} \mathrm{c}(\Delta y)\mathrm{c}(\Delta z) & \mathrm{c}(\Delta y)\mathrm{s}(\Delta z) & -\mathrm{s}(\Delta y) \\ \mathrm{s}(\Delta x)\mathrm{s}(\Delta y)\mathrm{c}(\Delta z) - \mathrm{c}(\Delta x)\mathrm{s}(\Delta z) & \mathrm{s}(\Delta x)\mathrm{s}(\Delta y)\mathrm{s}(\Delta z) + \mathrm{c}(\Delta x)\mathrm{c}(\Delta z) & \mathrm{s}(\Delta x)\mathrm{c}(\Delta y) \\ \mathrm{c}(\Delta x)\mathrm{s}(\Delta y)\mathrm{c}(\Delta z) + \mathrm{s}(\Delta x)\mathrm{c}(\Delta z) & \mathrm{c}(\Delta x)\mathrm{s}(\Delta y)\mathrm{s}(\Delta z) - \mathrm{s}(\Delta x)\mathrm{c}(\Delta z) & \mathrm{c}(\Delta x)\mathrm{c}(\Delta y) \end{bmatrix} \quad (5)$$

The *c* and *s* signify cosine and sine of the angle respectively. The angle is the rotation about the pitch (Δx), roll (Δz) and yaw (Δy) axis, with the roll axis being the axis in the direction of the target. The position and the beam direction in the target frame of reference is then found by

$$\bar{x}_I = [T_{rot}]\bar{x}_P \quad (6)$$

$$\bar{r}_I = [T_{rot}]\bar{r}_P \quad (7)$$

The subscript *I* indicates the target frame of reference coordinate system (inertial coordinate system in the case of the laboratory setup). The values of the intercept point *on* the last plane and the direction *from* the last plane must be in the target frame of reference and used in the calculation of *d* for the distance to the target in equation(4).

For the case of multiple mirrors, if the intercept point is another reflective surface, this process is repeated using the next mirrors orientation, the intercept point on the previous mirror, the beam direction after reflection and the distance *d* as calculated by equation(4). For multiple reflective surfaces, the following algorithm may be used:

$$\bar{x}_I = [T_{rot}]\left\{ {}^{o}x_P + \sum_{i=0}\left(\prod_{j=0} [T_{ref}] \right) {}^{o}r_P{}^{i+1} d \right\} \quad (8)$$

where k is the number of reflective surfaces, ${}^{0}[T_{refl}] = [I]$ (identity matrix), ${}^{k}d$ is in the target's frame of reference, and ${}^{j}[T_{refl}]$ is the reflection matrix for the j^{th} mirror. If this intercept point is the target, then the impact position is theoretically known and the error can be determined. This error can then be used in a feedforward compensation technique using adaptive filters to predict the beam's position

3.2 Proportional-Integral Control

A proportional-integral (PI) controller is used to correct for the platform induced jitter using both target feedback and the calculated feedforward signal. Proportional-integral-derivative (PID) controllers are very common in industry and can easily be adjusted on-site. In addition, PID controllers are very common because of their general applicability to most control systems and because it is not necessary to know the mathematical model of the plant being controlled. In this research, the derivative term, which is usually included in the traditional PID controller, is not used since derivative action is very sensitive to measurement noise. The PI controller calculates an error value as the difference between a measured process variable and a desired set-point. The controller attempts to minimize the error by adjusting the process control inputs. The proportional value determines the reaction to the current error and the integral value determines the reaction based on the sum of recent errors.[10] The block diagram for the PI controller with the calculated feedforward signal is shown below in Figure 8. P denotes the primary plant transfer function which the disturbance must pass through before the output, and S denotes the secondary plant or actuator transfer function the control signal must pass through before the summing junction.

---

[10] Ogata, K., *Modern Control Engineering,* 4th ed, Prentice Hall, Upper Saddle River, NJ, 2002.

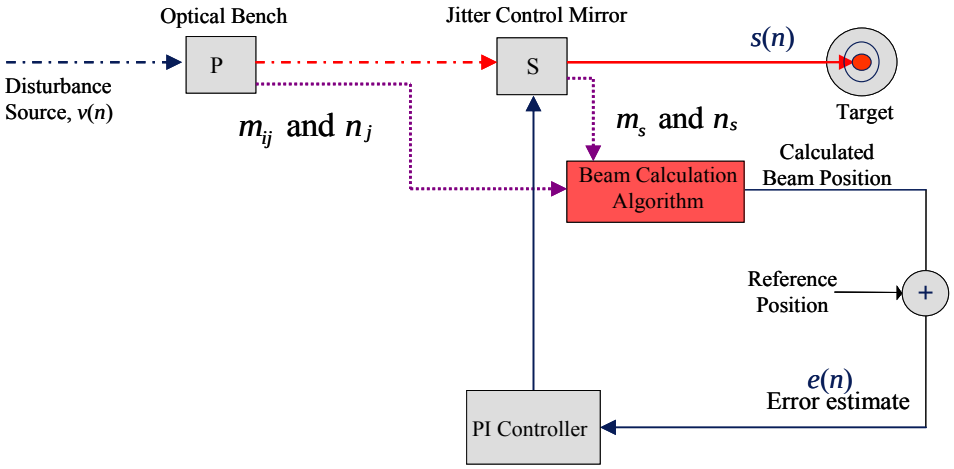

Figure 8. PI Controller Block Diagram

To determine the optimal gains for the PI controller, the Ziegler-Nichols method is used to tune the controller. The integral gain, K_i, is first set to zero and the proportional gain, K_p, is increased until it reaches the ultimate gain, K_u, at which the output of the loop starts to oscillate. The ultimate gain and the oscillation period, P_u, are used to set the PI gains as follows:[11]

$$K_p = 0.45K_u \qquad (9)$$

$$K_i = P_u / 1.2 \qquad (10)$$

As previously discussed, the FSM can rotate about its local x and y axes. As such, gains are needed for the both axes, thus each axis is tuned independently of the other. The gains are determined by giving the FSM a step input. The proportional gain is increased until the mirror goes unstable. Figure 9 shows the position of the mirror (in mV) in response to the step input right before the critical gain was reached. The mirror goes to the commanded step position and does not oscillate. Figure 10 shows the position of the mirror at the critical gain as can be seen by the oscillations. The ultimate gains, ultimate period, and PI gains are listed in Table 1.

[11] Ogata, K., *Modern Control Engineering,* 4th ed, Prentice Hall, Upper Saddle River, NJ, 2002, p. 685

Table 1. PI Controller Gains

	x axis	y axis
K_u	0.0532	0.0705
P_u	0.002 sec	0.002 sec
K_p	0.0239	0.0317
K_i	0.0017	0.0017

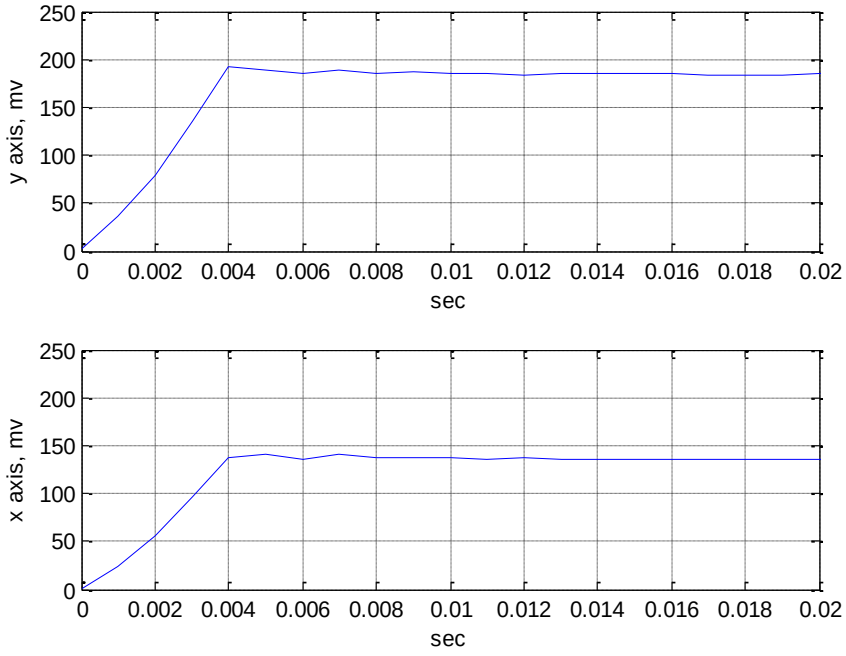

Figure 9. Mirror Position before Critical Gains

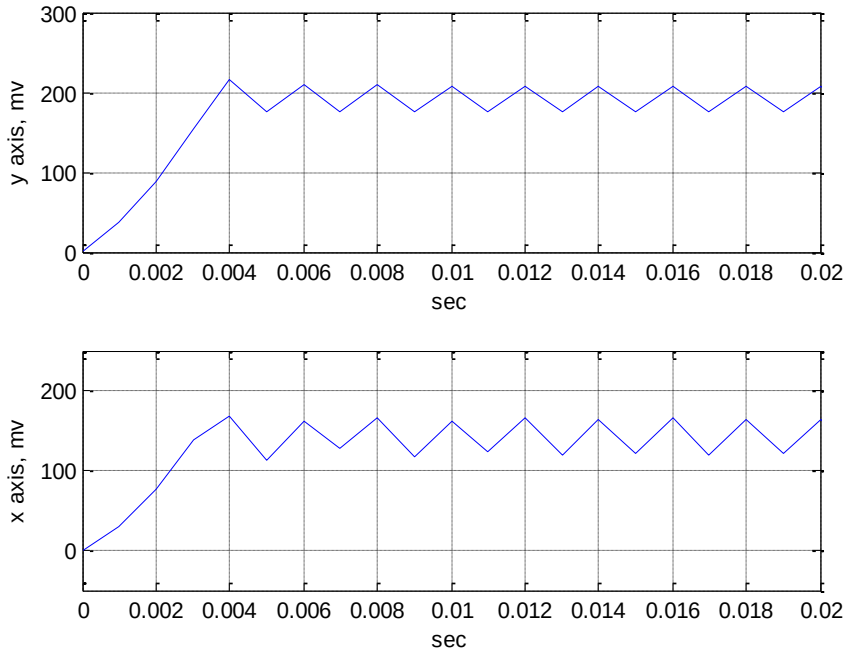

Figure 10. Mirror Position at Critical Gains

3.3 Least Mean Squares Control

The Least Mean Squares (LMS) algorithm is one of the simplest yet robust adaptive algorithms. In the LMS algorithm, the tap gains (w_M in Figure 11) are adjusted based on the response of the system to the error, a reference signal correlated with the disturbance, and the control input. The algorithm uses the method of Least Squares to find the optimum values for the tap gains. In particular, the algorithm relies on predicting its next input, which is simply the disturbance to the beam in the case of laser jitter control, to optimize the tap gains. The error, the difference between the predicted signal and the system output, is then used to recalculate the gains that minimize the error in return. For the experimental Testbed, the feedback or feedforward signal is used to provide the error signal, and the accelerometers or PSMs provide the correlated disturbance input signal.[12] This type of control algorithm not only calculates the necessary gains, but also identifies the system, simplifying the requirement to mathematically

[12] Watkins, R. and Agrawal, B., "*Use of Least Means Squares Filter in the Control of Optical Beam Jitter*", Journal of Guidance, Control and Dynamics, Vol. 30, No. 4, July-August 2007

model the system. The predictor in this LMS algorithm can be described as a transversal or ladder filter, as shown in Figure 11.

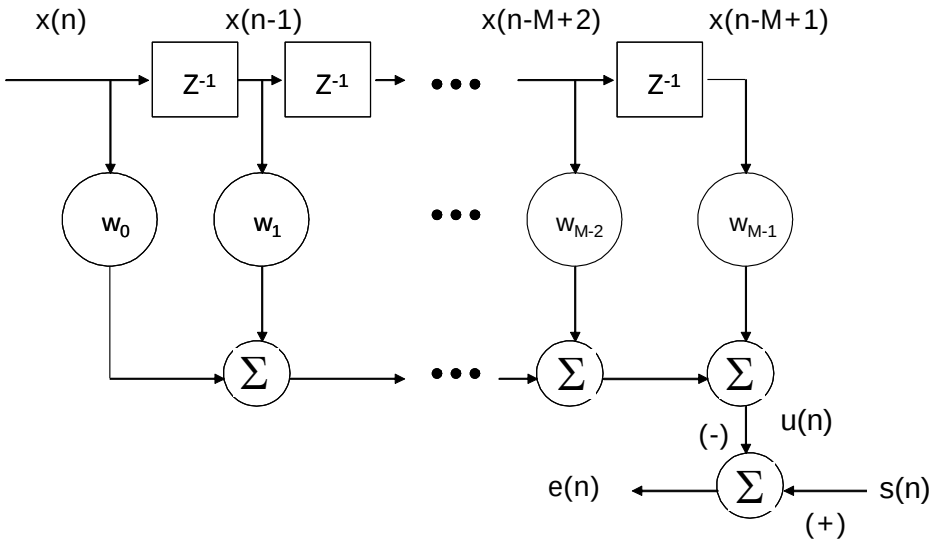

Figure 11. Filter for LMS Algorithm

The reference signal, $x(n)$, is delayed one time step for each of the M stages, with the exception of the current input, forming a vector of delayed inputs, $[x(n), x(n-1), \ldots, x(n-M+1)]^T$. The inner product of the vector of tap gains, $\bar{w}(n)$, and the vector of delayed inputs, $\bar{x}(n)$, produces the scalar control input, $u(n)$, to the FSM.

$$u(n) = \bar{w}^T(n)\bar{x}(n) \qquad (8)$$

The desired output, *s(n)*, is that FSM motion which results in the cancellation of any perturbation in the laser beam caused by the supporting structure and equipment vibration (the disturbance or *d(n)*, see figure below). The error is the difference between the target center and the laser beam's actual position at the target.

$$e(n) = d(n) - s(n) \qquad (9)$$

The tap gains are adjusted by means of the update equation developed by Widrow.[13] μ is the adaptation step size that controls the stability of the algorithm.

$$\bar{w}(n+1) = \bar{w}(n) + \mu \bar{x}(n) e(n) \qquad (10)$$

The block diagram of the algorithm in a form for implementation in the beam control system is shown in Figure 12 below. Again, P denotes the primary plant transfer function which the disturbance must pass through before the output, and S denotes the secondary plant or actuator transfer function the control signal must pass through before the summing junction. P includes the transfer function of the structure of the bench and mirrors for the case of vibration of the bench, the transfer function of the sensors, as well as the gain effect caused by the distance the light beam travels through the system to the target. S must include the effect of vibration to the control mirror, the transfer function of the mirror and sensors, and the delays inherent in the digital signal processing and the computation of the control signal.

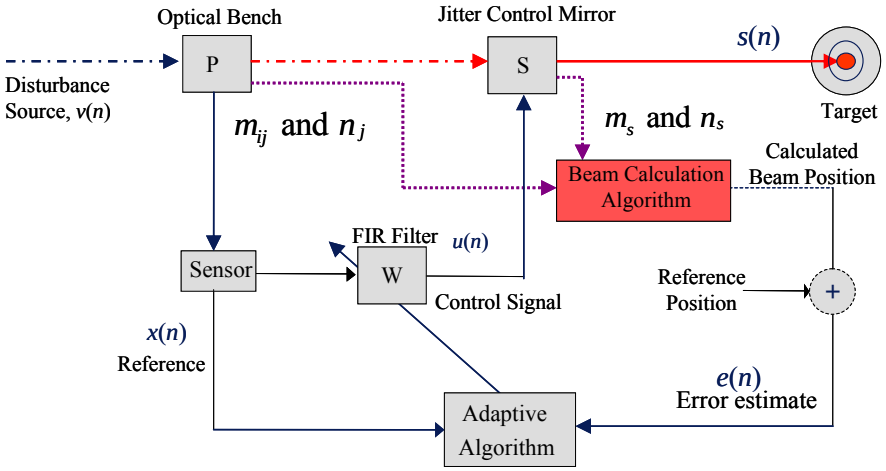

Figure 12. LMS block diagram

[13] Widrow, B., *Adaptive Signal Processing*, 1st Ed., Prentice-Hall, Upper Saddle River, NJ, 1985

3.4 SIMULINK Model

The Directed Energy Beam Control Laboratory is operated using a SIMULINK model built in MATLAB which is shown below in Figure 13. The model contains several blocks which perform all the operations necessary to running the laboratory. The first block (light green) inputs the PSM and FSM data. The second block (first pink block) is the beam calculation algorithm which includes all the calculations previously discussed that are required to compute the beam's position at the target. It uses the input data, performs the calculations, and outputs the beam's position at the target. The next blocks (blue and pink) are the controllers, one for the PI controller and another for the LMS controller. These controllers use either target feedback or the calculated feedforward signal to determine a command for the FSM that will correct for the platform induced jitter. The final block (last blue) is for the outputs of the model. It sends commands for the inertial actuators and the FSM to the experiment. The maximum execution time for one cycle was determined to be approximately 40 μsec. The time step used in the experiments was 500 μsec which means that the system is taking in data, performing the calculations, and outputting commands all within the experimental time step. Thus, the calculated feedforward signal can be thought of as a real-time signal, the same as the target feedback signal.

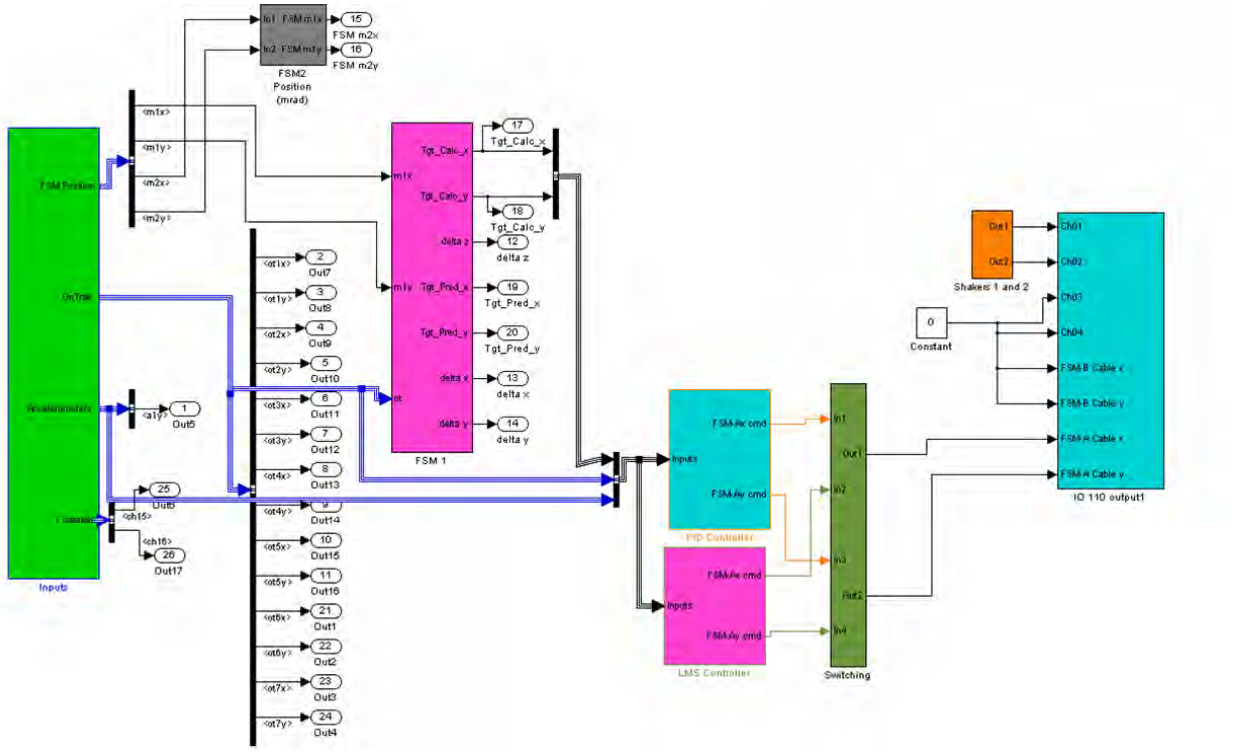

Figure 13. SIMULINK Model Block Diagram

Each of the blocks depicted in Figure 13 contains multiple sub-blocks that contain the necessary calculations for running the laboratory. Several of the sub-blocks are discussed below while the additional sub-blocks can be found in the Appendix.

Figure 14 contains the sub-blocks of the beam calculation algorithm. The first block (pink) contains the rotation matrix which inputs the PSM data and calculates the platform's rotations about the x, y, and z axis. The FSM block (gray) inputs the FSM position in volts and converts it to an angle in radians that can be used in future calculations. The green block is the heart of beam calculation algorithm. It inputs the platform rotations and FSM position and calculates the beam's position at the target. It contains the necessary normal calculations and the reflection matrix.

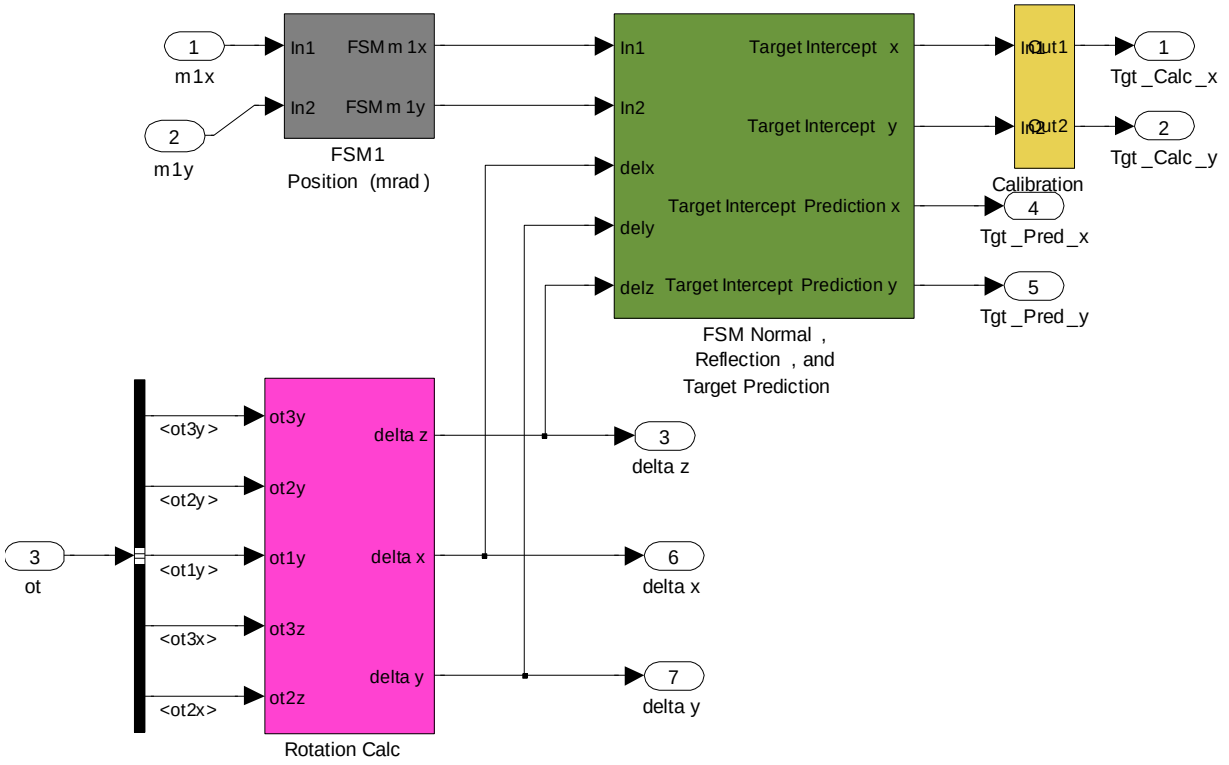

Figure 14. Beam Calculation Sub-Blocks

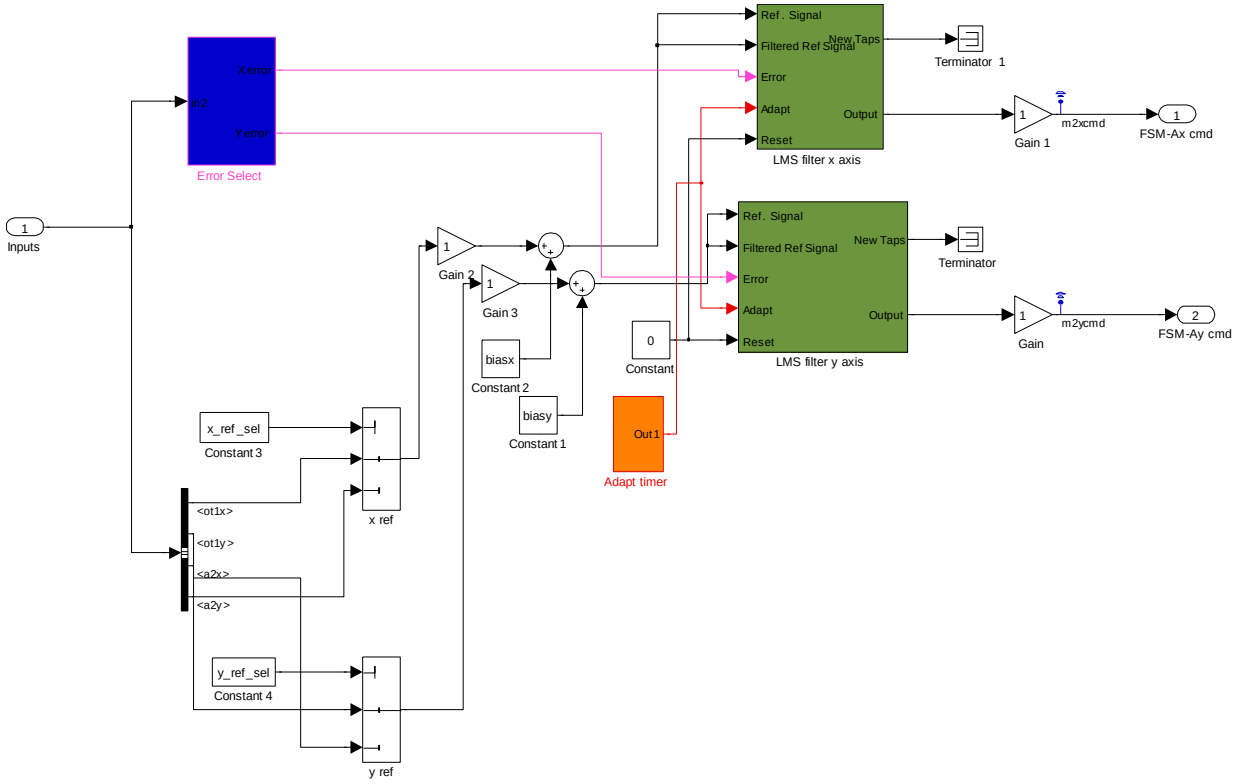

Figure 16 below are the block diagrams of the PI and LMS controllers respectively. As previously mentioned, both controllers can use either the feedback or feedforward signal to determine necessary FSM command to correct for platform induced jitter. The controllers can also be turned off in order to run experiments with no control.

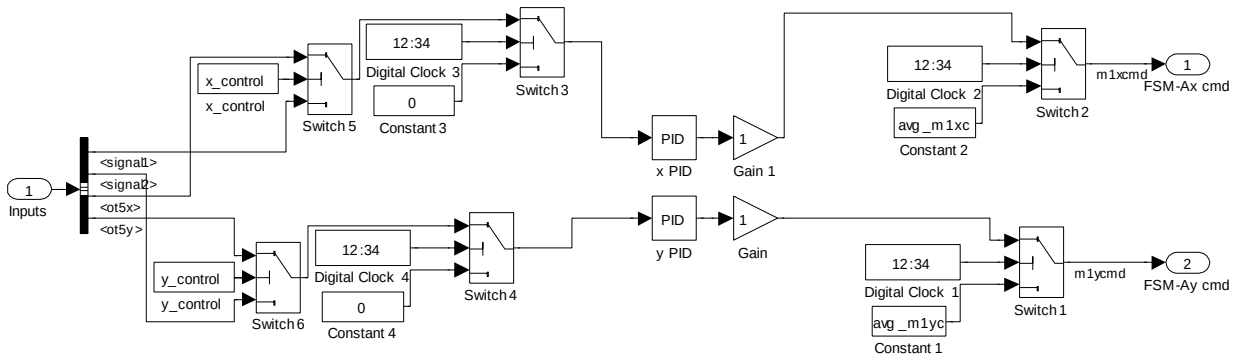

Figure 15. PI Controller

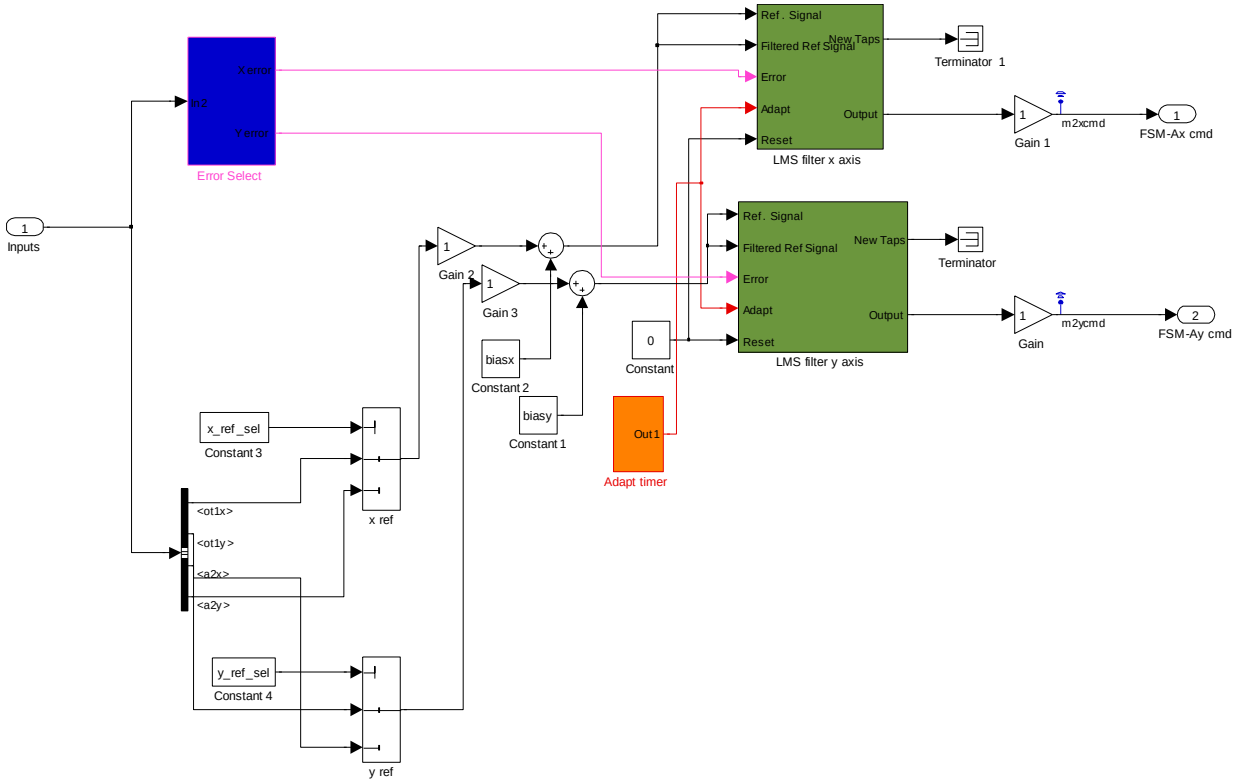

Figure 16. LMS Controller

4 Experimental Results

4.1 Platform Motion

The experiments were conducted using two inertial actuators which imparted a complex pitch, roll, and yaw motion to the platform. The first inertial actuator is mounted at a 45 degree angle to the horizontal axis of the platform and is located along the back edge of the platform in the center. The second inertial actuator is mounted vertically on the left side of the platform. The first case investigated used only the first inertial actuator disturbing the platform at 17 Hz. The platform motion for this first case is shown below in Figure 17. The second case used both inertial actuators disturbing the platform with the following frequencies: 10, 13, 17, 23, 27, 41, and 45 Hz. The platform motion for this second case is shown below in Figure 18. The rotations of the platform about the pitch, roll, and yaw axis are given in µrad.

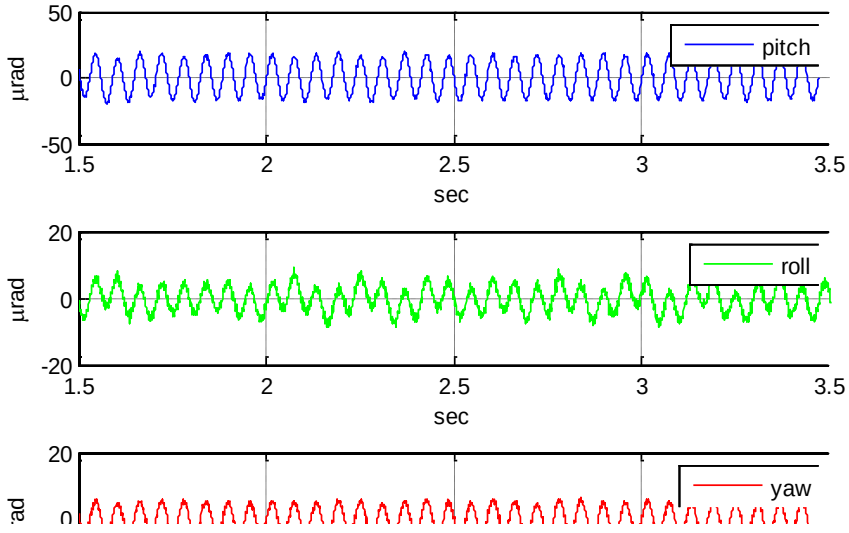

Figure 17. Platform Motion for 17 Hz Disturbance

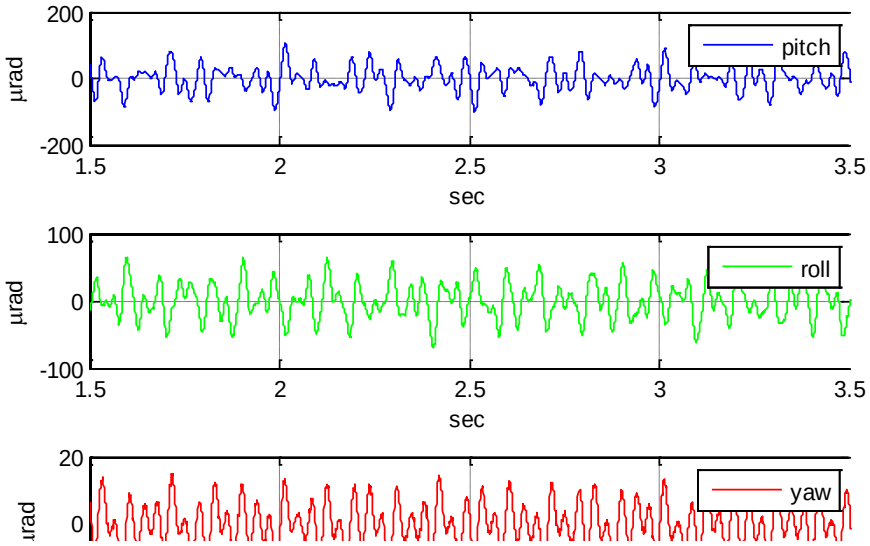

Figure 18. Platform Motion for Multiple Frequency Disturbances

4.2 Spectral Analysis of System with No Control and Residual Jitter

A spectral analysis is performed for each experimental run in this investigation. The spectral analysis depicts the frequencies that are present in the system. Before the platform is disturbed, a spectral analysis is done for the system at rest. The spectral analysis done in this investigation was performed by calculating the power spectral density of the signal using Welch's averaged modified periodogram method of spectral estimation, a window size of 8192 with no overlap, and 30 seconds of signal sampled at 0.001 seconds. In Figure 19, the spectral analysis of a representative accelerometer (accelerometer 2 in these cases) is shown on the top graph, and the spectral analysis of the position of the beam at the target is shown on the bottom graph (Figure 21 and Figure 22 in like manner). As can be seen in Figure 19, even when the platform is not being disturbed by the inertial actuators, there is still motion in the system at 5 Hz and 14 Hz. These frequencies correspond to two rigid body modes of the platform spring and isolator system which is excited by energy in the laboratory that can result from seismic or acoustic disturbances, with 5 Hz being the first transverse (vertical) mode, and 14 Hz

corresponding to the first rotational mode (about the pitch axis). The accelerometer (and to some extent the PSMs) shows instrument noise at 60 Hz.

In addition to this motion, there is residual jitter in the diode laser used for the main beam. By using a high pass filter, the effect of the platform motion is removed and the jitter in the laser can be determined. Figure 20 shows this beam motion at the target. This residual jitter is not included in the control analysis since it cannot be corrected. The standard deviation of the filtered residual jitter was calculated to be 0.525 μrad.

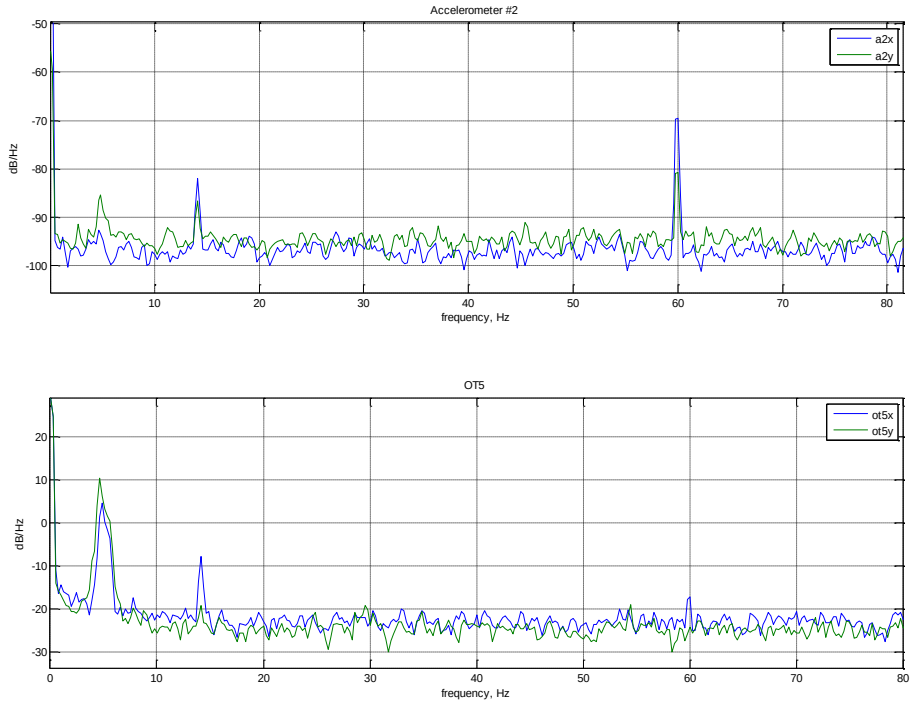

Figure 19. Spectral Analysis, No Disturbance, No Control

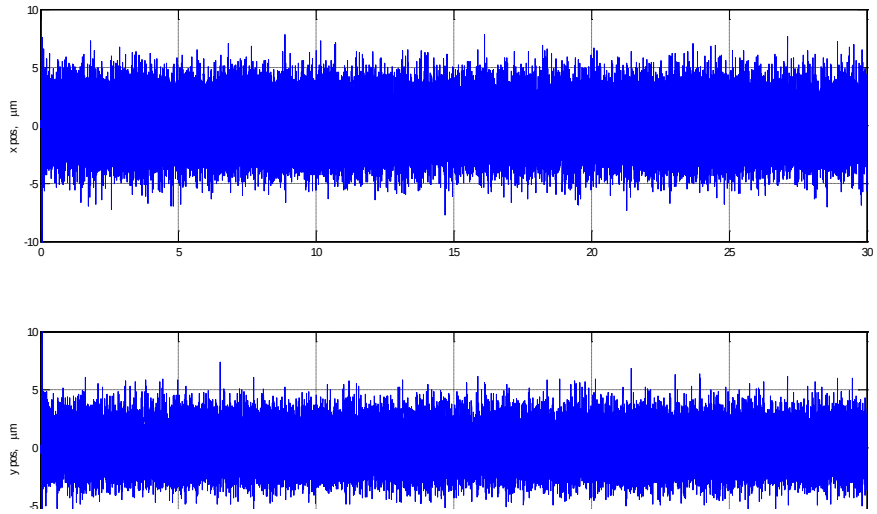

Figure 20. Filtered System Residual Jitter

Figure 21 and Figure 22 show the power spectral density for the system for both the 17 Hz and multiple frequency disturbance cases. Figure 21 shows frequencies at 5 Hz (the first transverse mode), 17 Hz (the disturbance), and 34 Hz (the first harmonic of the disturbance). Figure 22 shows frequencies at 5 Hz (again, the first transverse mode), at each disturbance frequency, and several harmonics of the disturbance frequencies. These spectral analysis plots confirm that the commanded disturbance frequencies are indeed present in the system as well as the rigid body modes of the platform excited by the disturbance input. Both the x and y directions in the platform coordinate system for accelerometer 2 and the horizontal (x) and vertical (y) directions at the target are shown in this and the following analysis figures.

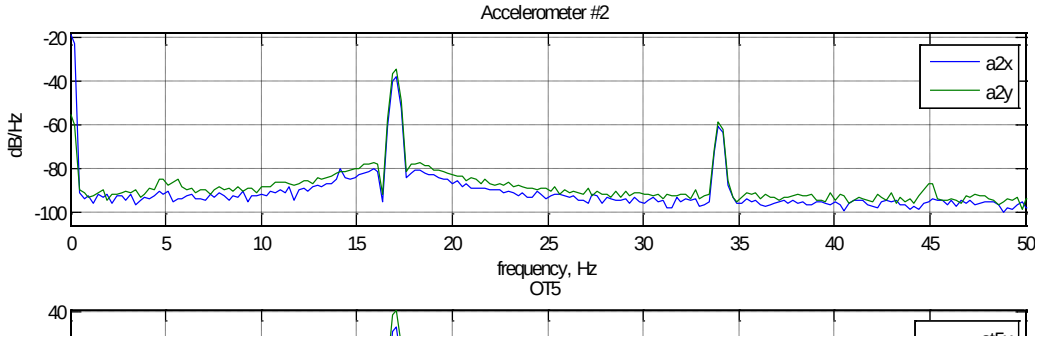

Figure 21. Spectral Analysis, 17 Hz Disturbance, No Control

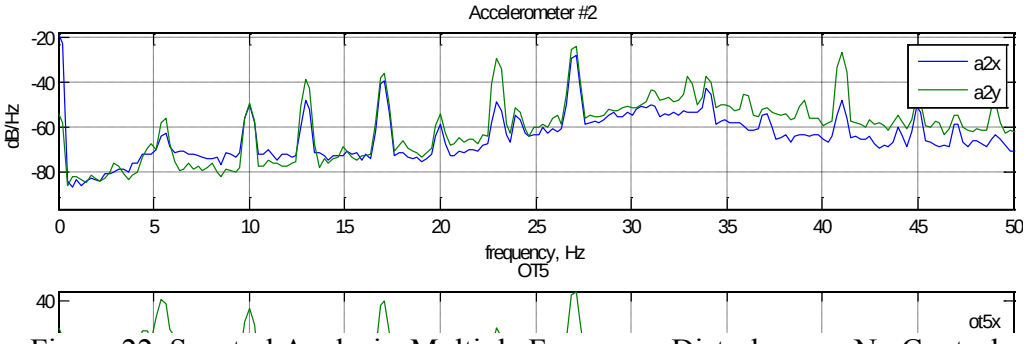

Figure 22. Spectral Analysis, Multiple Frequency Disturbances, No Control

4.3 Beam Calculation Results

As previously discussed, the primary objective of this research project was to calculate the position of the beam at the target using only the position and orientation of the platform and the FSM. Ideally, this calculated position would be the feedforward signal that could be used instead of target feedback for use with the PI and LMS controllers. Figure 23 and Figure 24

depict the actual position of the beam at the target in blue (feedback) and the calculated beam position at the target in green (feedforward) for the 17 Hz and multiple frequency disturbance cases respectively. As can be seen, the signals match very closely thus validating the feedforward calculated signal. The position of the beam at the target is given in µm.

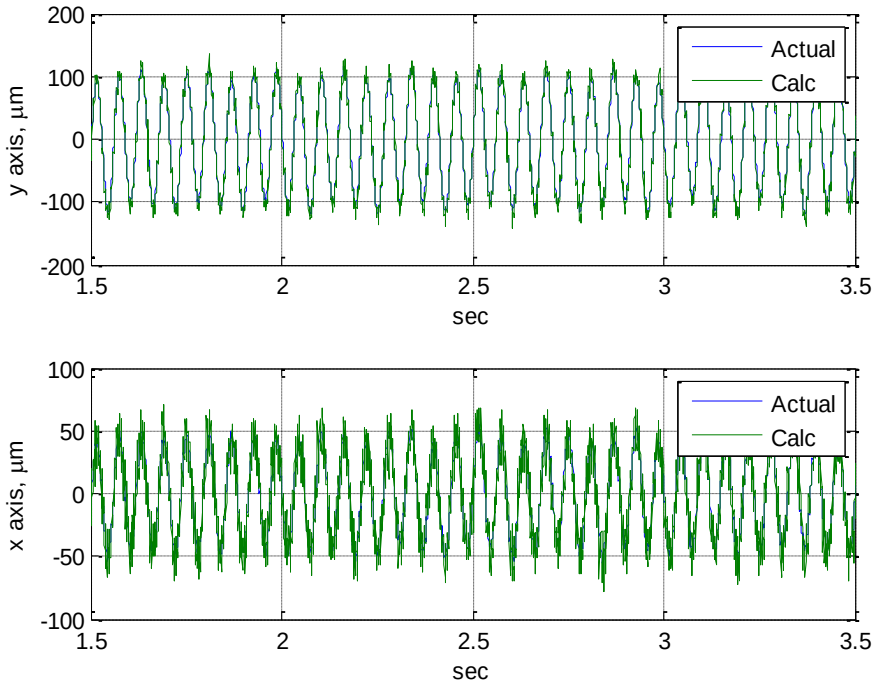

Figure 23. Actual vs. Calculated Beam Position at Target for 17 Hz Disturbance

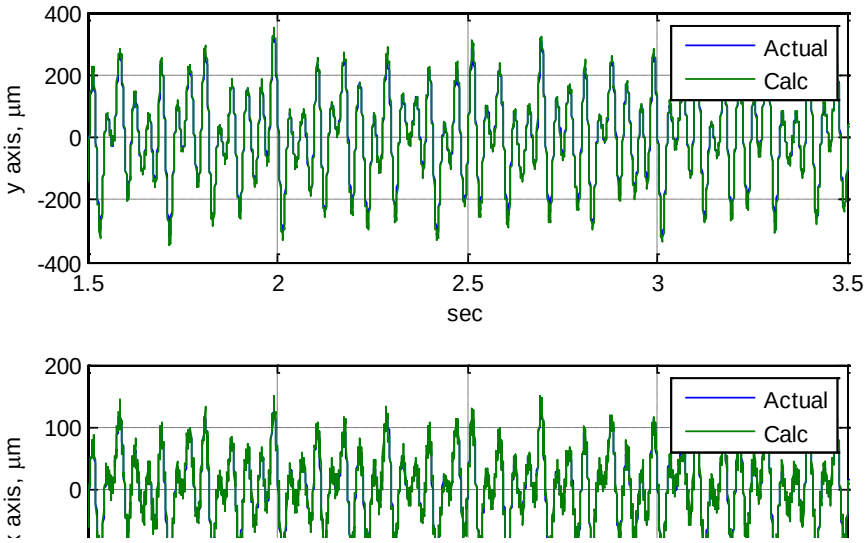

Figure 24. Actual vs. Calculated Beam Position at Target for Multiple Frequency Disturbances

While the actual and calculated beam positions appear very close in Figure 24, even the smallest error in the feedforward signal will adversely affect the ability to correct for the actual jitter in the system. Thus, a closer analysis is necessary. The jitter angle at the target with no control was determined for the feedback and feedforward signals. The feedforward signal was then subtracted from the feedback signal to determine the error in the feedforward signal. A 50 msec moving average of the error was calculated and plotted in Figure 25 and Figure 26. For the 17 Hz disturbance, the root mean squared (RMS) error of the feedforward signal prior to applying the moving average was 1.64 µrad. The 50 msec moving average error was less than 0.5 µrad for the entire run indicating the overall accuracy of the feedforward signal. For the multiple frequency disturbances, the root mean squared (RMS) error of the feedforward signal prior to applying the moving average was 1.88 µrad. The 50 msec moving average error was only greater than 1 µrad for 0.50 msec out of a 3.0 sec run indicating the overall accuracy of the feedforward signal.

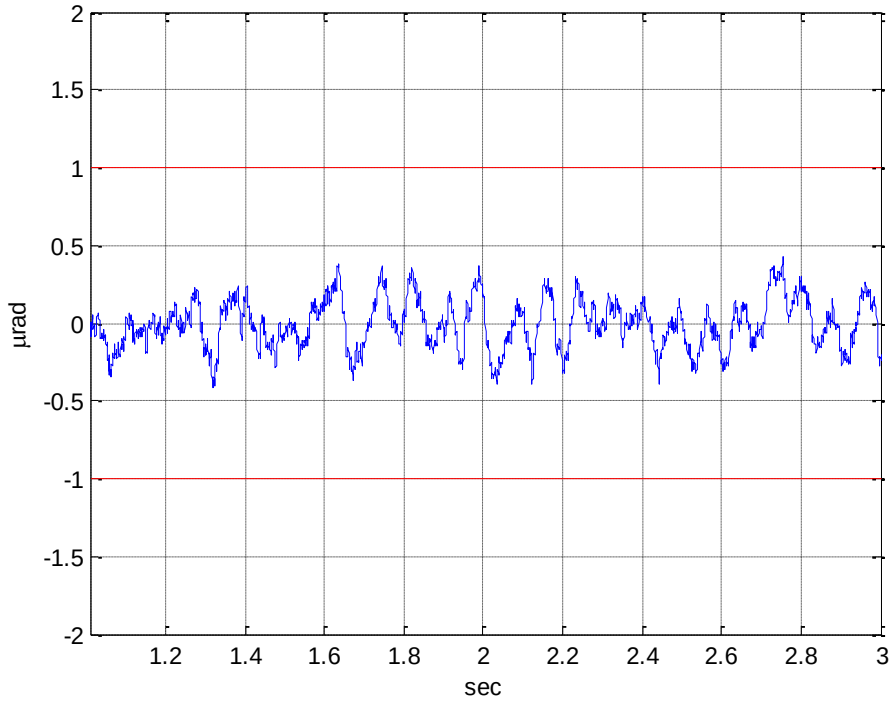

Figure 25. 50 msec Moving Average of Error between Actual and Calculated Jitter Angle at Target for 17 Hz Disturbance

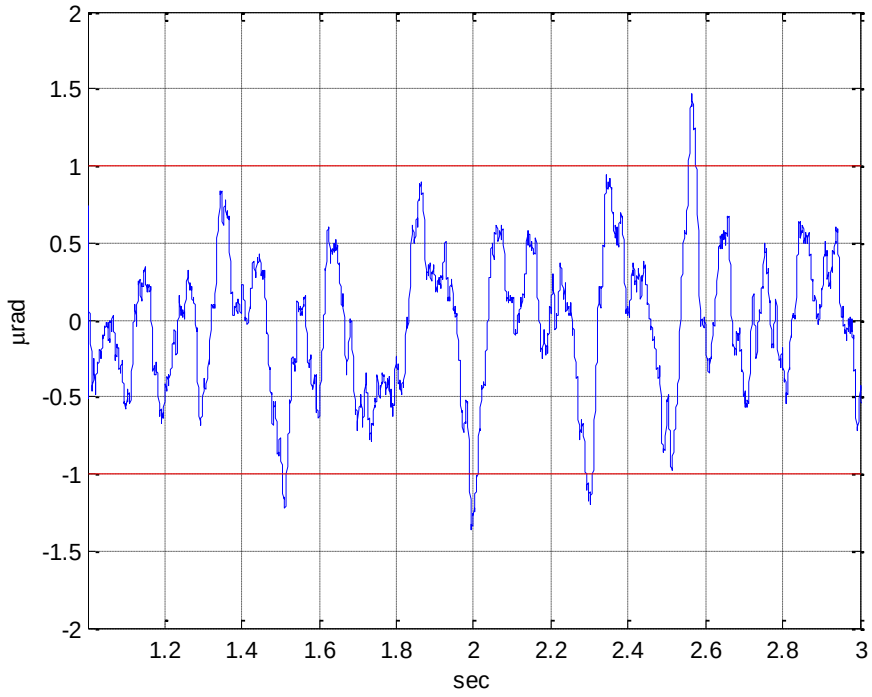

Figure 26. 50 msec Moving Average of Error between Actual and Calculated Jitter Angle at Target for Multiple Frequency Disturbances

4.4 Experiment Description

Eight experimental runs were conducted to investigate the mitigation of platform induced jitter using PI and LMS controllers. For each controller, both the 17 Hz frequency disturbance and the multiple frequency disturbances cases were investigated. Each case was investigated by first employing the feedback signal and then using the calculated feedforward signal. The runs lasted five seconds each. The platform was disturbed for 2 seconds while the mirror was held in a fixed position allowing the calculation and depiction of the jitter without control. The controller was then turned on and allowed to run for the remaining 3 seconds. The position of the beam at the target was recorded and then the jitter angle was calculated and plotted in the figures below. For the plots below, the red line represents no control, the blue line represents control using target feedback, and the green line represents control using feedforward.

4.5 PI and LMS Control Experimental Results

Experimental results for the mitigation of platform induced jitter using a PI or LMS controller are shown in the eight figures below. Figure 27 and Figure 29 depict the jitter angle at the target for the 17 Hz disturbance using both feedback and feedforward. As can be seen, the feedforward is not as effective in compensating for the platform motion.

The power spectral density in Figure 28 and Figure 30 shows the significant frequencies in the system. The peaks at 5 and 14 Hz are the rigid body modes of the platform as previously discussed. The peak at 5 Hz in the feedforward case is due to the fact that the prediction algorithm does not include the slight transverse motion that was expected in the experiment. As the 14 Hz peak (corresponding to rotation about the pitch axis) is much more evident in the feedforward case than in the feedback case, it is believed that this part of the beam calculation algorithm may have some error associated with it. The 17 Hz peak is the disturbance frequency and 34 Hz is the first harmonic of the disturbance. These 4 frequencies are present in all 3 cases (no control, feedforward and feedback). However, there are also frequencies present in the feedforward case at 33, 35, and 60 Hz that are not present in either of the other 2 cases. The 60 Hz is most likely a result of sensor noise, amplified by the beam calculation algorithm, but the source of the other 2 frequencies is unknown. In addition, the feedforward case has added energy at the higher frequencies while the feedback case is at a lower level (as compared to the no control case). These unknown frequencies and higher energy level indicate why the feedforward control is not quite as effective as feedback control.

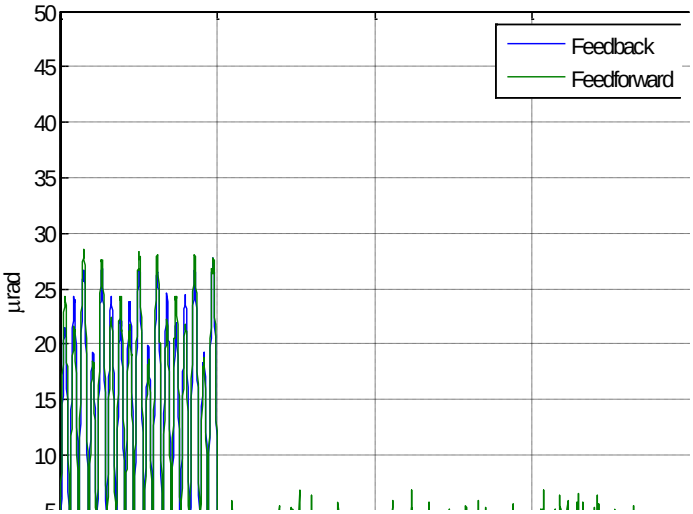

Figure 27. PI Jitter Control for 17 Hz Disturbance

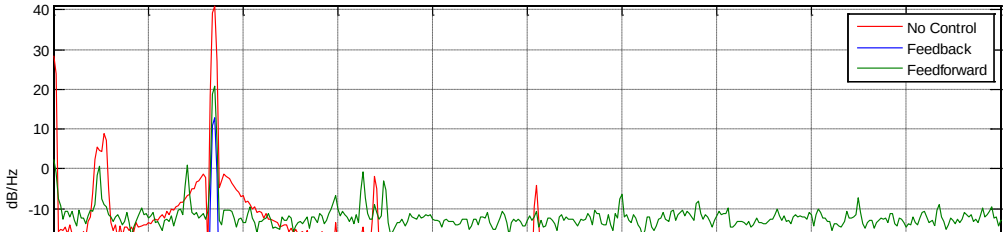

Figure 28. PI Spectral Analysis for 17 Hz Disturbance

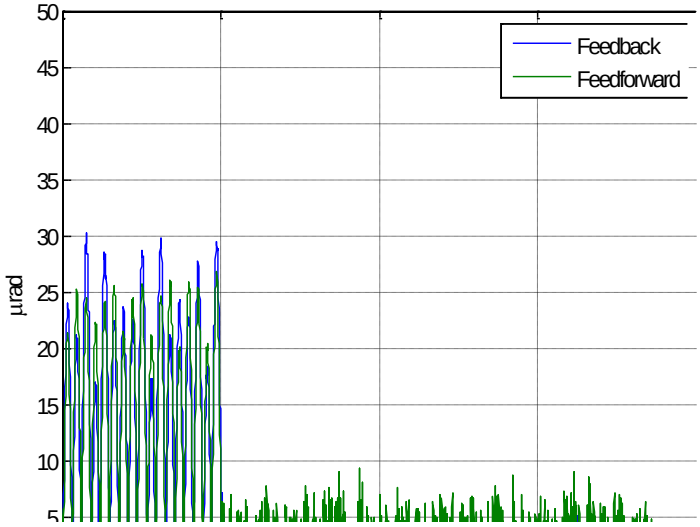

Figure 29. LMS Jitter Control for 17 Hz Disturbance

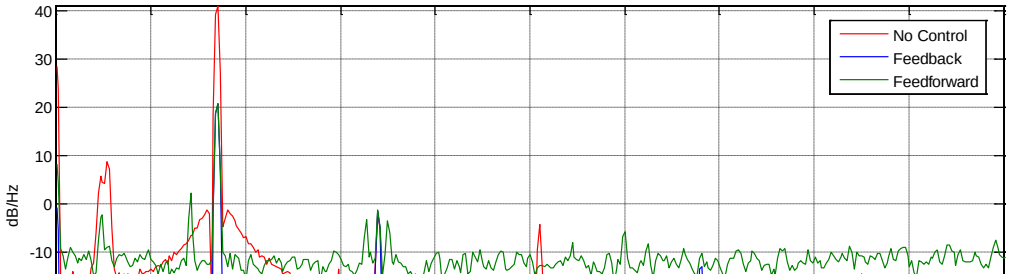

Figure 30. LMS Spectral Analysis for 17 Hz Disturbance

Below, Figure 31 and Figure 33 depict the jitter angle at the target for the multiple frequency disturbances using both feedback and feedforward control. In comparison to the single frequency case, the amount of jitter present in the system under control has increased as

would be expected for a higher overall disturbance level. It is noted, however, for multiple disturbances the magnitude response for the feedforward and feedback cases align more closely.

The power spectral density in Figure 32 and Figure 34 show the significant frequencies in the system. The frequency components at 5 and 14 Hz are the rigid body modes of the platform as previously discussed. Most of the remaining peaks are the 7 disturbances and their harmonics. However, there are also frequencies present in all three cases around 60 and 70 Hz that are not disturbance frequency harmonics. 60 Hz is most likely sensor noise, again amplified by the beam calculation algorithm but the source of the other frequencies is unknown. Lastly, the broad peak at around 31 Hz results from the resonance of the two actuators. Because of these unknown frequencies and the more complex motion, the remaining jitter in the system is about twice as much as what was recorded in the single frequency disturbance case. However, since the overall energy level of the disturbance is greater, the feedback and feedforward spectral results are much more closely aligned. In other words, while the errors in the feedforward calculation show up in the single frequency disturbance case, they are masked by the magnitude of the combination of multiple frequencies and harmonics in the multiple frequency case.

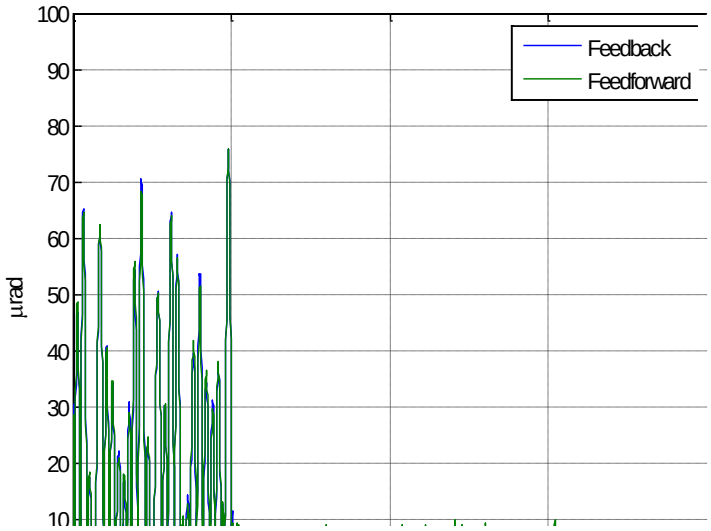

Figure 31. PI Jitter Control for Multiple Frequency Disturbances

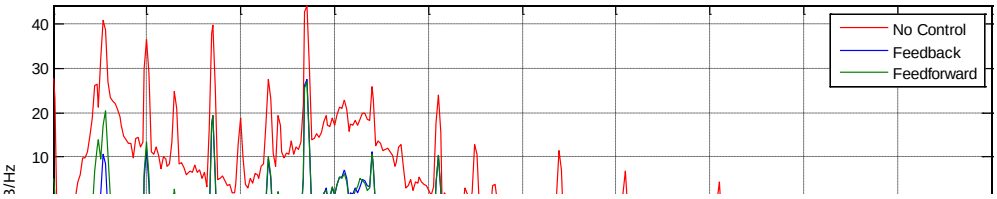

Figure 32. PI Spectral Analysis for Multiple Frequency Disturbances

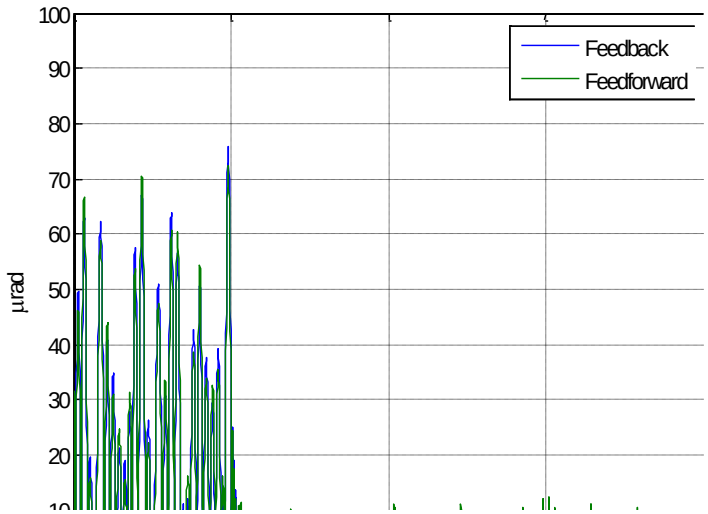

Figure 33. LMS Jitter Control for Multiple Frequency Disturbances

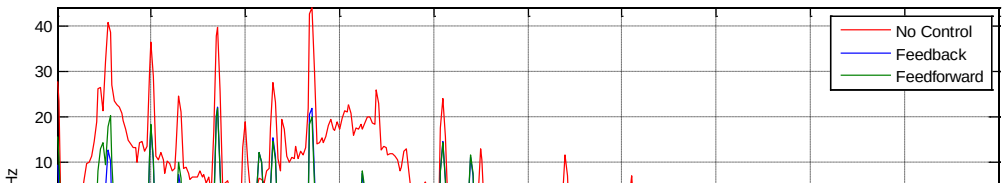

Figure 34. LMS Spectral Analysis for Multiple Frequency Disturbances

4.6 Comparison

In order to gain a better understanding of how well the controllers were able to mitigate the platform induced jitter, the standard deviation of the jitter was used as a scoring metric. The standard deviation of the jitter before and after the controller was turned on was calculated and

then used to find the percent improvement in the resulting jitter. In addition, the standard deviation of the laser's residual jitter of 0.525 μrad was subtracted from the before and after control results.

Table 2 and Table 3 show the percent improvement in the standard deviation of the jitter angle for the 17 Hz disturbance and multiple frequency disturbances cases respectively. As previously discussed, the feedback signal in the 17 Hz disturbance case performed the best in mitigating the platform induced jitter. There was a significant difference between feedback and feedforward for the 17 Hz disturbance case and the worst performer of all the experimental runs was the feedforward signal with the LMS controller. This occurred because of errors in the feedforward calculation which resulted in the addition of certain frequencies to the error signal which did not exist at the target that the LMS controller attempted to correct. As can be seen in Table 3, the feedback and feedforward signals were more closely aligned for the multiple frequency disturbances case. Again, this is because the errors in the feedforward calculation, which show up in the single frequency disturbance, are masked by the multiple frequencies and their harmonics.

Table 2. Improvement in Jitter Angle for 17 Hz Disturbance

	Feedback	Feedforward
PI	97.6%	90.7%
LMS	96.0%	84.5%

Table 3. Improvement in Jitter Angle for Multiple Frequency Disturbances

	Feedback	Feedforward
PI	91.9%	91.7%
LMS	92.9%	90.8%

5 Conclusion

5.1 Results

This research has demonstrated that it is possible to calculate a beam's position for a complex motion in real time based solely on platform and mirror positions. Using only three position sensors on the platform and a mirror orientation, this investigation was able to successfully calculate the position of a beam at a target approximately 5 m away with micrometer accuracy. This calculated beam position was then used in a feedforward compensation technique to mitigate platform induced jitter. Using either PI or LMS controllers, the feedforward signal reduced the standard deviation of the jitter by over 90%, except in the one case of LMS control of a single frequency (17 Hz – 84%). The feedforward control algorithm compared favorably to the feedback system, and while it did not produce as accurate a result, the ability to control a beam without the use of target feedback is significant. Experimental results also offered insights into ways the feedforward signal could be improved. For example, it was discovered that not including the platform's transverse motion, and only its rotations, degraded the performance of the feedforward calculation. In addition, it was discovered that the feedforward calculation had a 60 Hz component that was most likely the result of sensor noise, amplified by the algorithm. This 60 Hz component, along with the other unknown frequencies in the feedforward error signal, resulted in a power spectrum increase in the high frequency regime (greater than about 30 Hz). These added frequency components represent motion that does not exist in the platform disturbance, thus causing error in the controlled beam. Lastly, experimental results revealed the presence of error sources such as the residual jitter in the laser and the effect of the atmosphere the beam travels through. While these sources cannot be removed with this model, they are significant and must be accounted for in a control system.

5.2 Future Work

One of the most successful aspects of this project is that it has laid a foundation for future directed energy research here at USNA. Concerning this research, there are several areas that could be improved to make this system more applicable to real directed energy systems. The

first step would be to shift from off-board to on-board sensors to determine the position and orientation of the platform. As previously described in the experimental setup, the current sensors rely on a laser mounted off the platform which is obviously not realistic. One solution would be to use angular rate sensors and accelerometers. These could provide rate and acceleration data that could be integrated to find the position and orientation of the platform. This solution would be representative of an inertial measurement unit which is used in real-life to solve similar problems.

A second area that needs improvement is the actual jitter control system. Ideally, the system would be able to correct platform induced jitter to less than 1 μrad. One step would be to improve the feedforward signal by including the x, y, and z displacements of the platform in the feedforward algorithm. Currently, only the platform rotations are used to find the position and orientation of the platform. While the displacements are small compared to the rotations, they are significant as could be seen from the spectral analysis and would improve the accuracy of the beam calculation. In addition, more work is needed to remove the 60 Hz noise in the feedforward signal. This is most likely coming from one or more of the sensors and thus trouble shooting each sensor is required. If the source of the noise cannot be discovered and/or eliminated, some filtering technique may be required to eliminate the 60 Hz signal.

Other ways to improve the jitter control would be to improve the controller by adding a filtered-x reference signal for the LMS adaptive controller. This would place an estimate of the transfer function governing the FSM dynamics in the reference signal path to account for the delay in positioning the FSM. Another adaptive algorithm, such as the Recursive Least Squares (RLS) method or one of the lattice based algorithms could result in improved disturbance rejection.

Additional planned improvements include the shift from an external or inertial reference system to a line-of-sight reference frame. As the motion about the vector along the line of sight is the cause of the degradation in intensity seen at the target impact location, a line of sight reference frame would allow mitigation of the jitter without reference to an external frame.

APPENDIX A: Newport Fast Steering Mirror

Mirror Assembly	FSM-320
Number of Axes	2 (tip-tilt)
Angular Range from ±10 V	±26.2 mrad (±1.5°), Mechanical[1]
Resolution	≤1 µrad rms, Mechanical[1]
Repeatability	≤3 µrad rms, Mechanical[1]
Accuracy from ±26.2 mrad, 25°C[1]	≤0.262 mrad (0.015°), Mechanical[1]
Linearity from ±26.2 mrad, 25°C[1]	≤1.0%
Closed-Loop Amplitude Bandwidth for small signal inputs (-3 dB)	800 Hz at 10 mV (typical)
Closed-Loop Phase Bandwidth (60° lag)	400 Hz (typical)
Response Flatness[2]	Peaking ≤3 dB
Noise Equivalent Angle	≤3 µrad rms
Resolution of Local Position Sensor	≤0.5 µrad
Operating Temperature Range	0 to 35°C (32 to 95°F)
Storage Temperature Range	-20 to 55°C (-4 to 131°F)
Sensor Warm-up Time for Mirror Stability at 25°C	≤10 minutes
Mass	1lb (0.45 kg)
Interconnect Cable Length	9.8 ft (3 m)
Dialectric Mirror Substrate Material	Pyrex

Mirror Retaining Mechanism	Mirror bonded to aluminum carrier, field replaceable
Pivot Point of Axes (centered on mirror)	12.19 mm behind mirror surface
Mirror Diameter	25.4 mm
Mirror Thickness	6.0 mm
Mirror Wedge	≤5 arc min
Clear Aperture (at 0° angle of incidence)	≥20.3 mm
Clear Aperture (at 45° angle of incidence)	≥14.4 mm
Reflectivity(2)	Enhanced Aluminum: >93%, 450-700 nm
Surface Flatness(2) (after coating and bonding)	≤λ/10 at 632.8 nm over clear aperture
Surface Quality(2)	15-5 scratch-dig

1) Optical angular range is equal to twice the mechanical angular range.
2) Optical parameters apply to central 80% of mirror aperture.

Controller/Driver

Command Input and Position Output	Analog, ±10 V = ±26.2 mrad
Peak Operating Power to Mirror	30 W
Continuous Maximum Operating Power to Mirror	15 W
Thermal Protection	60°C at mirror coil
Current Protection	3 A
Operating Temperature Range	0 to 50°C (32 to 122°F)

Storage Temperature Range	-20 to 55°C (-4 to 131°F)
Power	100-240 Vac ±10%, 47-63 Hz
Mass	5.45 lb (2.5 kg)
Envelope [w x h x d]	9 x 3.45 x 10 in. (229 x 88 x 254 mm)

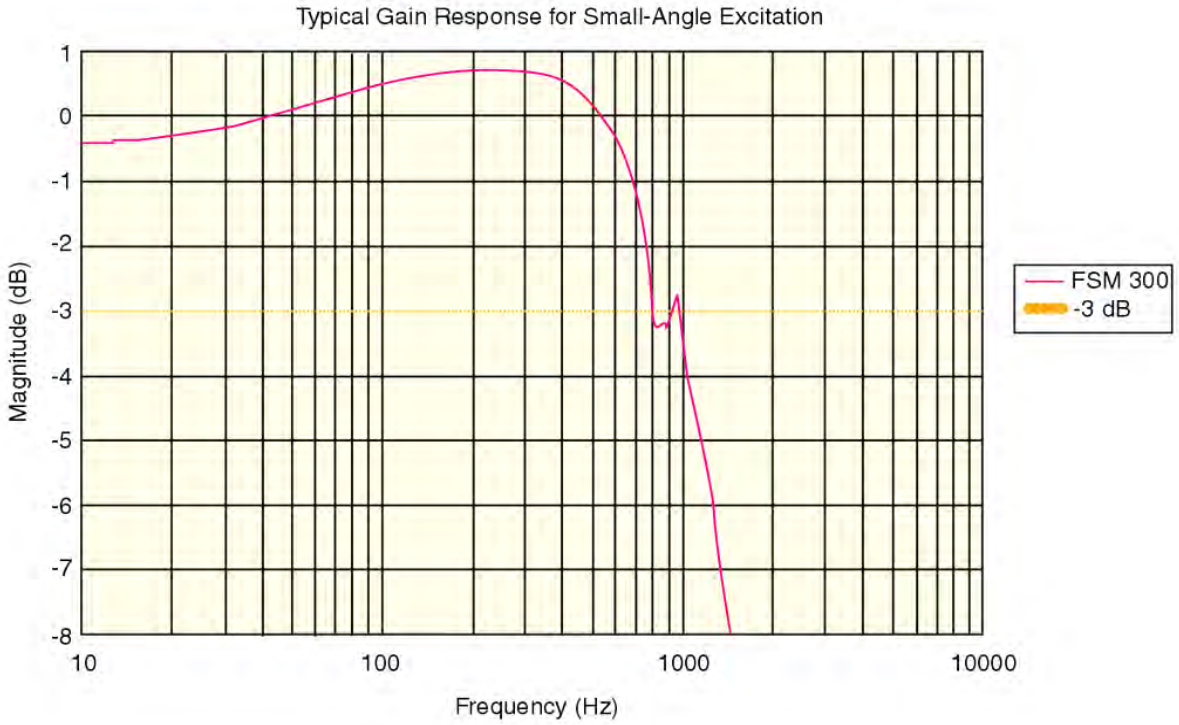

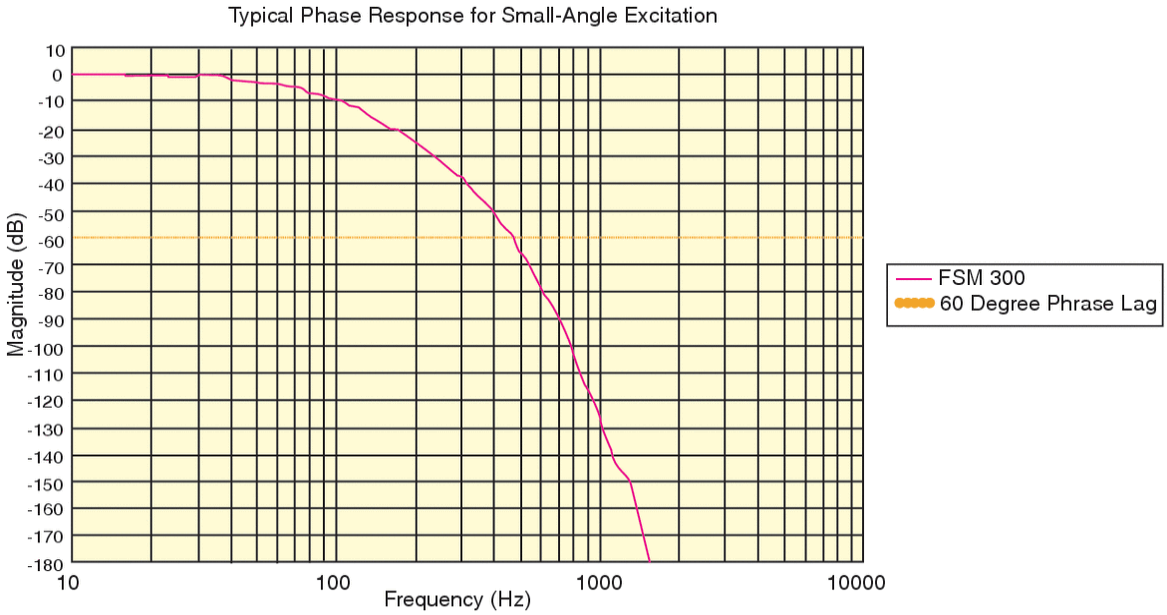
Typical Phase Response for Small-Angle Excitation
Magnitude (dB)
10
0
-10
-20
-30
-40
-50
-60
-70
-80
-90
-100
-110
-120
-130
-140
-150
-160
-170
-180
10
100
1000
10000
Frequency (Hz)
FSM 300
60 Degree Phrase Lag

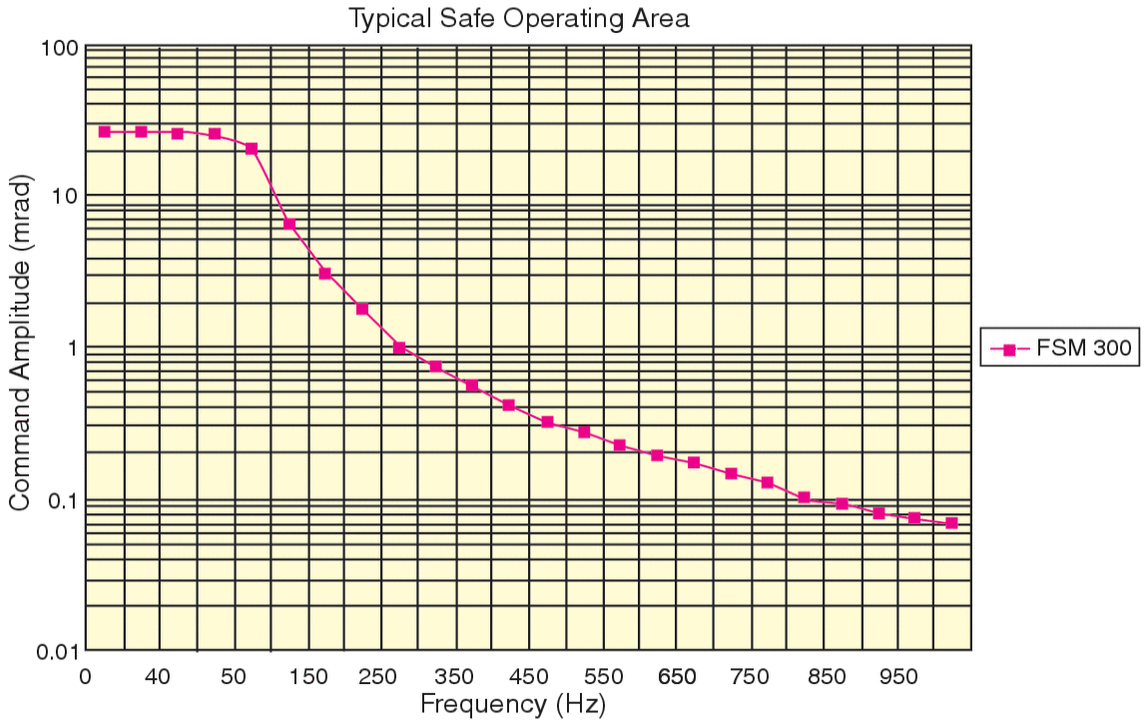
Typical Safe Operating Area
Command Amplitude (mrad)
100
10
1
0.1
0.01
0
40
50
150
250
350
450
550
650
750
850
950
Frequency (Hz)
FSM 300

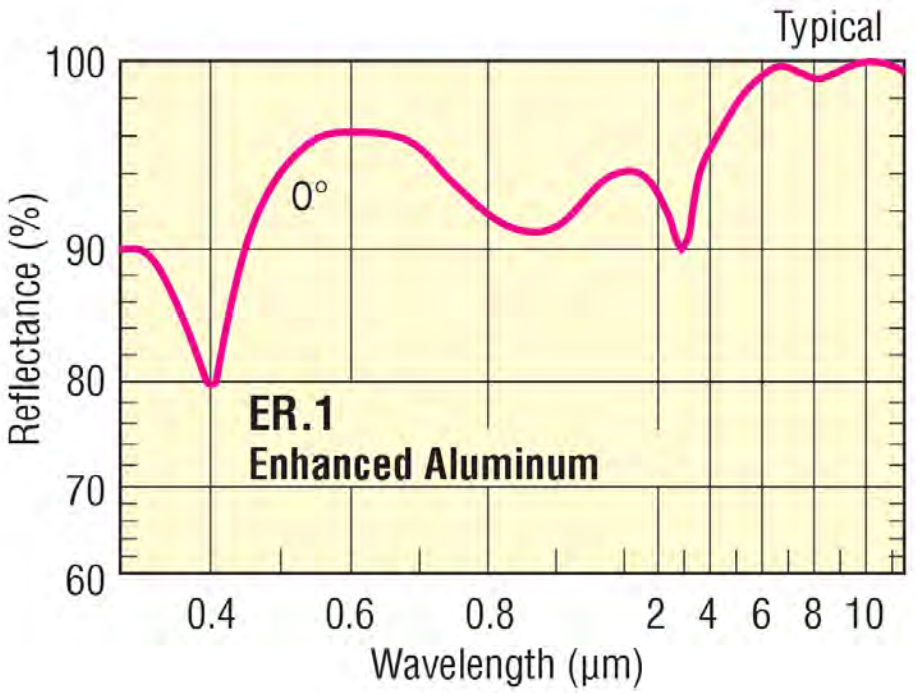
Typical
100
90
80
70
60
Reflectance (%)
0°
ER.1
Enhanced Aluminum
0.4
0.6
0.8
2
4
6
8
10
Wavelength (µm)

APPENDIX B: Newport Breadboard

Model	IG-33-2
Width	3 ft.
Length	3 ft.
Thickness	2.3 in. (58 mm)
Thread Type	1/4-20
Mounting Hole Pattern	1.0 in. grid
Surface Flatness	±0.006 in. over 2 ft. (±0.15 mm over 600 mm)
Working Surface	400 Series ferromagnetic stainless steel
Core Design	Trussed honeycomb, vertically bonded closed cell construction, 0.010 in. (0.25 mm) Steel sheet materials, 0.030 in. (0.76 mm) triple core interface
Broadband Damping	Integrated Damping including constrained layer core, damped working surface and composite edge finish

Mounting Hole Type	Cut (not rolled) threads with countersink
Hole/Core Sealing	Easy clean conical cup 0.75 in. (19 mm) deep Non-corrosive high impact polymer material
Maximum Dynamic Deflection Coefficient	$<17 \times 10^{-4}$
Maximum Relative Motion Value	$<13 \times 10^{-7}$ in. ($<3.3 \times 10^{-5}$ mm)
Deflection Under Load	$<15 \times 10^{-5}$ in.
Top and Bottom Skins	0.134 (3.4 mm) thick with integrated damping layer

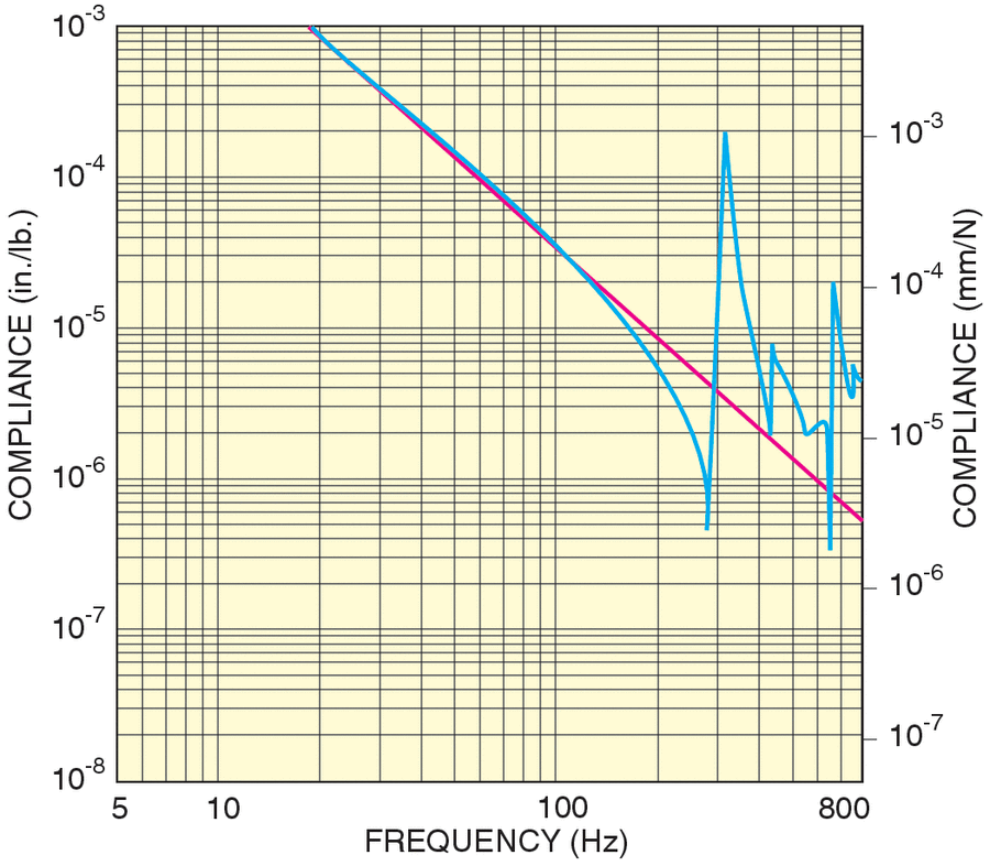
COMPLIANCE (in./lb.)
10-3
10-4
10-5
10-6
10-7
10-8
5
10
100
800
FREQUENCY (Hz)
COMPLIANCE (mm/N)
10-3
10-4
10-5
10-6
10-7

APPENDIX C: CSA Engineering Inertial Actuator

SA Series Inertial Actuators

CSA Engineering, Inc.

- Inertial force generator
- 1-10 lbf broadband output (0 - peak)
- Peak outputs greater than 100 lbf
- Wide bandwidth (20 to 1000 Hz)
- Self contained

SA series actuators deliver inertial force over a wide bandwidth in compact, rugged, electromagnetically efficient forms. The actuators use an electromagnetic circuit with a moving magnet that allows the coil to be thermally grounded to the housing. Magnets are suspended by specially designed long life flexures. The force is generated along the axis of the cylindical units.

Typical applications include active damping or vibration cancellation, mounts for active vibration isolation, or disturbance generation. Dynamic amplification at frequencies near the actuator resonance results in large force outputs. A rigid housing enables direct insertion of the SA into structural load paths.

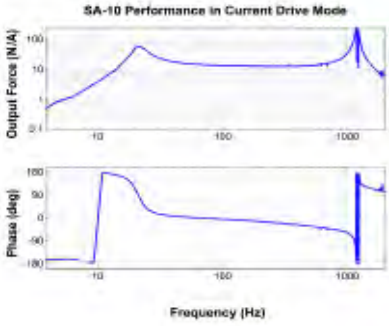

Actuators are specified by force capacity and internal suspension resonance. Standard options/accessories include alternative end caps, coils of specified impedance, a variety of cable interfaces, and current or voltage drive mode amplifiers. The overall design is easily customizable to meet the requirements of mounting configurations, drive electronics, or mass budgets.

The SA1, SA5, and SA10 are standard products. Also available are the SA2, SA35 and other non-standard models. Actuators are specified as SA*x-f* where *x* is the zero-peak force output at high frequency in pounds and *f* is the primary resonant frequency in Hz. For example, the SA5-60 produces 5 pounds force and has a 60 Hz resonance.

SPECIFICATIONS				
	SA1	SA5	SA10	Units
Rated Force Output*	1	5	10	lbf (0-peak)
Bandwidth	40-1000	20-1000	20-1000	Hz
Motor Constant**	0.5	2	5	lbf/Amp
Resonant Frequency***	30-200	30-200	30-200	Hz
Resistance**	2	2	2	Ohm
Total Mass	0.25	2.9	5.5	lbm
Diameter	35	76	93	mm
Height	30	66	92	mm

* Significantly greater forces possible with good heatsinking
** Typical values
*** User-specified. Manufactured to ± 2-3%

For more information, email *actuators@csaengineering.com*

APPENDIX D: On-Trak PSM

Description (From On-Trak Website: http://www.on-trak.com/theory.html)

Position Sensing Detectors "PSD's" are silicon photodiodes that provide an analog output directly proportional to the position of a light spot on the detector active area. The PSD allows you to simultaneously monitor position and light intensity. The PSD is a continuous analog position sensor. Compared to discrete element devices, the PSD offers outstanding position linearity, high analog resolution, fast response time, and simple operating circuits.

Theory Of Operation

A Position Sensing Detector consists of n-type silicon substrate with two resistive layers separated by a p-n junction. The front side has an ion implanted p-type resistive layer with two contacts at opposite ends. The back side has an ion implanted n-type resistive layer with two contacts at opposite ends placed orthogonally to the contacts on the front side. On a single axis PSD, the electrodes are placed at opposite ends of the p-type resistive layer. A light spot within the spectral range of silicon will generate a photocurrent that flows from the incident point through the resistive layers to the electrodes. The resistivity of the ion implanted layer is extremely uniform so the photogenerated current at each electrode is inversely proportional to the distance between the incident spot of light and electrodes. The PSD outputs track the motion of the "centroid of power density" to an extremely high resolution and ultra-high linearity. On-Trak Position Sensing Amplifiers take the photocurrent from each electrode and process the signals to provide X, Y outputs independent of light intensity.

Position Resolution

The position resolution of a PSD is the minimum detectable displacement of a spot of light on the detector surface. The position resolution of On-Trak PSDs are proven better than one part in a million. Resolution dependent on:

- Detector Size
- Detector Noise
- Light Input Intensity
- Bandwidth of the Electronic Signal Processing Circuits

Position Linearity

Position non-linearity is defined as geometric position error divided by detector length and is measured within 80% of the detector length. Position non-linearity is typically better than 0.05% for the single axis PSD and better than 0.3% for the duolateral. The On-Trak vs competitor two-dimensional linearity plot shows the ultra linear characteristic of these PSDs.

One-Dimensional PSD

The one-dimensional PSD detects a light spot moving over its surface in a single direction. The photoelectric current generated by the incident light flows through the device and is seen as an input bias current divided into two output currents. The distribution of the output currents show the light position on the detector.

Duolateral Two-Dimensional PSD

The duolateral two-dimensional PSD detects an incident light spot position on its square surface. The photoelectric current generated by the incident light flows through the device and is seen as two input currents and two output currents. The distribution of the output currents show the light position of one dimension (Y), and the distribution of the input currents show the light position of the second dimension (X).

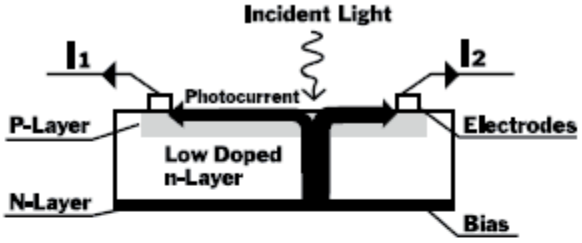

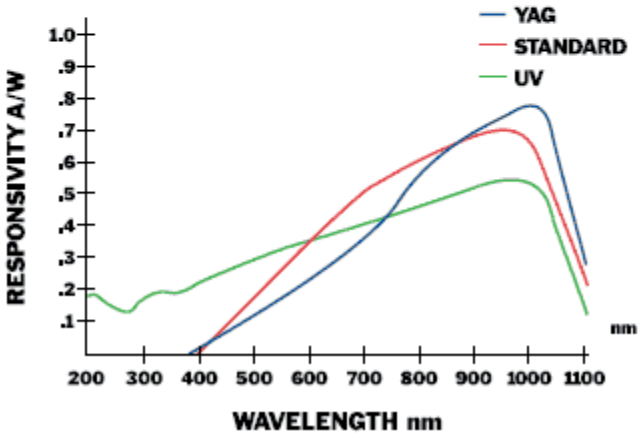

PSD Type	Spectral Range	Responsivity
Standard	400-1100 nm	0.70 A/W @ 940 nm

APPENDIX E: Newport Compact Air-Mount

Model	SLM-1A
Load per Isolator	100 lb (45 kg)
Load Capacity	100 lb (45 kg)
Max. Air Pressure	60 psi
Natural Frequency (Nominal), Max.	5
Natural Frequency (Nominal), Min.	3 Hz
Isolator Weight	1 lb (0.45 kg)
Operating Temperature Range	-40 to 83 °C

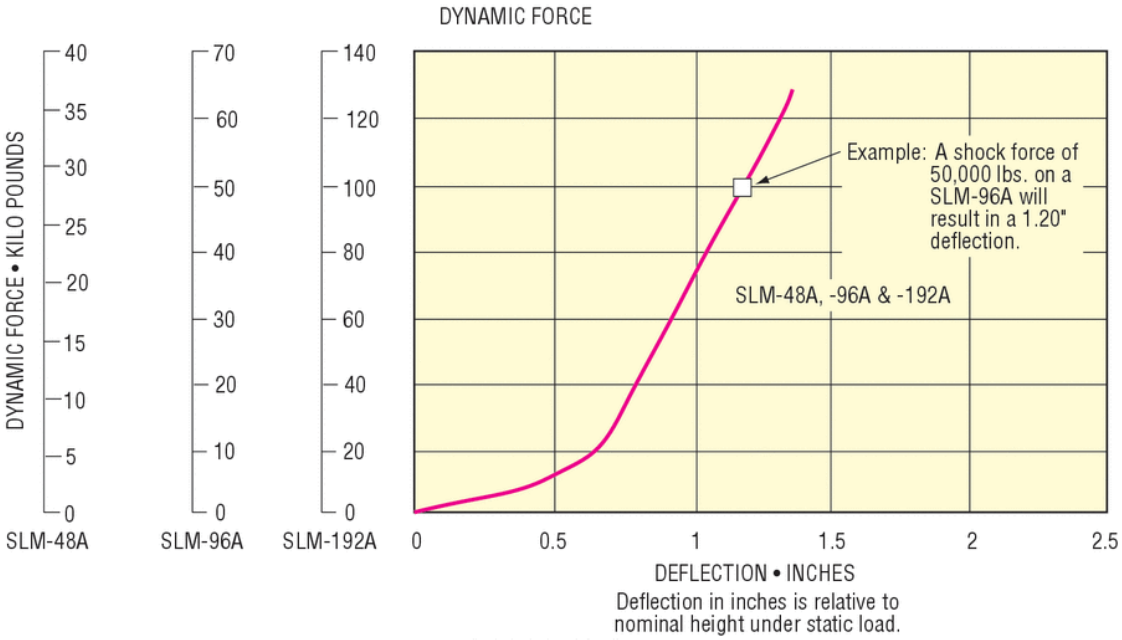
DYNAMIC FORCE
DYNAMIC FORCE • KILO POUNDS
40
35
30
25
20
15
10
5
0
SLM-48A
70
60
50
40
30
20
10
0
SLM-96A
140
120
100
80
60
40
20
0
SLM-192A
Example: A shock force of 50,000 lbs. on a SLM-96A will result in a 1.20" deflection.
SLM-48A, -96A & -192A
0
0.5
1
1.5
2
2.5
DEFLECTION • INCHES
Deflection in inches is relative to nominal height under static load.

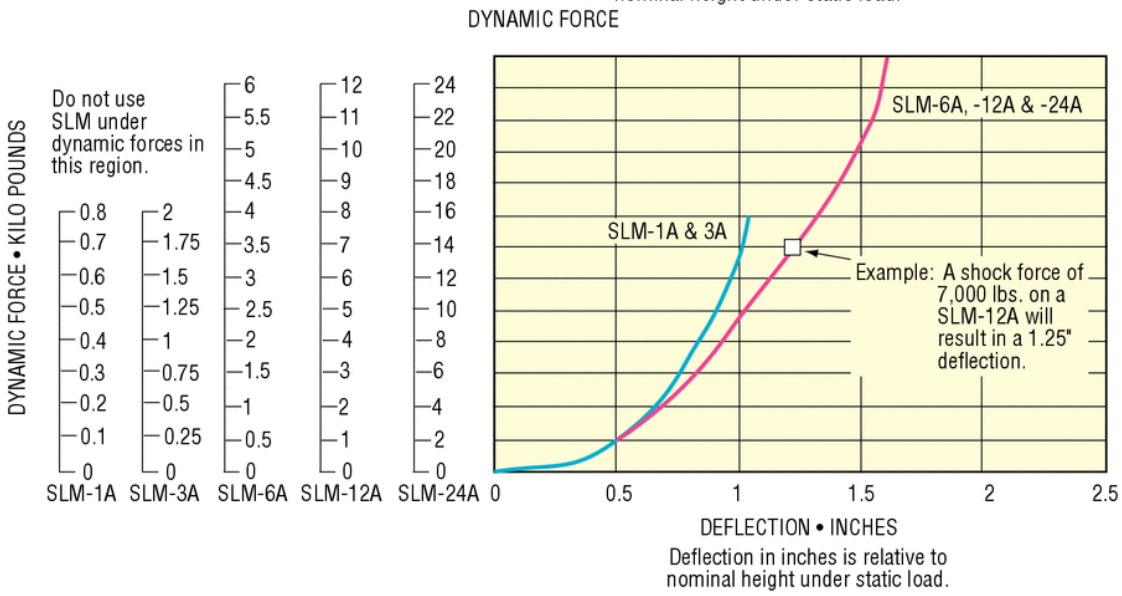
DYNAMIC FORCE
DYNAMIC FORCE • KILO POUNDS
Do not use SLM under dynamic forces in this region.
0.8
0.7
0.6
0.5
0.4
0.3
0.2
0.1
0
SLM-1A
2
1.75
1.5
1.25
1
0.75
0.5
0.25
0
SLM-3A
6
5.5
5
4.5
4
3.5
3
2.5
2
1.5
1
0.5
0
SLM-6A
12
11
10
9
8
7
6
5
4
3
2
1
0
SLM-12A
24
22
20
18
16
14
12
10
8
6
4
2
0
SLM-24A
SLM-6A, -12A & -24A
SLM-1A & 3A
Example: A shock force of 7,000 lbs. on a SLM-12A will result in a 1.25" deflection.
0
0.5
1
1.5
2
2.5
DEFLECTION • INCHES
Deflection in inches is relative to nominal height under static load.

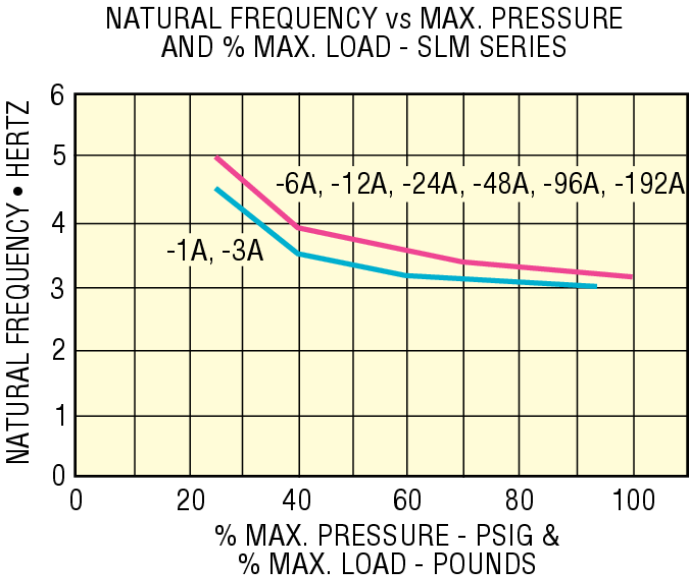
NATURAL FREQUENCY vs MAX. PRESSURE
AND % MAX. LOAD - SLM SERIES
NATURAL FREQUENCY • HERTZ
6
5
4
3
2
1
0
-6A, -12A, -24A, -48A, -96A, -192A
-1A, -3A
0
20
40
60
80
100
% MAX. PRESSURE - PSIG &
% MAX. LOAD - POUNDS

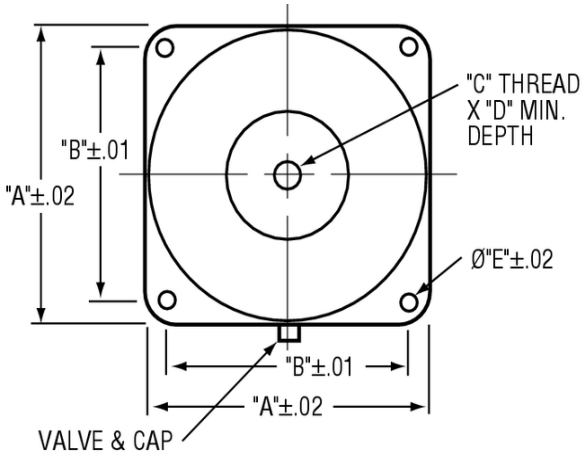
"C" THREAD
X "D" MIN.
DEPTH
"B"±.01
"A"±.02
Ø"E"±.02
"B"±.01
"A"±.02
VALVE & CAP

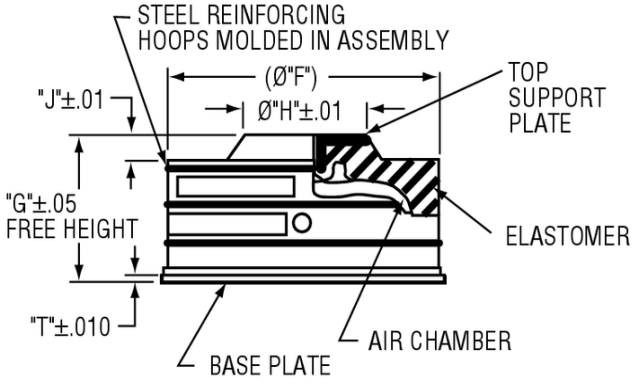
STEEL REINFORCING
HOOPS MOLDED IN ASSEMBLY
(Ø"F")
Ø"H"±.01
"J"±.01
TOP
SUPPORT
PLATE
"G"±.05
FREE HEIGHT
ELASTOMER
"T"±.010
AIR CHAMBER
BASE PLATE

APPENDIX F: Newport Optical Table

Model	RS4000-46-18
Mounting Hole Type	1/4-20
Mounting Hole Pattern	1 in. grid
Length	6 ft.
Width	4 ft.
Thickness	18 in.

Working Surface	400 series ferromagnetic stainless steel
Deflection Under Load	$<5.0 \times 10^{-5}$ in. in. ($<1.3 \times 10^{-3}$ mm mm)
Maximum Dynamic Deflection Coefficient	0.4×10^{-3}
Core Design	Trussed Honeycomb, Vertically Bonded Closed Cell Construction, 0.010 in. Steel sheet materials, 0.030 in. triple core interface
Broadband Damping	Constrained layer core, damped working surface and composite edge finish
Hole/Core Sealing	Easy clean conical cup 0.75 in. (19 mm) deep, Non-corrosive high impact polymer material
Top and Bottom Skins	3/16 in. (4.8 mm) thick with integrated damping layer
Crated Weight	1234 lb (548 kg)

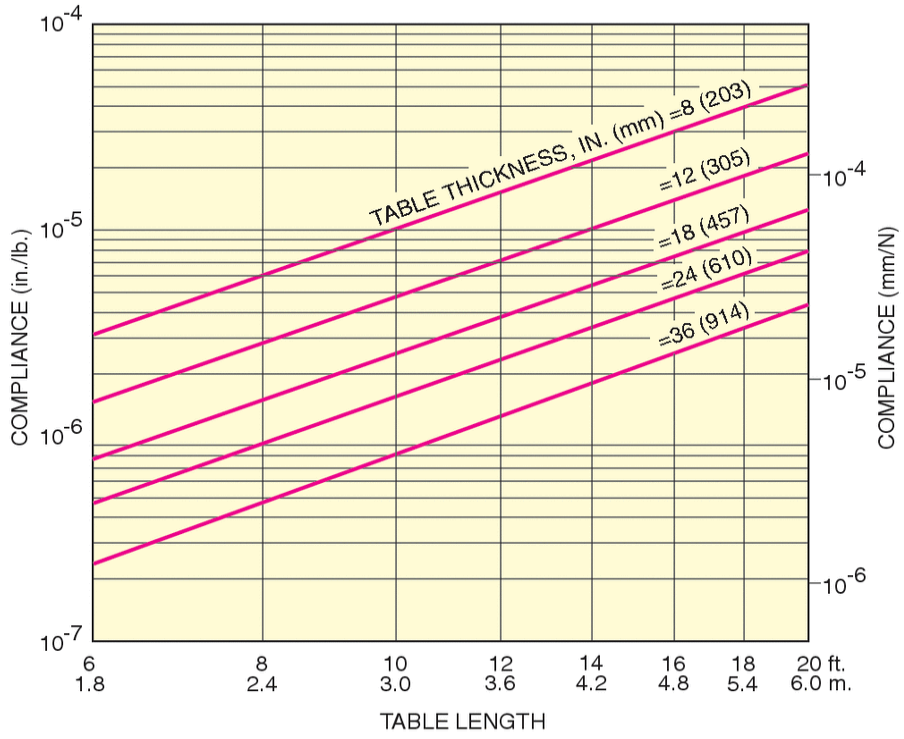
10^{-4}
10^{-5}
10^{-6}
10^{-7}
COMPLIANCE (in./lb.)
TABLE THICKNESS, IN. (mm) =8 (203)
=12 (305)
=18 (457)
=24 (610)
=36 (914)
10^{-4}
10^{-5}
10^{-6}
COMPLIANCE (mm/N)
6 1.8
8 2.4
10 3.0
12 3.6
14 4.2
16 4.8
18 5.4
20 ft. 6.0 m.
TABLE LENGTH

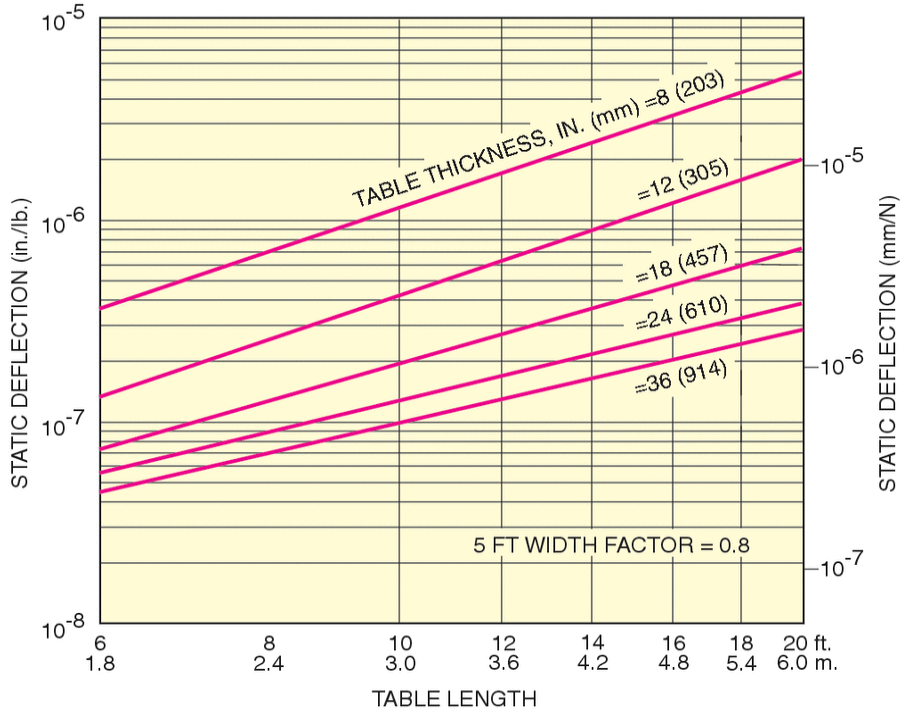
10^{-5}
10^{-6}
10^{-7}
10^{-8}
STATIC DEFLECTION (in./lb.)
TABLE THICKNESS, IN. (mm) =8 (203)
=12 (305)
=18 (457)
=24 (610)
=36 (914)
5 FT WIDTH FACTOR = 0.8
10^{-5}
10^{-6}
10^{-7}
STATIC DEFLECTION (mm/N)
6 1.8
8 2.4
10 3.0
12 3.6
14 4.2
16 4.8
18 5.4
20 ft. 6.0 m.
TABLE LENGTH

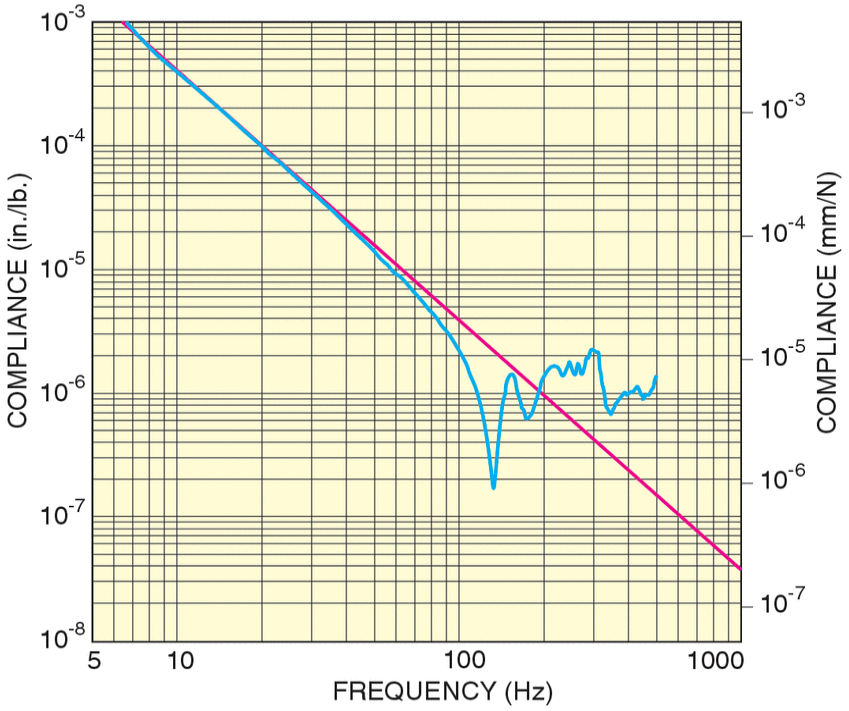
COMPLIANCE (in./lb.)
10^{-3}
10^{-4}
10^{-5}
10^{-6}
10^{-7}
10^{-8}
COMPLIANCE (mm/N)
10^{-3}
10^{-4}
10^{-5}
10^{-6}
10^{-7}
5
10
100
1000
FREQUENCY (Hz)

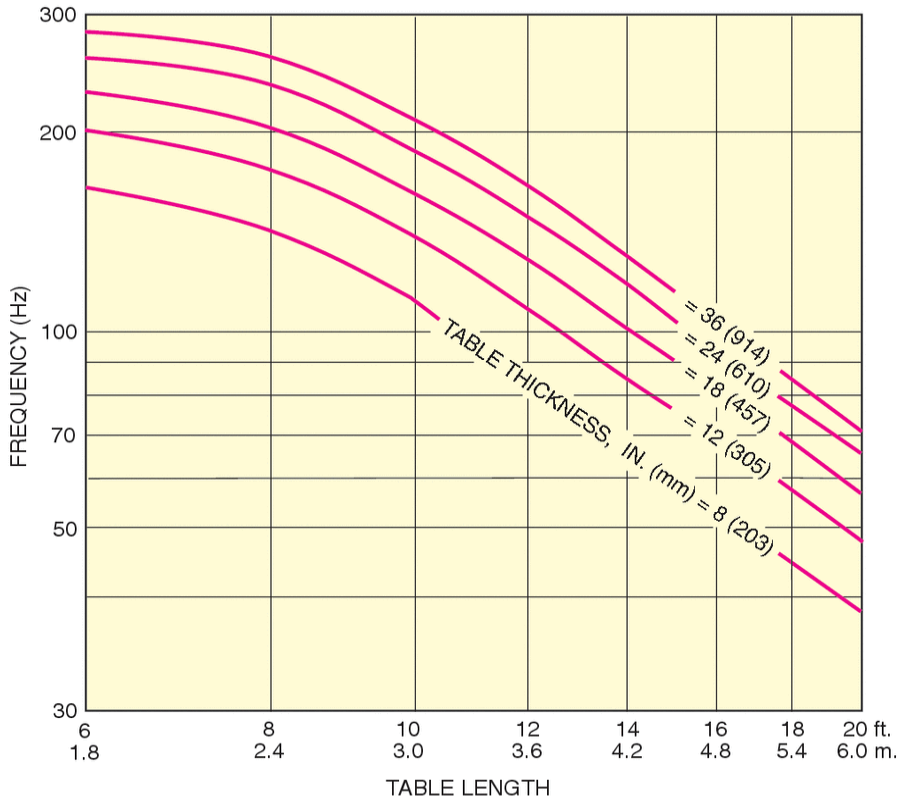
FREQUENCY (Hz)
300
200
100
70
50
30
TABLE THICKNESS, IN. (mm)
= 36 (914)
= 24 (610)
= 18 (457)
= 12 (305)
= 8 (203)
6
1.8
8
2.4
10
3.0
12
3.6
14
4.2
16
4.8
18
5.4
20 ft.
6.0 m.
TABLE LENGTH

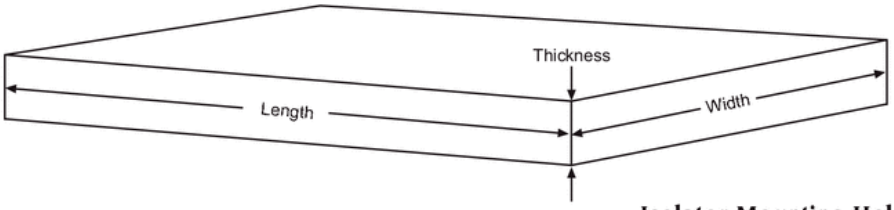

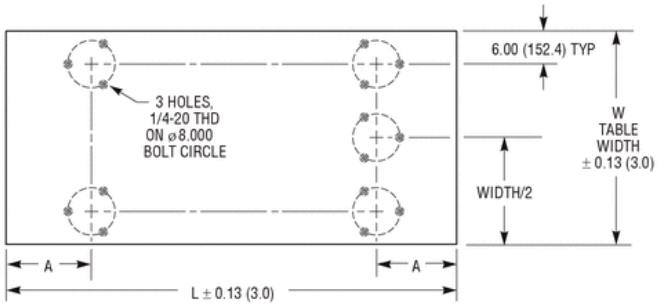

Isolator Mounting Hole Dimensions

WIDTH (W)	LENGTH (L)	DIMENSION (A)
in.	ft	in.
36.0	20.0	53.0
48.0	18.0	47.0
59.1	16.0	42.0
	14.0	37.0
	12.0	32.0
	10.0	27.0
	8.0	22.0
	6.0	16.0

APPENDIX G: Newport Pneumatic Isolators

Specifications

Table Tops:	
Flatness:	±0.005in. (0.13mm)*
Compliance:	Consult your Newport Catalog or Newport directly for the specific compliance and other pertinent table top specifications of your particular table top model.
Isolators:	Stabilizer™ I-2000
Vertical Resonant Frequency:	<1.1 Hz at 80 psi
Horizontal Resonant Frequency:	<1.5 Hz
Recommended Load Range: (per 4 isolators)	660 to 8,000 lb (300 to 3,600 kg)
Automatic Leveling Accuracy:	±0.010 inch (0.25 mm) standard, higher accuracy available on special order
Vertical Adjustment Range:	1.3 inches (33 mm)
Settling Time: (after 5-lb. weight removal)	<1.5 sec.
Typical Air Pressure Range:	10 to 85 psi (0.7 to 6.0 kg/cm^2)

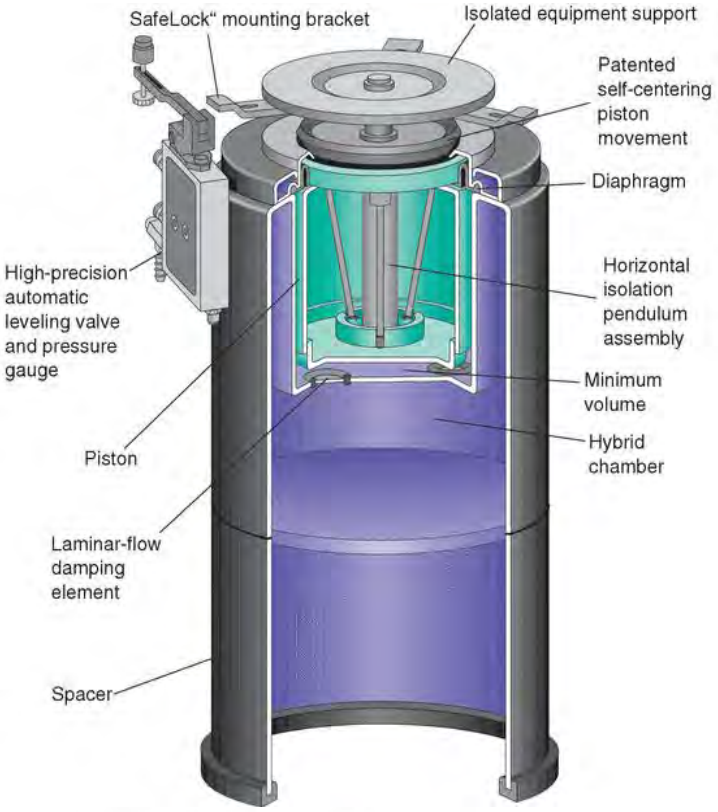

Isolation System Transmissibility

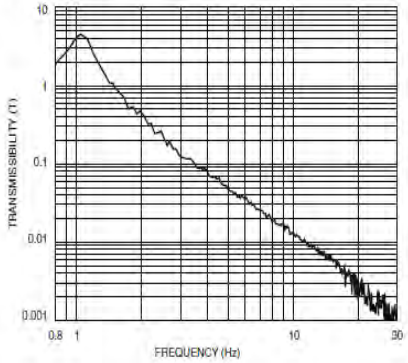

Vertical Transmissibility (at maximum recommended load)

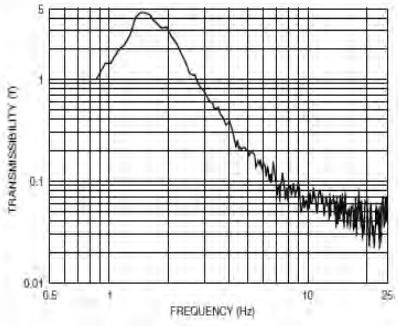


Clamp
(3 per Isolator)
Wrench Holes
Level
Adjustment
Screw
Leveling Valve
(3 per system)
Newport

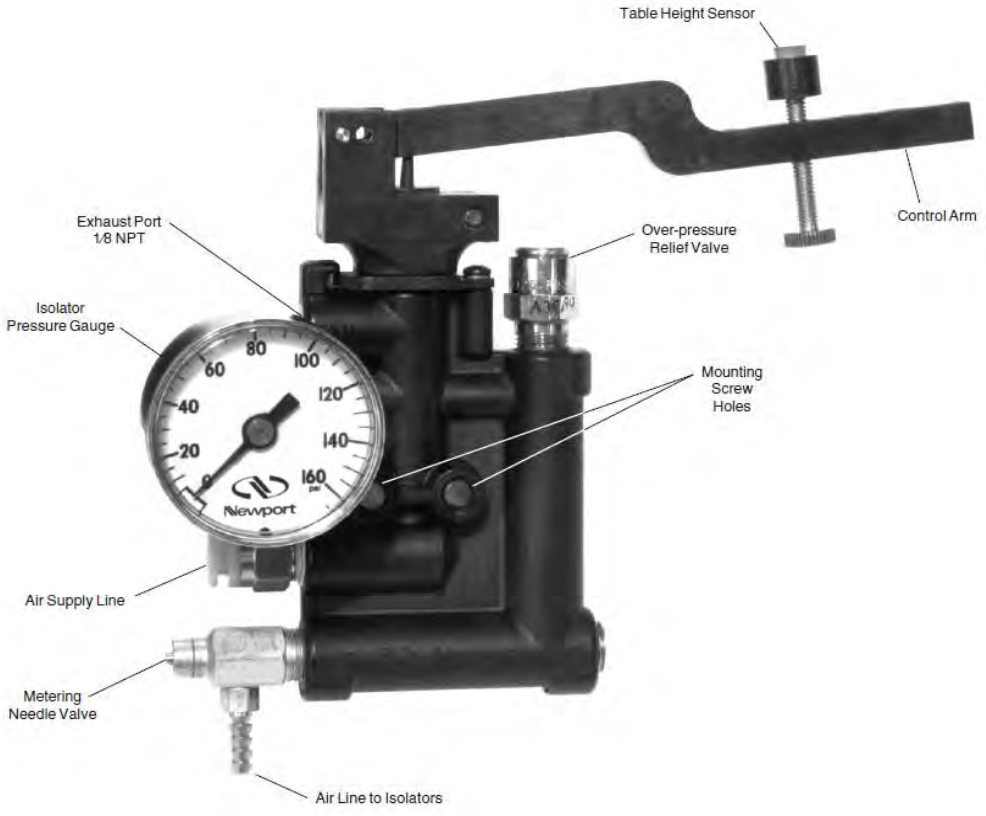
Table Height Sensor
Control Arm
Exhaust Port
1/8 NPT
Over-pressure
Relief Valve
Isolator
Pressure Gauge
Mounting
Screw
Holes
Air Supply Line
Metering
Needle Valve
Air Line to Isolators
Newport

APPENDIX H: Laser Diode

Class	5mW, Class IIIa
Typical Power Output	~75% of max. output power
Beam Diameter	3.8 x 0.9mm, typical collimated beam
Beam Divergence	0.45 x 0.95 mrad, typical collimated beam
Line Width, Focused Spot	<0.001" (25 microns) user adjustable
Focusing Distance	Face of module to past collimation
Dimensions	
Module only	0.750" Diameter +0/-0.005"
Projection Head	0.734" Diameter
Bore Sighting (Beam vs. Housing Alignment)	<3 mrad, collimated beam
Temperature Range	+10°C to +48°C
Frequency Drift	0.25nm / °C
ESD Protection	+8,000 volts
Diode MTBF, calc.	50 - 100,000 hrs, varies with model
Current Draw	65 - 150 mA, varies with model
Input Voltage	5 - 6V DC
Weight	~65 grams
Housing Material	Black Anodized Aluminum
*Class IIIb Models	CDRH certified with key box

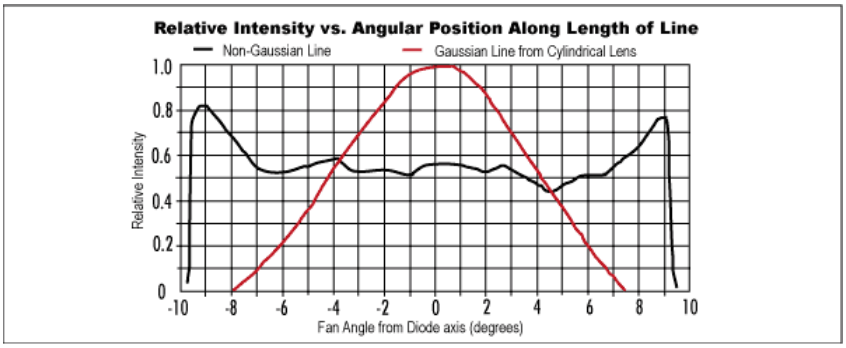

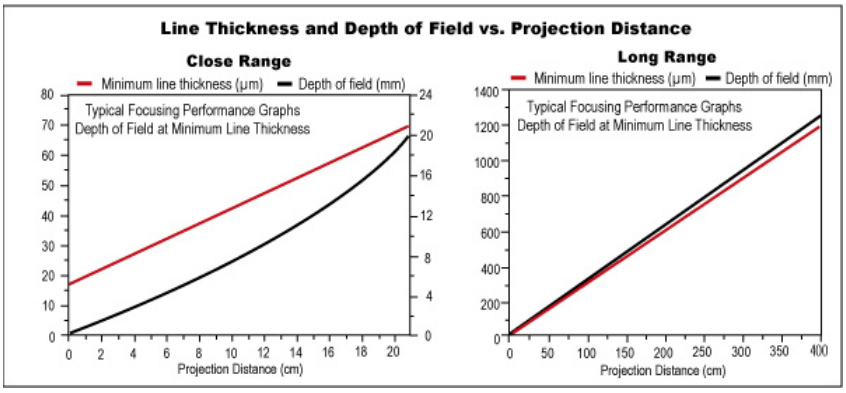

APPENDIX I: Kistler Accelerometer Model 8690C5

Acceleration - ATP

KISTLER
measure. analyze. innovate.

PiezoBeam™

Type 8690C...

Light Weight, Voltage Mode Triaxial Accelerometer

High sensitivity triaxial accelerometers that simultaneously measure vibration in three, mutually perpendicular axis (x, y and z).

Designed primarily for modal analysis applications, the triaxial accelerometer can also find selective use as a general purpose vibration sensor.

- Low impedance, voltage mode
- High sensitivity
- Low cost, lightweight triaxial design
- High accuracy and stability
- Choice of ranges and sensitivities
- Excellent thermal stability
- Conforming to CE

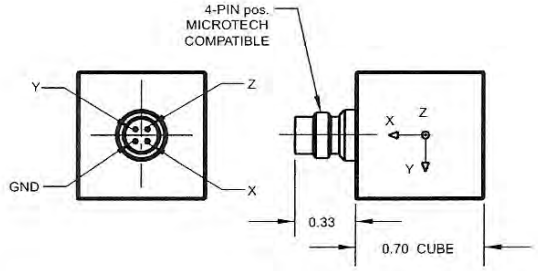

Description
Internal of the PiezoBeam accelerometer is a uniquely configured sensing element consisting of a ceramic beam supported by a center post that when bending occurs as a result of being subjected to vibration, the cantilevered beam element yields an electrical charge. The charge signal is converted by the internal charge amplifier to a proportional high level voltage signal at a output impedance of less than 500 ohms.

The lightweight units reduce mass loading on thin-walled structures in multichannel general vibration measurements or modal applications. This series of triaxial sensors, with an integral four-pin connector, is designed for simplified installation in confined areas. Each unit may be mounted on any of three surfaces.

The 8690C triaxial series offer outstanding phase response, thermal stability, as well as wide frequency range. They are constructed of hard, anodized aluminum which provides ground isolation and environmentally sealed with epoxy.

The accelerometers will operate directly from the internal power source found in most FFT analyzers, from several Kistler Piezotron™ power supply couplers or any industry standard IEPE (Integrated Electronic Piezo Electric)compatible power source.

Application
This light weight, triaxial accelerometer series is ideally suited for multiple channel modal vibration measurement on aerospace vehicle, air frame, flight flutter and automotive structural testing.

Technical Data

Type	Units	8690C5	8690C10	8690C50
Acceleration Range	g	±5	±10	±50
Acceleration Limit	g_{pk}	±8	±16	±80
Threshold nom.	μV_{rms}	120	140	100
	μg_{rms}	120	280	1000
Sensitivity ±5 % (at 100Hz, 3 g_{rms})	mV/g	1000	500	100
Resonant Frequency mounted, nom.	kHz	9	22	22
Frequency Response ±5%	Hz	1... 3000	1... 5000	1...6000
Phase Shift, < 5°	Hz	4...2000	4...2000	4...4000
Amplitude Non-linearity	%FSO	±1	±1	±1
Time Constant nom.	s	1	1	1
Transverse Sensitivity	%	<1	<1	<1
Long Term Stability	%	±1	±1	±1
Environmental:				
Base Strain Sensitivity @ 250 με	g/με	<0.001	<0.001	<0.001
Shock Limit (0.2ms pulse width)	g_{pk}	5000	10000	10000
Temperature Coefficient of Sensitivity	%/°F	- 0.02	+0.04	+0.04
Temperature Range Operating (4mA supply current)	°F	32 ...150	32 ...150	32 ...150
Temperature Range Operating Storage	°F	- 10 ... 200	- 10 ... 200	- 10 ... 200
Output				
Bias	VDC	11	11	11
Impedance	Ω	<500	<500	<500
Current, (4mA supply)	mA	2	2	2
Voltage full scale	V	±5	±5	±5
Source				
Constant Current	mA	2 ... 20	2 ... 20	2 ... 20
Voltage	VDC	20 ... 30	20 ... 30	20 ... 30
Construction				
Sensing Element	type	ceramic bimorph/ bender	ceramic bimorph/ bender	ceramic bimorph/ bender
Housing	material	Al, hard anodized	Al, hard anodized	Al, hard anodized
Sealing housing/connector	type	Epoxy	Epoxy	Epoxy
Connector	type	4-pin pos. Microtech Equivalent	4-pin pos. Microtech Equivalent	4-pin pos. Microtech Equivalent
Ground Isolation	MΩ	10	10	10
Weight	grams	11.2	11.2	11.2
Mounting	type	adhesive/wax	adhesive/wax	adhesive/wax

1 g = 9.80665 m/s², 1 inch = 25.4 mm, 1 gram = 0.03527 oz, 1 lbf-in = 0.1129 Nm

Mounting

The cube shape configuration of the triaxial accelerometer allows for the unit to be attached to the test surface using any available side. Attachment can be by wax or by adhesive. Reliable and accurate measurements require that the mounting surface be clean and flat. The Operating Instruction Manual for the 8690C series provides detailed information regarding mounting surface preparation.

Ordering Information

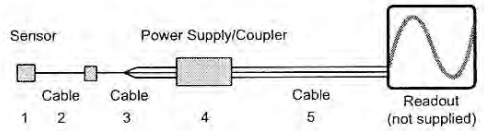

X = specify range; 5g, 10g, 50g
sp = specify cable length in meters

1 - 8690C(X)	triaxial accelerometer, specify range
2 - 1578Asp	optional extension cable, 4-pin pos. Microtech equivalent to 4-pin neg. Microtech equivalent
3 - 1756B(Y)	cable, 4-pin Microtech neg., to 3x BNC pos., length Y = 0.5, 3, 10 meters
4 - 5100	coupler series, or
5134	four-channel coupler
5 - 1511sp	output cable BNC pos. to BNC pos.

Supplied Accessories

8432	mounting wax

Optional Accessories

8476	mounting clip, black derlin

APPENDIX J: MATLAB Scripts

The following code is used to calibrate the beam control lab:

```
%     M-file to calibrate DEV3
%
%******************************
Ts=0.001;           %sample time
fintime = 7;        %Length of data run.
calibrate=0;
%-----------------------------------
%Control Selection
    %2=Control Off
    %0=Control On
    On_Off=2;
        x_On_Off=On_Off;
        y_On_Off=On_Off;

    %2=Feedback
    %0=Feedforward
    control=2;
        x_control=control;
        y_control=control;

    %2=PI
    %0=LMS
    PI_LMS=2;
        x_PI_LMS=PI_LMS;
        y_PI_LMS=PI_LMS;
            PI_LMS=2;
        x_PI_LMS=PI_LMS;
        y_PI_LMS=PI_LMS;

        if PI_LMS >= 2;
            title_control='PI Control';
        end
        if PI_LMS <=0;
            title_control='LMS Control';
        end
%-----------------------------------------
%   Shaker input (sinusiod, max 4 signals)
%       amp in volts, freq in Hz
%-----------------------------------------
shakeramp = [0      0        0       0];
shakerfreq= [0      0        0       0];
shakeramp2 = [0     0        0       0];
shakerfreq2= [0      0        0       0];
shaker_start=0;         %start time of vibrations in secs
shaker_end=fintime;
shakephase= [0 0 0 0];
```

```
chirp_on = 0; IA_chirp_gain=1;
IA_init_freq = 1;  IA_final_freq = 1000; IA_targ_time = 120;  %Chirp
Parameters

xzero = 0; yzero = 0;   % calibration const of mirror (to be determined)

FSM_position=[0,0,0];

dist_targ = 4.775; %distance to tgt (m)

mirror_angle = 45;  mirror_angle = mirror_angle*pi/180*1000; % mounted angle
for mirror
                    %rotation from x axis toward z is positive about y
                    %(mrad);

cal_ot1y = 0;   cal_ot1x = 0;
cal_ot2y = 0;   cal_ot2z = 0;
cal_ot3y = 0;   cal_ot3z = 0;
cal_ot4x = 0;   cal_ot4z = 0;

cal_ot5y = 0;   cal_ot5x = 0;

cal_ot6z = 0;   cal_ot6x = 0;
cal_ot7z = 0;   cal_ot7x = 0;

cal_tgty = 0;   cal_tgtx = 0;
%-----------------------------------------
%   LMS parameters for FSMB controller
%-----------------------------------------
    mux=0.015;      leakx=1.0;      % x axis adaption rate and leakage factor
    muy=0.035;      leaky=1.0;      % y axis adaption rate and leakage factor
    w0x = 0;        w0y = 0;        % initial tap gains
    adapt = 0.5;                    % adaption start time in secs
    biasx=-0.005*1;   biasy=0.002*1;     % estimate of bias correction
    ax_to_mx=1;       ay_to_my=14;   % estimate of gain correction for FSM to
accel
    ot2y_to_m2y = -1/10;
    mu_y_error = 0.05; leak_y_error = 1.0;
    adapt_y_error = 0.0;
    mu_x_error = 0.05; leak_x_error = 1.0;
%-----------------------------------------
%   Reference Signal Selection
%       1=OT-1, 2=Accel-2 (a2x and a2y)
%-----------------------------------------
    x_ref_sel=1;    y_ref_sel=2;
    zz=1;  % number of delays for the predictor ref signal
%-----------------------------------------
%   Error source selection
%       1=mirror postion, 2=OT3 position, 3=OT2 position
%-----------------------------------------
    x_error_sel=2;  y_error_sel=2;
```

```
    accel_lag = 1.05;
    OT2y_lag = 1;
    mirror_zero_bc = [0.318;0;0.572];
beam_dir_source = [0.408;0;0.572];
beam_start_source = [0.508;0;0.572];
d_1_2 = 0.762e6;    % distance in micrometers (
d_2_3 = 0.864e6;
d_1_3 = 1.152e6;
sd_1_2 = d_1_2^2;
sd_1_3 = d_1_3^2;
rmeanx = 0;  rmeany = 0;
xdist_2_3 = 1/0.862;
xdist_1_3 = 0.4826;
xdist_2_3p = 1.5;
zdist_3_1 = 1/0.7491*1.15;

%   Additional LMS parameters for Prediction
    adapt_y_error = 0.0;
    mu_y_error = 0.05; leak_y_error = 1.0;
    mu_x_error = 0.05; leak_x_error = 1.0;
%----------------------------------------
%   PID gains for FSM Controller A
%----------------------------------------
fsm1px=0.0532*0.45;   fsm1ix=(0.07*1.2/0.002);   fsm1dx=0.0;
fsm1py=0.0705*0.45;   fsm1iy=(0.1*1.2/0.002);   fsm1dy=0.0;
avg_m1xc = 0;
avg_m1yc = 0;

%Plot Parameters
%----------------------------------------
    plot_time=2.0;              %length of plot in seconds
    delay_time=shaker_start+1;             %delay before start of example
plot
    adapt=adapt+delay_time+plot_time;     %modify adaption to be after delay
    x_plot_bias=200;    y_plot_bias=200;    %amt to bias example signal
    pbiasy = 300; pbiasx = 300;
    pidstart = (adapt-0.1)+1*0;   % PID control start, sec, before adaption
%----------------------------------------
%   Load Model
%----------------------------------------
tg=xpctarget.xpc;
C1 = (get(tg,'Application'));C2='DEV3_rev19';C3 = get(tg,'Connected');
C4 = 'Yes';
TF1=strcmp(C1, C2);TF2=strcmp(C3, C4);
if ~TF1;
    unload(tg);
    load(tg,'DEV3_rev19');
    tg=xpctarget.xpc;
end
if ~TF2
    error('Connection with target cannot be established - aborting');
end
reply=input('connect model (if not connected) and press enter    ')
set_param('DEV3_rev19', 'SimulationCommand', 'update')
```

```
    tg.StopTime=999;
+tg
reply1=input('press enter when beam is centered on all three detectors   ');
pause(2.5)

-tg
clear tt oo
tt=tg.Time;
last2 = 2/Ts;  endtt = length(tg.Time);
f2 = endtt - last2;
oo = tg.Output(f2:end,:);

cal_ot1y = mean(oo(:,3));
cal_ot1x = mean(oo(:,2));
cal_ot2y = mean(oo(:,5));
cal_ot3y = mean(oo(:,7));
cal_ot4z = mean(oo(:,9));
cal_ot4x = mean(oo(:,8));
cal_ot2z = mean(oo(:,4));
cal_ot3z = mean(oo(:,6));

cal_ot5y = mean(oo(:,11));
cal_ot5x = mean(oo(:,10));

cal_ot6x = mean(oo(:,22));
cal_ot6z = mean(oo(:,21));
cal_ot7x = mean(oo(:,24));
cal_ot7z = mean(oo(:,23));

ot5y=tg.Output(:,11);
ot5x=tg.Output(:,10);

%% 2nd Calibration
cal_tgty = 0;   cal_tgtx = 0;

tg=xpctarget.xpc;
C1 = (get(tg,'Application'));C2='DEV3_rev19';C3 = get(tg,'Connected');
C4 = 'Yes';
TF1=strcmp(C1, C2);TF2=strcmp(C3, C4);
if ~TF1;
    unload(tg);
    load(tg,'DEV3_rev19');
    tg=xpctarget.xpc;
end
if ~TF2
    error('Connection with target cannot be established - aborting');
end
%reply=input('connect model (if not connected) and press enter    ')
set_param('DEV3_rev19', 'SimulationCommand', 'update')
    tg.StopTime=999;
+tg
%reply1=input('press enter when beam is centered on all three detectors   ');
pause(2.5)
```

```
-tg
clear tt2 oo2
tt2=tg.Time;
last2 = 2/Ts;  endtt2 = length(tg.Time);
f2 = endtt2 - last2;
oo2 = tg.Output(f2:end,:);

ot5y_calc=tg.Output(:,18);
ot5x_calc=tg.Output(:,17);
cal_tgty=mean(oo2(:,18));
cal_tgtx=mean(oo2(:,17));

figure(10)
    subplot(2,1,1)
    plot(tt,ot5y*500,tt2,(ot5y_calc*500)),grid,
    line([0 2],[cal_ot5y*500 cal_ot5y*500])
    line([0 2],[cal_tgty*500 cal_tgty*500],'color','r')
    title('Calculation based on FSM and plate motion')
    xlabel('sec'),ylabel('y axis, \mum')
    legend('Actual','Calc')
    subplot(2,1,2)
    plot(tt,ot5x*500,tt2,(ot5x_calc*500)),grid
    line([0 2],[cal_ot5x*500 cal_ot5x*500])
    line([0 2],[cal_tgtx*500 cal_tgtx*500],'color','r')
    xlabel('sec'),ylabel('x axis, \mum')
    legend('Actual','Calc')
```

The following code is used to run the beam control lab:

```
%M-file to Run DEV3_rev19

%Must run Calibration first!

%Save Experimental Data
savefile     = 0;   %   Set to one to save data
% If want to save data, need to create the folder for c1
c1= 'C:\Documents and Settings\Trident1\My
Documents\Experiments\2010\03_05\ex';

if savefile==1;
    reply1 = input('input experiment number   ','s');
    reply2 = input('input run number   ','s');
else
    reply1 = 0;
    reply2 = 0;
end

%*******************************
Ts=0.001;          %sample time (s), if change, have to rebuild model
fintime = 6;        %Length of data run (s)
```

```
calibrate=1;        %just a variable for use in calibration, do not change
%---------------------------------
%Control Selection
    %2=Control Off
    %0=Control On
        x_On_Off=0;
        y_On_Off=0;

    %2=Feedback
    %0=Feedforward
    control=0;
        x_control=control;
        y_control=control;

        if control >= 2;
            title_control2='Feedback';
        end
        if control <=0;
            title_control2='Feedforward';
        end
    %2=PI
    %0=LMS
    PI_LMS=2;
        x_PI_LMS=PI_LMS;
        y_PI_LMS=PI_LMS;
        if PI_LMS >= 2;
            title_control='PI Control';
        end
        if PI_LMS <=0;
            title_control='LMS Control';
        end
%-----------------------------------------
%   Shaker input (sinusiod, max 4 signals)
%       amp in volts, freq in Hz
%-----------------------------------------
a=1; %shaker 1
b=1; %shaker 2
shakeramp = [3*1   2*a        2*a     0.2*a]; %shaker 1
shakerfreq= [17      10        27       45];  %shaker 1
shakeramp2 = [3*b    2*b        1*b       0];  %shaker 2
shakerfreq2= [13      23        41       0];  %shaker 2
shaker_start=1;         %start time of vibrations in secs
shaker_end=fintime;
%Chirp Parameters
chirp_on = 0; IA_chirp_gain=1;
IA_init_freq = 1;  IA_final_freq = 1000; IA_targ_time = 120;

%   LMS parameters for FSMB controller
%-----------------------------------------
    mux=0.015*0.3;      leakx=1;      % x axis adaption rate and leakage
factor
    muy=0.035*0.3;      leaky=1;      % y axis adaption rate and leakage
factor
    w0x = 0;        w0y = 0;        % initial tap gains
```

```
    adapt = 2;                    % adaption start time in secs
    biasx=-0.005*1;   biasy=0.002*1;     % estimate of bias correction
    ax_to_mx=1;       ay_to_my=14;   % estimate of gain correction for FSM to
accel
    ot2y_to_m2y = -1/10;
    mu_y_error = 0.05; leak_y_error = 1.0;
    adapt_y_error = 0.0;
    mu_x_error = 0.05; leak_x_error = 1.0;
%----------------------------------------
%   Reference Signal Selection
%       1=OT-1, 2=Accel-2 (a2x and a2y)
%----------------------------------------
    x_ref_sel=1;    y_ref_sel=1;
    zz=1;  % number of delays for the predictor ref signal
%----------------------------------------
%   Error source selection
%       1=mirror postion, 2=OT3 position, 3=OT2 position
%----------------------------------------
x_error_sel=2;  y_error_sel=2;
accel_lag = 1.05;
OT2y_lag = 1;
mirror_zero_bc = [0.318;0;0.572];
beam_dir_source = [0.408;0;0.572];
beam_start_source = [0.508;0;0.572];
d_1_2 = 0.762e6;    % distance in micrometers
d_2_3 = 0.864e6;
d_1_3 = 1.152e6;
sd_1_2 = d_1_2^2;
sd_1_3 = d_1_3^2;
rmeanx = 0;  rmeany = 0;
xdist_2_3 = 1/0.862;
xdist_1_3 = 0.4826;
xdist_2_3p = 1.5;
zdist_3_1 = 1/0.7491*1.15;

%   PID gains for FSM Controller A
%----------------------------------------
fsm1px=0.0532*0.45;   fsm1ix=(0.07*1.2/0.002);   fsm1dx=0.0;
fsm1py=0.0705*0.45;   fsm1iy=(0.1*1.2/0.002);   fsm1dy=0.0;
avg_m1xc = 0;
avg_m1yc = 0;
%For Ziegler Tuning
    % Kpx=0.0532;
    % Kpy=0.0705;

pidstart=shaker_start + 1 %when control will start
%----------------------------------------
clear ot1x ot1y ot2x ot2y ot3x ot3y
clear ot5x ot5y
clear ot5x_calc ot5y_calc
clear delta_z delta_y delta_x
clear m1x m1y m2x m2y

%****Need to Change this if using a different Model****
```

```
set_param('DEV3_rev19', 'SimulationCommand', 'update')
    tg.StopTime=fintime;
+tg
pause(fintime+0.1)
-tg
clear tt oo

%Output Variables
%Output in volts, multiply by 500 to convert to micro meters
tt=tg.Time; %time (s)
ot5y=tg.Output(:,11); %target y-axis (volts)
ot5x=tg.Output(:,10); %target x-axis
ot3y = tg.Output(:,7)*-500; %(micro meter)
ot2y = tg.Output(:,5)*-500;
ot1y = tg.Output(:,3)*-500;
ot3z = tg.Output(:,6)*-500; %neg b/c pos reading means plate moved in neg z-
dir
ot2z = tg.Output(:,4)*500;
ot1x = tg.Output(:,2)*-500; %neg b/c pos reading means plate moved in neg x-
dir

% Rotations (micro rad)
delta_z=tg.Output(:,12);
delta_x=tg.Output(:,13);
delta_y=tg.Output(:,14);

%Target Calculation (volts)
ot5y_calc=tg.Output(:,18);
ot5x_calc=tg.Output(:,17);

% Calculate Miss Distance and Jitter at Target
ot5r = ((ot5y.^2+ot5x.^2).^0.5)*500; % miss dist in um
ot5j = ot5r./dist_targ;  % jitter in urad

% Jitter in Calculated Signal
ot5r_calc=((ot5y_calc.^2 + ot5x_calc.^2).^.5)*500;
ot5j_calc=ot5r_calc./dist_targ;

% Error Between Actual and Calculated Jitter angle
jitter_error=ot5j_calc-ot5j;
RMS=sum(sqrt(jitter_error.^2))/length(jitter_error)

% Percent Improvement with Control
shake=find(tt>=shaker_start);
shake=shake(1);
control=find(tt>=pidstart);
control=control(1)-1;
done=length(tt);
ot5j_shake=mean(ot5j(shake:control,:));
ot5j_control=mean(ot5j(control:done,:));
jstdin=sqrt(var(ot5j(shake:control)));
jstdout=sqrt(var(ot5j(control:done)));
ystdin=sqrt(var(ot5y(shake:control)));
```

```
xstdin=sqrt(var(ot5x(shake:control)));
ystdout=sqrt(var(ot5y(control:done)));
xstdout=sqrt(var(ot5x(control:done)));
impj=(1-(jstdout/jstdin))*100;
impy=(1-(ystdout/ystdin))*100;
impx=(1-(xstdout/xstdin))*100;

if savefile==1;
    c2= reply1;  c3='_run'; c4=reply2;c5='.mat';
    strsave = strcat(c1,c2,c3,c4,c5);
    save(strsave,...
        'tt','ot5y','ot5x','ot3y','ot2y','ot1y','ot3z','ot2z','ot1x',...
        'delta_z','delta_x','delta_y',...
        'ot5y_calc','ot5x_calc')
end

%Plots
figure(5)
    subplot(3,1,1)
        plot(tt,delta_x,'b'),grid,title('Plate Rotations'),xlabel('sec'),...
        ylabel('\murad'),legend('pitch')
    subplot(3,1,2)
        plot(tt,delta_z,'g'),grid,xlabel('sec'),...
        ylabel('\murad'),legend('roll')
    subplot(3,1,3)
        plot(tt,delta_y,'r'),grid,xlabel('sec'),...
        ylabel('\murad'),legend('yaw')
figure(2)
    subplot(3,1,1)
    plot(tt,ot5y*500),grid
    title(['Laser Position at Target using ',num2str(title_control),...
        ' with ',(num2str(title_control2))])
    xlabel('sec'),ylabel('\mum'),legend('y axis')
    axis([-inf inf -500 500]);
    subplot(3,1,2)
    plot(tt,ot5x*500,'r'),grid
    xlabel('sec'),ylabel('\mum'),legend('x axis')
    axis([-inf inf -500 500]);
    subplot(3,1,3)
    plot(tt,ot5j,'Color',[0 0.502 0]),grid,legend('Jitter')
    title(['Percent Improvement in Jitter Angle = ',num2str(impj,4),'%'])
    xlabel('sec'),ylabel('\murad'),axis([-inf inf 0 100]);
figure(7)
    subplot(2,1,1)
    plot(tt,ot5y*500,tt,(ot5y_calc*500)),grid
    title('Calculation based on FSM and plate motion')
    xlabel('sec'),ylabel('y axis, \mum')
    legend('Actual','Calc')
    axis([-inf inf -500 500]);
    subplot(2,1,2)
    plot(tt,ot5x*500,tt,(ot5x_calc*500)),grid
    xlabel('sec'),ylabel('x axis, \mum')
    legend('Actual','Calc')
    axis([-inf inf -500 500]);
```

The following code is used to run a demonstration of the beam control system:

```
%      demo_DEV3

clear signals beam_int_in beam_int_out radstd radstdin n_cuton
clear tin h_radstdin h_radstd
delayj=5;                    %delay in secs before jitter cut-on
dswx=2;  dswy=11;           % delay in secs for regulator cut-on
Gm=(52.4e-3)/20;
bmint=1;                     % set to > 0 to plot beam intensity
ns=10;
bot1=400;   % dist from dist to ot1
not3=318;   % dist from control to ot3
bot3=715;   % dist from dist to ot3

    %   20 microns at OT3 correspond to about 30 micro-Rad input disturbance

seed1=23499;  seed2=23475;
Ts=0.001;
    np=0.000005;    %0.000005 is about 35 microns at 200 Hz

%   set selx/sely for regulator control:
%       1 = LMS  2 = LQG,  3 = LQG+GAL,   4 = Test Input
%       5 = GAL  6 = GAL+LQG

    selx=3;         sely=3;

scdata=150;     %  10    50   100
shaker_end=40;  %40 seconds if using 150

%   build xPC application lms_rev_3 or Lattice_1 and download it onto the
target
%   initialize above vars manually

% is connection with target working?
if ~strcmp(xpctargetping, 'success')
  error('Connection with target cannot be established');
end

    %develop bullseye
for vx=0:0.1:6.3
      ii=round(10*vx+1);
      ytarg(ii)=10*sin(vx);
      xtarg(ii)=10*cos(vx);
      ytarg2(ii)=20*sin(vx);
      xtarg2(ii)=20*cos(vx);
end
clear vx
```

```
set_param('DEV3_rev19', 'SimulationCommand', 'update')
tg = xpc;                                % create an xPC Object

tg.SampleTime = 0.001;                             % set sample time
tg.StopTime   = 10000;                              % set stoptime to a high
value

start(tg);                               % start execution
tic
% get property name of Parameter to tune
%tPar = getparamid(tg, 'Gain1', 'Gain');

sc = addscope(tg, 'host');               % define (add) a scope object

% get indices of signals
signals(1) = getsignalid(tg, 'Inputs/IO 106 AD input/Gain1');
signals(2) = getsignalid(tg, 'Inputs/IO 106 AD input/Gain2');
% signals(3) = getsignalid(tg, 'OT output Scopes/On Trac/Gain', 'numeric');
% signals(4) = getsignalid(tg, 'OT output Scopes/On Trac/Gain1', 'numeric');

                   % add signals to signal list of scope object
addsignal(sc, signals);
sc.NumSamples  = 50; n_samples=50;                    % set number of samples
to 50
sc.Decimation  = 4;  dec_samples=4;                   % set decimation to 4

                        %  for Ts=0.0005 and Decimation = 4,
                        %  2 msec per sample, 0.1 sec per picture
                        %  (50 "asterisks" per snapshot)

sc.TriggerMode = 'Freerun';                      % set TriggerMode to FreeRun

figh = findobj('Name', 'Laser Control');         % Does the figure exist?
if isempty(figh)
  figh = figure; set(figh, 'Name', 'Laser Control', 'NumberTitle', 'off');
else
  figure(figh);
end
n_cuton=round(dswx/(n_samples*dec_samples*Ts));          % number of scope
samples till cut-on
m = 1; flag = 0; flag1=1; beam_int_std=1;                %60e-3/0.5^2/pi

ro=3000;                                                 %beam diameter in
microns
dratio=400/not3*1000;                                    % ratio of demo
distance to actual distance in m
stdv_val=0.63;                                           %  one standard
deviation from mean
dtx=-380;dty=-200;
for n = 1 : scdata           %   100 50 loop to acquire data packages from
the scope object
```

```
  if isempty(find(get(0, 'Children') == figh)), flag = 1; break; end

  mt = rem(m + 1,  5);

  start(sc);                % start scope object

  while ~strcmpi(sc.Status,'finished');     % wait until scope-object has
state 'finished'
  end;

  % create time vector, upload scope data and display it
  t = sc.Time;
  tin(n)=0.3*n;
  x1=1e3*sc.Data;  % input scope data and convert to microns
  %x1(:,3:4)=x1(:,3:4)*bot3/bot1;  %  account for diff in distance between
OT3 and OT2
  stdvy=sqrt(var(x1(:,2)));
  %stdvyin=sqrt(var(x1(:,1)));
  meany=mean(x1(:,2));
  %meanyin=mean(x1(:,1));
  stdvx=sqrt(var(x1(:,1)));
  h_stdvx(n)=stdvx;
  %stdvxin=sqrt(var(x1(:,3)));
  %h_stdvxin(n)=stdvxin;
  meanx=mean(x1(:,1));
  %meanxin=mean(x1(:,3));
  radstd=sqrt(stdvy^2+stdvx^2);
  h_radstd(n)=radstd;
  ang_radstd=radstd/not3*1000;   % angular measure in mRad
  %radstdin=sqrt(stdvyin^2+stdvxin^2);
  %h_radstdin(n)=radstdin;
  %ang_radstdin=radstdin/bot1*1000;  % angular measure in mRad
  for vx=0:0.1:6.3
      ii=round(10*vx+1);
      yvr(ii)=radstd*sin(vx)+meany;
      xvr(ii)=radstd*cos(vx)+meanx;
      %yvrin(ii)=radstdin*sin(vx)+meanyin;
      %xvrin(ii)=radstdin*cos(vx)+meanxin;
  end

  % upload and plot acquired data

  figure(figh)
  plot(x1(:,1),x1(:,2),'*r'),grid;
  axis square
  hold on
  plot(xvr,yvr,'k','LineWidth',1.2);
  %plot(xvr,yvr,xtarg,ytarg,'k',xtarg2,ytarg2,'k','LineWidth',1.2);
  hold off
  title(['Position on Target'])
%   text(dtx,dty,[' Incoming Std Dev
',round(num2str(radstdin)),'\mu'],'HorizontalAlignment',...
%       'left','VerticalAlignment','bottom','FontWeight','bold')
```

```
%   if toc>dswx
      text(dtx,dty/1.5,[' Beam Std Dev
',round(num2str(radstd)),'\mu'],'HorizontalAlignment',...
          'left','VerticalAlignment','bottom','FontWeight','bold')

%   end
  xlabel('X-Position,microns')
  ylabel('Y-Position,microns')
%   ax1=[(meanx-100) meanx+100 meany-100 meany+100];
  %if toc>dswx+3;ax1=[-150 150 -150 150];dtx=-40;dty=40;end
  %if toc>dswx+10;h_n=n;end
  %axis([-50 50 -50 50])      % for closeup view
  ax1=[-500 500 -500  500];
  axis(ax1);
  drawnow;
end
remscope(tg)
stop(tg);
```

The following code is used to determine the error in the calculated beam position from experimental data:

```
% Code to Find Error in Feedforward Calculation
act = Actual_Jitter(2001:end)*500;
calc = Calc_Jitter(2001:end)*500;
tt2 = tt(2001:end);
figure(1)
plot(tt2,act),grid,zoom
error = (act-calc)-mean(act-calc);
time = 0;

figure(2)
plot(tt2,error),grid,zoom
% rms_err = sqrt(sum(error.^2))
rms_err = norm(error)/sqrt(length(error))
y = smooth(error,101);
for i=1:length(y(1:(3/0.005)))
    if abs(y(i))>1
        time = time+0.0005;
    end
end
time = time*1000;
figure(3)
plot(tt2,y),grid,zoom
axis([1.0005 3 -2 2]);
line([1.0005 3],[1 1],'Color','r')
line([1.0005 3],[-1 -1],'Color','r')
text(1.5,1.2,['time outside \pm 1 \murad = '...
    ,num2str(time),' msec'],'BackgroundColor','w')
```

The following code is used to determine and plot the spectral analysis of experimental data:

```
% Spectral Analysis Code
    window= 8092;
    noverlap = [];
    nfft = [];
    Ts=0.001;
Fs=1/Ts;

[Pot5y,ff]=pwelch((500*ot5y_calc(5/Ts:end)),window,noverlap,nfft,Fs);Pot5y=10
*log10(Pot5y);

[Pot5x,ff]=pwelch((500*ot5x_calc(5/Ts:end)),window,noverlap,nfft,Fs);Pot5x=10
*log10(Pot5x);

figure(30)
        plot(ff,Pot5x,ff,Pot5y),grid,zoom
        title('Power Spectral Density using Welchs method - OT5 ')
        xlabel('frequency, Hz')
        ylabel('dB/Hz')
        legend('ot5x','ot5y')
        axis([0 100 -inf inf]);
```

APPENDIX K: Additional Simulink Blocks

Plots the sensor inputs:

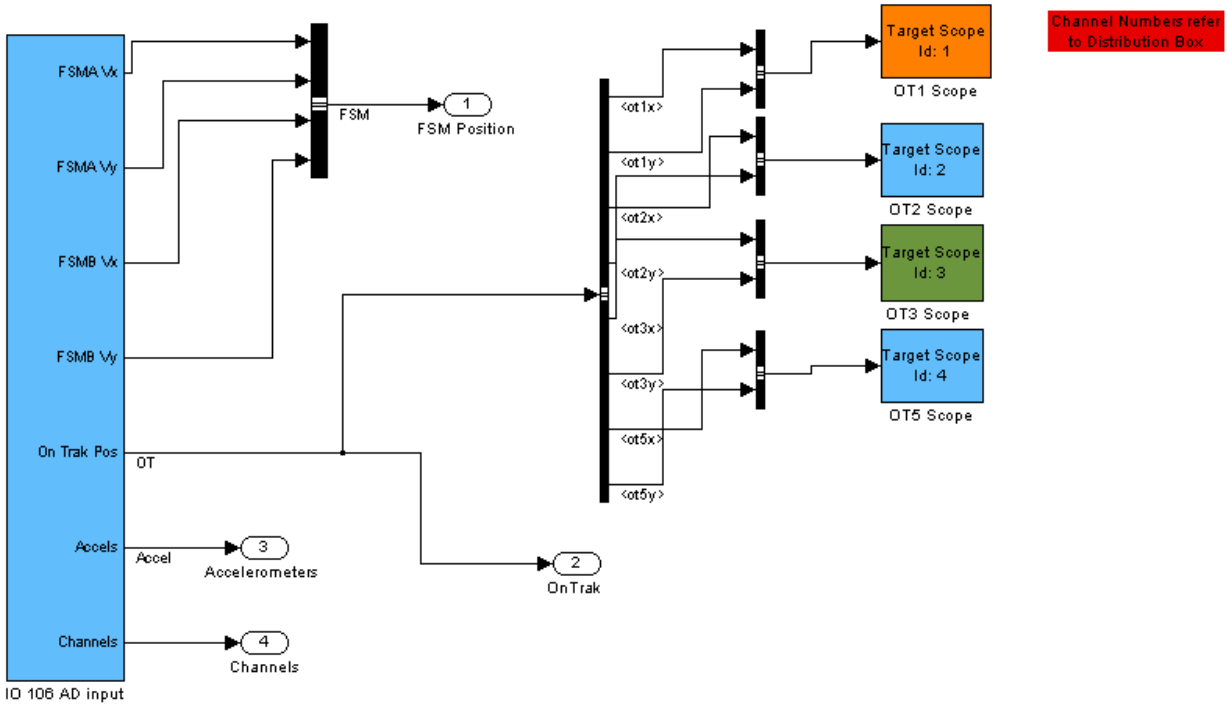

Inputs of all the sensors in the system:

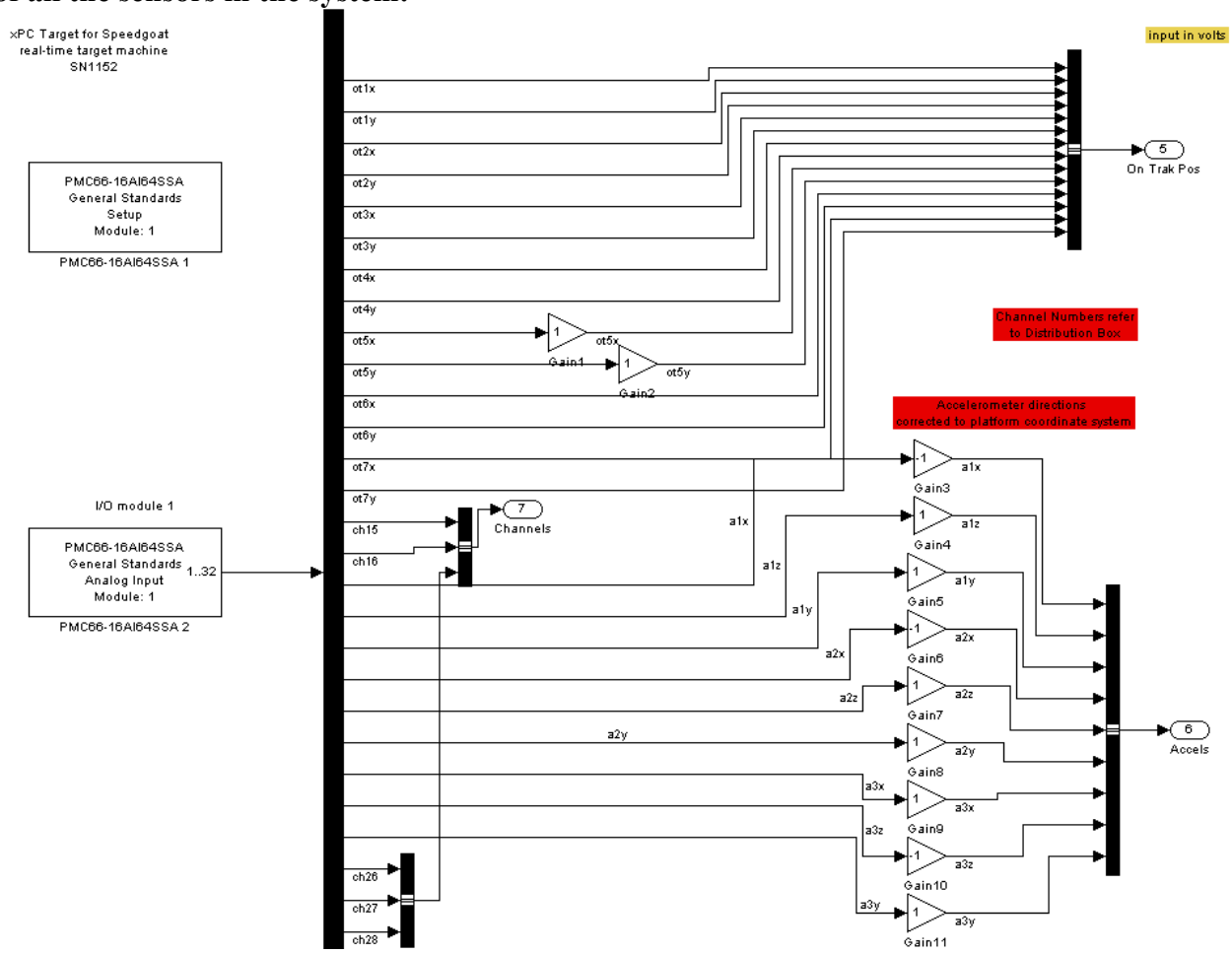

Fast steering mirror (FSM):

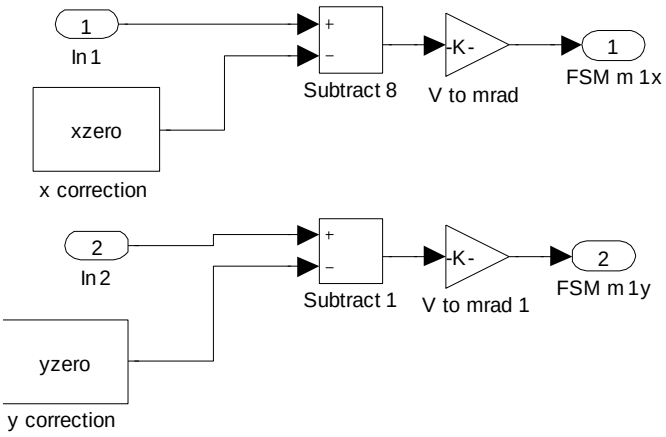

Calculates the rotations of the platform about the x, y, and z axes:

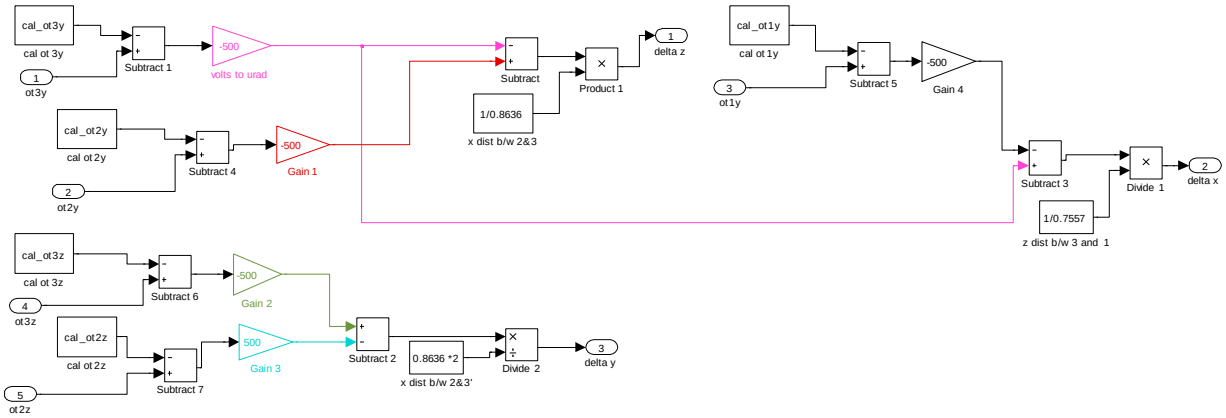

Overall model for computing the beam position at the target:

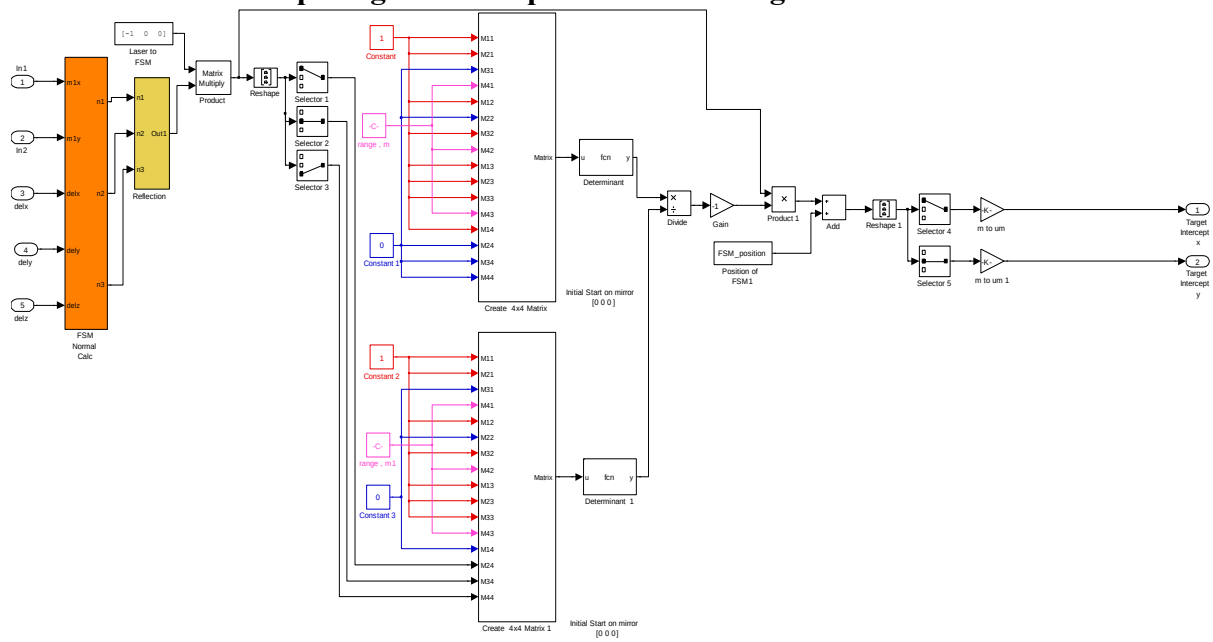

Computes the normal to the mirror based on the platform's rotations and the position of the FSM:

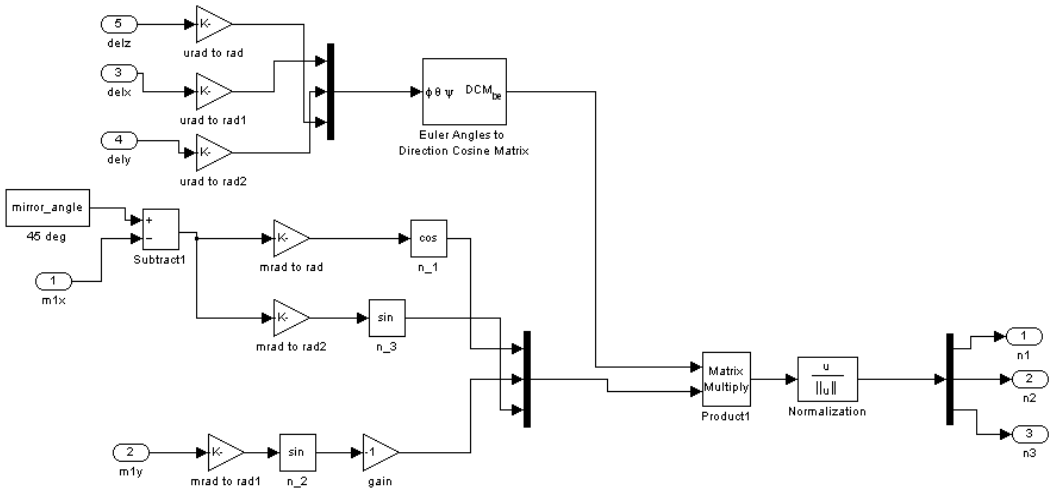

Uses the normal to the mirror to compute the reflected direction of the beam:

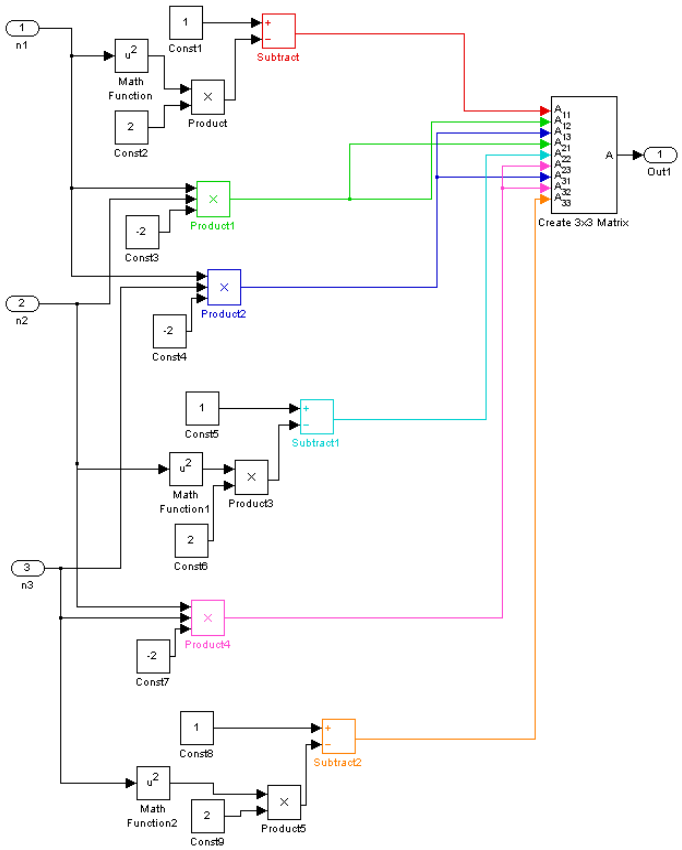

Allows one to select either feedback or feedforward for the LMS controller:

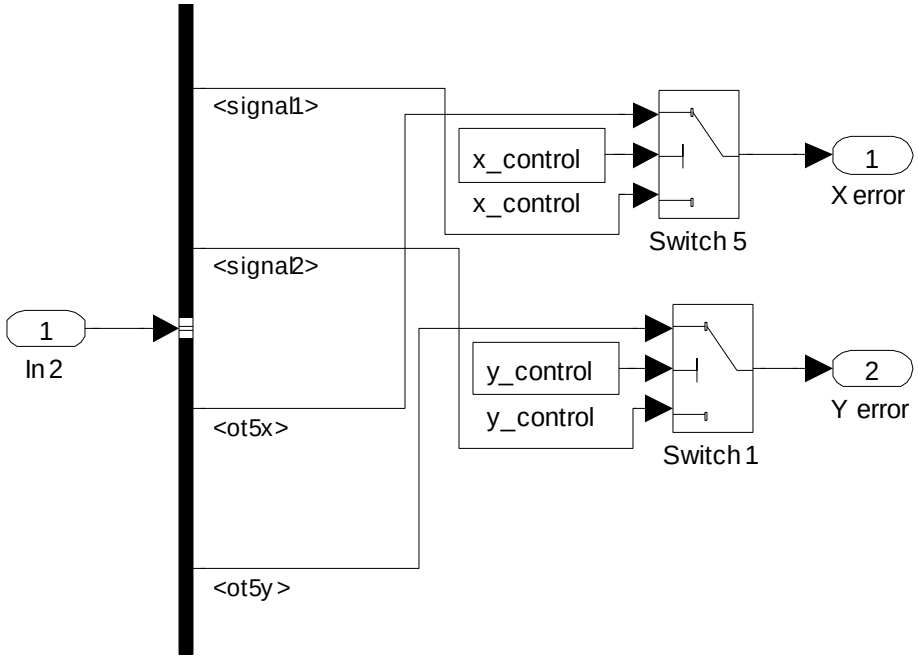

LMS filter:

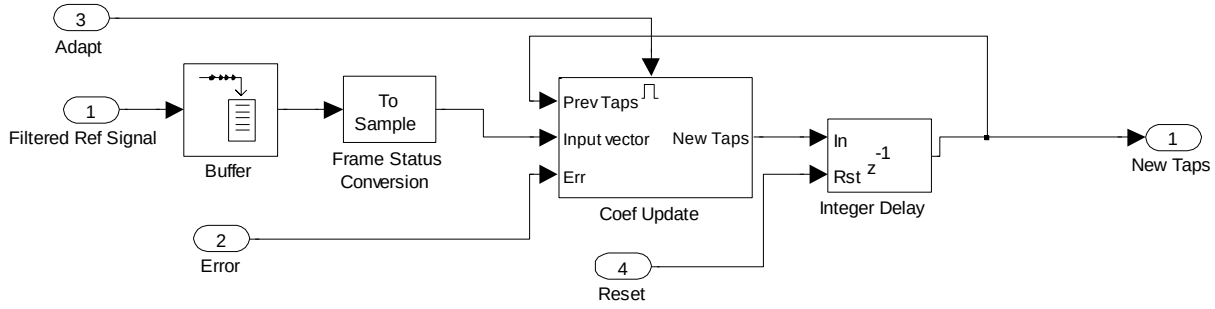

Allows one to turn on/off the control and to switch between using PI or LMS control:

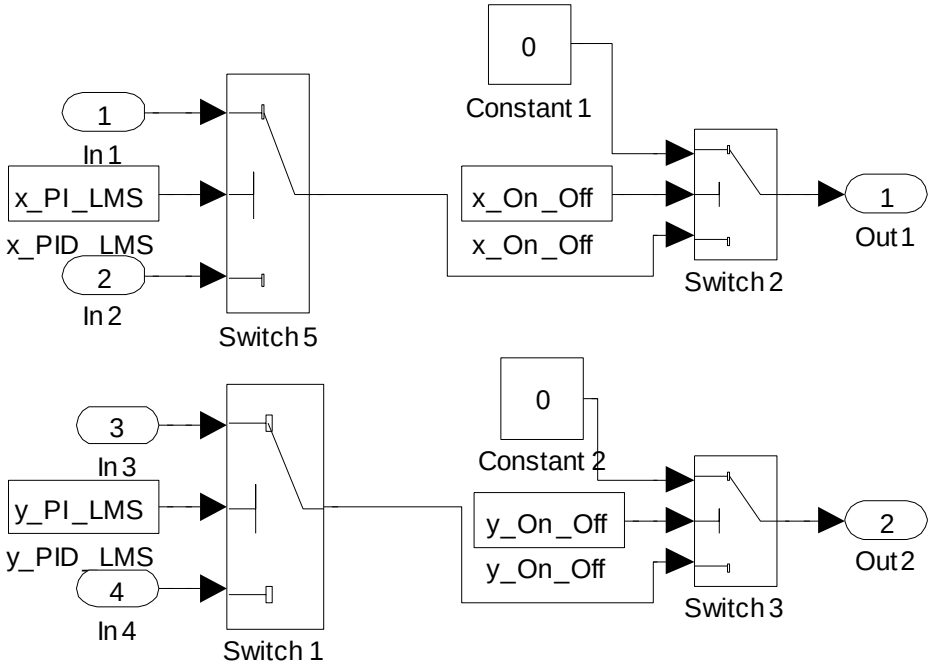

Controls the inertial actuator:

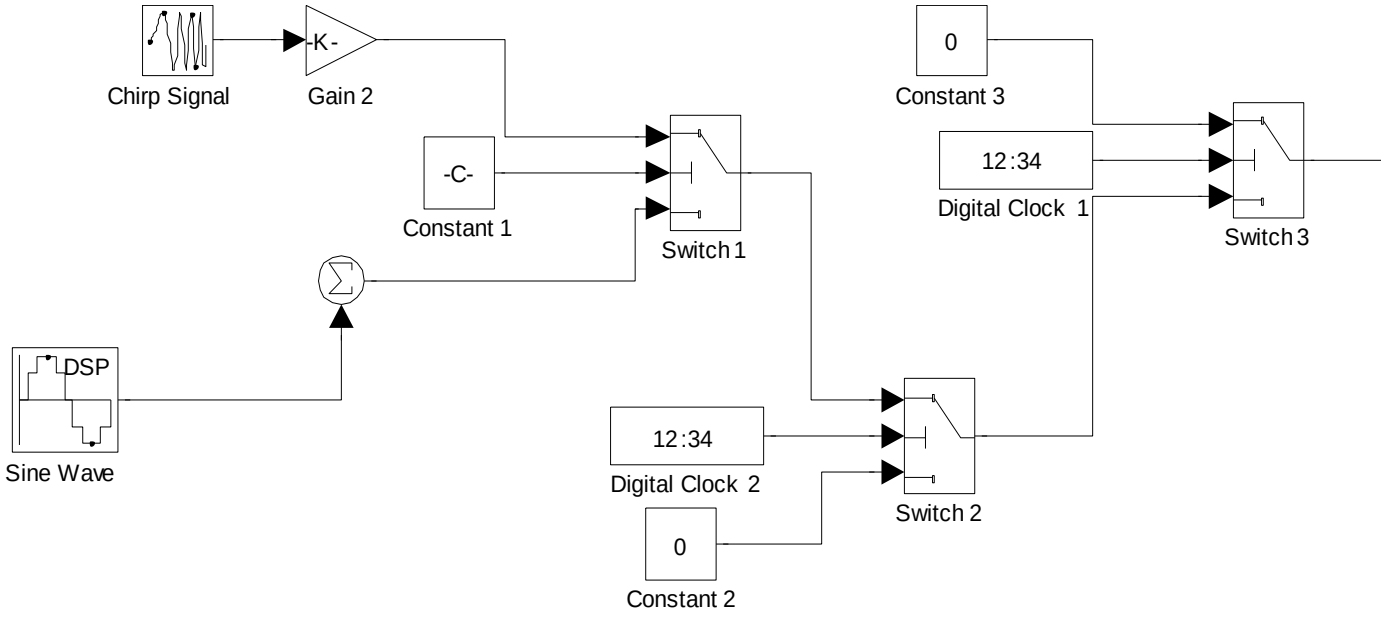

Outputs commands to laboratory: